2013-04-19

Gas Recharging Process Study in Heavy Oil Reservoirs

Zhang, Jihong

UNIVERSITY OF CALGARY

Gas Recharging Process Study in Heavy Oil Reservoirs

by

Jihong Zhang

A THESIS

SUBMITTED TO THE FACULTY OF GRADUATE STUDIES

IN PARTIAL FULFILMENT OF THE REQUIREMENTS FOR THE

DEGREE OF MASTER OF SCIENCE

DEPARTMENT OF CHEMICAL AND PETROLEUM ENGINEERING

CALGARY, ALBERTA

APRIL, 2013

Abstract

Gas recharging process, as a supplemental technique for heavy oil reservoirs with thin layers, has attracted researchers' attention. This thesis focused on three post-cold production process studies-CH_4 recharging and depletion, CO_2 and C_3H_8 huff-puff, and C_3H_8 flooding. Two 18m in length glass beads and sand packed cores and one 1.5m in length sand packed core were used for testing. The mechanisms of each process were investigated. Foamy oil flow under the solution gas drive mechanism was clearly observed during two long core methane depletion processes. The effects of core length and permeability on oil recovery were discussed. CT scanning technique was applied to capture core saturation variations after each process at the 1.5m core, which helped better understanding of the mechanisms of the three gas recharging processes and also was successfully applied to explain what happened in two long cores.

Acknowledgements

I would like to sincerely thank Dr. Kantzas for his supervising throughout my graduate studies. Many thanks are also expressed to Ruiping Shi and Bangyou Wu for mentoring my thesis studies.

I would like to thank all the staff and students of the Tomographic Imaging and Porous Media Laboratory. Their assistance and advice have been very valuable to me. I especially appreciate Igor Tanski and Xiaodong Ji for helping running all the computer assistant tomography (CAT) X-ray scanning for 1.5m in length core at different stages and NMR measurements of produced fluids while I was pregnant. Also, many thanks are expressed to Sam Wu for data acquisition system (DAS) modification for two 18m length cores and set up for 1.5m length core. I also acknowledge Nina Goodarzi for leaving me related information of two 18m in length cores.

I also would like to thank Nexen Inc. and U.S. Silica Company for donating the Luseland dead oil samples and Ottawa silica sand.

Finally, I would like to thank my family for all their support which has continuously motivated me throughout all the challenging times to make this work finished.

Table of Contents

List of Tables

List of Figures and Illustrations

List of Symbols, Abbreviations and Nomenclature

Symbol	Definition
ASP	Alkaline Surfactant Polymer
BPR	Back pressure regulator
CAT	X-ray Computed Assisted Tomography
CCP	Cubic close packing
CHOPS	Cold heavy oil production with sand
CH_4	Methane
C_3H_8	Propane
CO_2	Carbon dioxide
DAS	Data acquisition system
GC	Gas chromatography
GOR	Gas oil ratio
H_2	Hydrogen
IPA	Isopropyl alcohol
MFC	Mass flow controller
MMP	Minimum miscibility pressure
MME	Minimum miscibility enrichment
MPC	Methane pressure-cycling
NMR	Nuclear magnetic resonance
OOIP	Original oil in place, %
P	Pressure, kPa
SAG	Soak-alternating-gas
SAGD	Steam Assisted Gravity Drainage
SCP	Simple cubic packing
SOR	Solvent gas oil ratio
S_{or}	Residual oil saturation, %
T	Temperature, ℃
V	Volume, ml
VEPEX	Vapour Extraction
W	Weight, g
WAG	Water-alternating-gas

Chapter One: Introduction

1.1 Background

The two largest oil deposits in the world are the heavy and extra heavy oil deposits of Venezuela and Canada[1]. With the oil demand and price increase and conventional oil reserves decrease, heavy oil production occupies increasingly important situation in the future energy industry. Compared to conventional oil, heavy oil is much more viscous; therefore, its production is much more complicated and difficult. Substantial work has been done to maximize heavy oil recovery from primary recovery methods (cold heavy oil production with sand-CHOPS) to non-thermal and thermal production methods.

It is well known that thermal recovery methods can dramatically reduce the viscosity of heavy oil. However, they could not be applied in the majority of Canadian heavy oil reservoirs economically after the primary production as formations are thin or bottom water exists[2]. Thermal recovery methods will result in extensive heat losses through the surrounding formations. Non-thermal recovery methods or post-cold production, as a supplementary technique, play an important role to these depleted or near depleted thin heavy oil reservoirs.

Gas injection as a non-thermal recovery method is mainly used for light oil recovery. Since the early 1963, a natural-gas-injection project was successfully conducted in a heavy oil reservoir (14-20 API) located in Eastern Venezuela[3]. Normally used injection gases include[4] acidic gas (CO_2 and sour gas), hydrocarbon gases, nitrogen and flue gas. Injection methods include single and mixture gas injections or combination with other EOR techniques (e.g. WAG[5-7], CO_2-ASP-WAG[8], CO_2-chemical[9], CO_2-foam[10-11], gas-steam[12-14], C_4H_{10}-SAGD[15] etc.).

Although much research work on improving oil recovery is ongoing for years, most of the experiments to date were applied at small scale core samples. It is always difficult at the laboratory level to carry out such experiments in real representative field condition, but it is no doubt that larger scale experiment is one step closer[29] to the reservoir scale and is very helpful to understanding the prevailing mechanisms which may occur in the reservoir. To the best of our knowledge, the longest cores[16-28] which have ever been used in the past are two 18m in length cores (glass beads packed and sand packed separately) tested by Goodarzi[17,19]and Shi[18].

1.2 Objective

The objective of this study is to further understand the recovery mechanism of heavy oil production by single gas and gas mixture recharging processes in heavy oil reservoirs. The effects of oil recovery methods, core permeability and core length are also investigated.

1.3 Methodology

To generate data that is a step closer to the reservoir scale, in this work, several gas recharging processes were presented at two 18m in length large-scale core systems used by Goodarzi[17, 19] and Shi[18] before. Tests were conducted in the absence of sand production, after primary production. To further understand what happened in these processes, a 1.5m in length sand packed core system was designed and tested with all the same processes done at the two long cores. At the same time, X-ray Computed Assisted Tomography (CAT) was used as the tool to monitor the core saturations before and after each process. Density profiles as a function of core length were investigated. An attempt was made to use the results from the 1.5m smaller core experiments to explain the long core results.

In total, three gas recharging processes were performed and studied in order after primary depletion at these three cores. Methane recharging (above bubble point pressure) and depletion, propane and carbon dioxide (mixture in liquid phase) huff-puff, and propane (gas phase) flooding.

Pressure and temperature variations along the core, injected and produced gas composition, produced oil viscosity and water cut, core density before and after each process, were the collected data.

Chapter Two: Literature Review

As mentioned in chapter one, the focus of this study is the further understanding of the behaviour of several gas recharging processes. As such, the literature review is concentrated on this subject only.

Due to high viscosity, the bulk of oil is left behind after primary production in heavy oil reservoirs. The natural energy has been depleted; more energy is needed to be added into the deposit for further recovery of the oil left in place. Gas injection is one option to do so. At the early stages, pressure maintain once is the main purpose for gas injection. Increasing ultimate recovery is also a goal for this operation.

To better investigate the gas injection process, the secondary recovery method, clearly understanding heavy oil primary production process is an important foundation.

2.1 Heavy Oil Primary Depletion-Foamy Oil Flow under Solution Gas Drive

It is widely reported[29-31] that primary production of heavy oil reservoirs has demonstrated higher oil recovery than expected based on conventional reservoir engineering principles. Understanding of this complex phenomenon has been developed from not only experimental studies but also field tests. The higher than expected level of primary well productivity of many heavy oil areas is mainly governed by the processes of sand production (Cold Heavy Oil Production-CHOPS) and foamy oil flow under solution gas drive[2]. In this study, we limit our work to the situation without sand production.

Foamy oil mechanism under solution gas drive was first presented by Smith[32] in 1988. He suggested that tiny gas bubbles tend to remain dispersed within heavy crude oil for a relatively long period of time and flow with the oil together. Following this, efforts have been made to interpret the mechanisms of heavy oil solution gas drive for the last three decades by many researchers.

First of all, what is solution gas drive? It needs to be defined clearly. This process has been well described by R. T. Johns[33]. Many oil reservoirs are initially under saturated with dissolved gas at

reservoir pressure which is above the bubble point pressure. If there is no water influx from the periphery of the reservoirs, the oil and water compressibilities are the primary energy for recovery. As pressure decreases, liquids expand to cause oil to flow to the production wells and to the surface. Because of the smaller liquid compressibilities, there is often a rapid decline in average reservoir pressure during the liquid expansion period until the bubble point pressure is reached. Once the average reservoir pressure drops below the bubble point pressure, solution gas evolves from the oil. The solution gas developing in the pores provides additional energy beyond liquid expansion with which to recover oil. Because of larger gas compressibilities, the average reservoir pressure does not decrease as rapidly as it did when the reservoir pressure was above the bubble point pressure.

Secondly, what is foamy oil? It should be defined. D.D. Joseph[34] defined that "foamy oil is heavy oil that gives rise to stable dispersed bubbles under moderate depressurization and to stable foam under severe depressurization". He also explained that "Stable dispersed bubbles are protected against coalescence. At least they are resistant to coalescence. Stable foam means that foam does not collapse for a long time." L. Andarcia et al.[35] explained the conceptual difference between foamy and non-foamy oil. They introduced that foamy oil is the oil that its phase separation between oil and gas would occur after a "long time". That is, the released solution gas could be entrapped in the oil for extended periods of time. A definition from the TermWiki -the global social learning network website (http://www.termwiki.com/EN:foamy_oil) is as follows:

Oil-continuous foam that contains dispersed gas bubbles produced at the wellhead from heavy oil reservoirs under solution gas drive. The nature of the gas dispersions in oil distinguishes foamy oil behavior from conventional heavy oil. The gas that comes out of solution in the reservoir does not coalesce into large gas bubbles nor into a continuous flowing gas phase. Instead it remains as small bubbles entrained in the crude oil, keeping the effective oil viscosity low while providing expansive energy that helps drive the oil toward the producing well. Foamy oil accounts for unusually high production in heavy oil reservoirs under solution-gas drive". B. B. Maini[36] reported that "Foamy-oil flow is a non-Darcy form of two-phase flow of gas and oil encountered in many Canadian and Venezuelan heavy-oil reservoirs during production under

solution-gas drive. Unlike normal two-phase flow, which requires a fluid phase to become continuous before it can flow, it involves flow of dispersed gas bubbles."

2.1.1 Differences of Conventional Solution Gas Drive and Foamy Solution Gas Drive

Various studies have been conducted to investigate the mechanism of primary production in heavy oil reservoirs. Considerable studies indicate that mechanisms of the solution gas drive in heavy oil reservoirs are complex and quite different from those in conventional oil reservoirs.

In conventional oil reservoirs[29], solution gas drive generally does not achieve very high recoveries. As pressure declines, the gas is evolved from the oil within the pore space and grows there until it forms a free and continuous phase. At this point the gas is produced out, leaving the oil in place.

However, in the case of heavy oil reservoirs[29-31], due to higher viscosity, after the gas is formed it tends to remain trapped longer within the oil as a result of the low viscosity and density[37], high compressibility and reduced gas mobility. A two-phase gas in oil dispersion (foamy oil) forms within the oil, the foamy oil flow under solution gas drive results in a higher primary recovery, lower produced gas oil ratios and slower-pressure decline rate within the reservoir.

Field data also showed that solution gas drive in heavy oil reservoirs was more successful and had higher oil production rates and lower produced gas oil ratios than those expected. For example, heavy oil reservoirs in Canada produced 12-20% OOIP by CHOPS technique. On the contrary, conventional primary production (no sand produced) in such case only recovered 0-2% OOIP[1].

S. Akin et al.[38] conducted a laboratory study of solution gas drive in viscous mineral oil and heavy oil. A series of primary depletion experiments were performed to differentiate the mechanisms of heavy-oil solution gas drive by using X-ray computerized-tomography (CT) to monitor these processes. The mineral oil experiments showed conventional solution-gas drive behaviour. Moreover, a continuous gas phase accumulated at the top of the sand pack by gravity segregation was demonstrated by CT-derived gas saturation images. The heavy crude oil experiments showed some aspects of foamy-oil behaviour. From the gas phase growth pattern, it

was surmised that the bubbles nucleated randomly, never grew to appreciable size before mobilization, and remained discontinuous throughout the whole experiments. Furthermore, bubbles were observed to nucleate on the sides of the visualization cell. Visual cell observations also showed that bubbles in the heavy oil were widely separated and flowed together with the oil. The frequency of bubble–bubble coalescence events in the visualization cell was virtually zero.

B.B. Maini[36] made a clear comparison in pore level between foamy solution gas drive and conventional solution gas drive. It is shown below:

Table 2.1 Comparison of pore-level processes[36] in solution gas drive

No.	Conventional Solution Gas Drive	Foamy Solution Gas Drive
1	Pressure depletion creates supersaturation.	
2	Bubbles nucleate in rough cavities of pore walls.	
3	Some bubbles detach and start growing in pore bodies.	
4	Bubbles continue to grow in place without vacating the pore in which they originated.	Bubbles start migrating with the oil after growing to a certain size.
5	Different bubbles originating in different pores grow large enough to contact each other.	Migrating bubbles keep dividing into smaller bubbles.
6	Bubbles coalesce to form a continuous gas phase.	Dispersed flow is achieved by breakup of large bubbles into smaller bubbles.
7	Producing GOR increases rapidly once the gas starts to flow as a continuous phase.	Producing GOR remains low.
8	Reservoir energy is depleted at a low recovery factor.	High recovery factors are obtained.

2.1.2 Effect of Oil Viscosity on Stability of Foamy Oil

Wang et al.[39] studied the influence of viscosity on foamy oil stability through sand pack experiment. He reported that the stability of foamy oil became better as oil viscosity increased. Large solution viscosity is a key role in retarding the transport of gas from solution to the growing bubble in the foamy oil. That is, gas bubble increases much more slowly in viscous oils; therefore, coalescence is slowed dramatically.

George et al.[40] also investigated the effect of viscosity on bubble coalescence in viscous oils under solution gas drive. Micro-models, cornered capillary tubes, and a bubble growth model were applied for further understanding. It is shown that oil viscosity has a profound effect on

coalescence dynamics during both earlier and later time regimes. In the earlier stage, when coalescence occurs mainly due to bubble growth by diffusion, high viscosity of the oil-phase slows the diffusion of dissolved solution gas in the oil, thus reducing the rate of bubble growth. These results in longer time for coalescence of bubbles trapped in more viscous oils. At the later stage, coalescence is governed by the pressure drop across the bubbles, pushing them together, draining the oil lens between the bubbles, and finally resulting in coalescence. Intuitively, it should be more difficult to drain the oil between the bubbles as oil-phase viscosity increases. Furthermore, heavy-oil reservoirs are able to maintain substantial drive energy because gas bubble coalescence is delayed partially by viscous oil and low bubble coalescence rates lead to substantial disconnected gas that is difficult to mobilize. Figure 2.1 showed the heterogeneous bubble nucleation and expansion at the same site during the pressure depletion of a micro model saturated with CO_2.

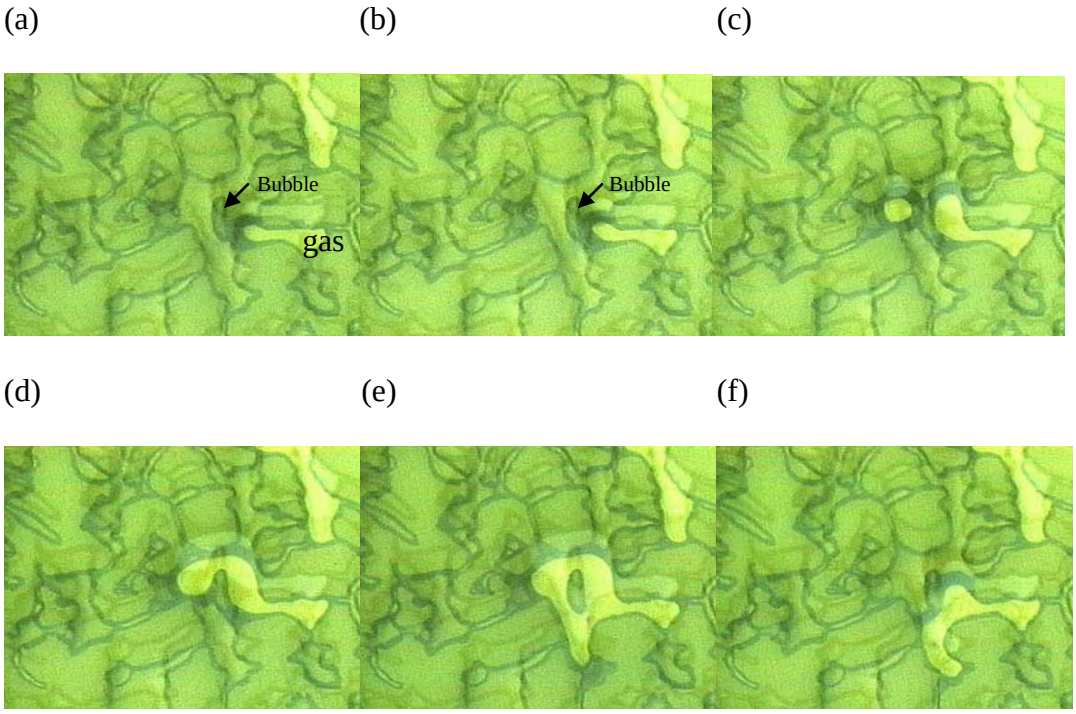

Figure 2.1 Bubble nucleation and growth in CO_2-saturated water[40]

(a) Recently nucleated bubble at 0 s,
(b) Bubble growth at 0.2 s,
(c) Gas bubble at 0.9 s after growing to fill pore body,
(d) Bubbles expand and coalesce at 1.2 s,
(e) At 2.4 s bubble expands,
(f) Bubble is mobilized and leaves the pore space where it was nucleated at 2.8 s.

2.1.3 Effect of Oil Composition

Peng et al.[41] investigated the role of oil composition on heavy oil solution gas drive. It was found that oil composition plays a role in determining metastability of dispersed gas bubbles in foamy oil by core-level depletion and significant asphaltene content as well as substantial acid number and base number are indicators of whether oil is foamy. It is also reported that a high concentration of asphaltenes that exhibits acid and base functional groups tends to increase foamability and film lifetime of gas/crude-oil dispersions. Inversely, the deasphalted fraction is not foamy despite possessing significant acid and base number. That is, acid and base groups within asphaltenes, and their interaction at the gas–oil interface, are a source of interfacial stability. Finally, they concluded that the role of solution viscosity on bubble coalescence and film rupture appeared to be relatively minor compared to the oil chemistry effect.

2.1.4 Effect of Gas Nucleation on Heavy Oil Mobility

The effect of gas nucleation on mobility of heavy oils in primary production under solution gas drive was investigated by Maini et al.[42, 43]. Based on their experiments conducted at a 2m in length sand packed core, they concluded that the mechanism of heavy oil primary production under solution gas drive is complex process involving interplay of several mechanisms including the nucleation, growth and coalescence of gas bubbles, formation of foam and multi-phase fluid flow in porous media. It is reported that the formed foam formation has no mobility enhancing potential, but it can be very beneficial for increasing the oil recovery.

2.1.5 Effects of Two Types of Non-Equilibrium Processes

Maini[36] introduced two types of non-equilibrium processes involved in foamy solution-gas drive in heavy oils. The first non-equilibrium is between solution gas and free gas that leads to a possibility of significant supersaturation of dissolved gas in the oil phase. The second non-equilibrium is related to fluid distribution in the rock. Being different from the traditional two-phase-flow situations governed by capillary forces, due to high oil viscosity and drawdown pressure, the local capillary number ($k\Delta\Phi/\sigma_{og}$) can be high enough to mobilize isolated bubbles to lead dispersed flow in heavy oil cold production. This type of non-equilibrium is affected by the surface tension of the oil, the absolute permeability, and the value of the gradient of flow

potential in the vicinity of the isolated bubbles. The first one is likely to be more significant in laboratory experiments on a much smaller time scale case, the second one is more important in causing the unexpected more production in the field. He also concluded that the pressure gradient, rather than the decline rate of average reservoir pressure, is the driving force for foamy-oil flow.

2.1.6 Effect of Depletion Rate and Pressure Gradient

Based on micro-model observations and linear sand-pack depletion tests, Maini[44] concluded that the pore scale flow behaviour was dramatically different in slow and fast depletion tests. The pressure depletion rate played a key role in determining the structure of gas-oil dispersion in porous media, and the performance of the solution-gas drive process. The slow depletion experiments behaved in a classical solution-gas-drive type displacement. On the other hand, the fast depletion tests resulted in a foamy solution gas drive process. Table 2.2 shows the behaviour comparisons of these different depletion rates.

Table 2.2 Behaviour comparisons at different depletion rates[44]

No.	Slow depletion rate	Fast depletion rate
1	A smaller number of bubbles nucleate.	The number of nucleated bubbles is somewhat higher than slow depletion test. The nucleation is not instantaneous and new bubbles keep being nucleated throughout the entire depletion.
2	Bubbles do not become mobilized with the oil and grew in size within the pore in which they originated.	Bubbles start to migrate with the flowing oil soon after nucleation. The bubbles keep growing while moving. The mobilized bubbles tend to break into smaller bubbles during moving.
3	Coalescence of the gas bubbles is more likely to occur when the liquid velocity is low and the bubbles remain in contact for a longer period.	The dispersed gas flow is achieved by the continued migration and bubble breakup instead of explosive nucleation.
4	Low pressure-gradient	High pressure-gradient persists throughout the duration of the high depletion rate test. It strongly showed that the gas phase is not continuous.
5	Low oil recovery factors	High oil recovery factors

Finally, he suggested that it was the pressure gradient generated within the sand-pack not the depletion rate on its own had a clear link to the depletion performance. A high pressure gradient may be required to generate the dispersed flow that results in high recovery factors.

Kumar et al.[45] also investigated the effect of depletion rate by varying the rate more than two orders of magnitude. They agreed with Maini that gas mobility decreased with the depletion rate increasing and high depletion rate resulted in more efficient oil recovery. They further reported that the maximum super saturation increased with increasing depletion rate and was found to be proportional to log of rate of pressure drop. The critical gas saturation was 3 to 4% and increased slightly with depletion rate.

Sheikha and Pooladi-Darvish[46] further studied the effect of pressure decline rate and pressure gradient on the behaviour of solution gas drive in heavy oil. They suggested that a high pressure decline rate results in larger super-saturation and faster nucleation and therefore leads to more dispersed gas bubbles. A high pressure gradient improves the viscous forces acting on the gas phase enhancing bubble break-up and gas dispersion. Both effects result in lower gas mobility improving oil recovery, but pressure gradient plays a more important role than pressure decline rate.

2.2 Post-Cold Production-Gas Injection

2.2.1 Immiscible and Miscible Gas Flooding

Johns[33] described two gas injection processes: immiscible and miscible gas flooding.

Immiscible gas injection is similar to the recovery process that occurs during a gas cap drive. The volume and driving of gas can be controlled to improve sweep efficiency and maintain reservoir energy or pressure like water flooding.

Typical gases for immiscible flooding are methane, nitrogen, carbon dioxide, and air. Many of them are not completely immiscible with the oil. For example, carbon dioxide nearly always has some limited miscibility with the oil and, therefore, can swell the oil and reduce its viscosity, both of which can improve recovery.

Miscible gas injection, when the inject gas is miscible with the oil, is much more efficient and commonly used method today. The oil recovery for miscible gas flooding can increase significantly beyond primary recovery processes because the interfacial tension between the residual oil and injected gas is reduced to zero. The reduced interfacial tension between the fluids can decrease capillary pressure, therefore, the residual oil saturation decreases in many cases to values of less than 1 or 2%.

One commonly used miscible fluid today is carbon dioxide, which is injected as a supercritical fluid at temperatures and pressures beyond its critical point. Methane and nitrogen can also be miscible with oil, although these gases require much higher reservoir pressures to achieve miscibility. The type of gas used also depends on its cost and its availability at the field site.

There are two types of miscibility that can occur between resident oil and injected gas-first-contact miscible and multi-contact miscible. First-contact miscibility occurs when the gas and oil are miscible when mixed in any proportions. This type of miscibility is ideal but is seldom achieved. Multi-contact miscibility occurs more often and is the process by which gas and oil develop miscibility in the reservoir by repeated contact with each other.

Historically, there are two multi-contact miscible processes which were thought to occur either by vaporizing contacts or by condensing contacts. In vaporizing drives, fresh gas mixes with equilibrium oil and vaporizes the intermediate-weight components in the oil, whereas in condensing drives, fresh oil mixes with equilibrium gas and condenses intermediate-weight components in the gas into the oil. Vaporizing drives occur when components, such as methane and nitrogen, are injected at pressures above the minimum pressure for miscibility (or MMP). Condensing drives were thought to occur when gases are sufficiently enriched with hydrocarbon components, such as ethane and propane, to a composition called the minimum enrichment for miscibility (or MME).

A combined condensing/vaporizing mechanism has been showed for both enriched hydrocarbon gas floods and carbon dioxide floods recently. In the combined process, the gas at the leading edge of the gas front swells oil, the gas at the trailing edge vaporizes the residual oil, and between the condensing and vaporizing regions, miscibility is approached.

2.2.2 First Application in Heavy Oil Reservoirs

Since 1963, a successful natural gas-injection project in a heavy oil reservoir (14-20 °API) located in Eastern Venezuela was conducted, reported by Garcia[3], gas injection applied to heavy oil deposits began to be thought attractive and possible. Dynamic miscibility and gravity segregation both contributed to the high recovery. The cumulative recovery in a relatively high oil-gas viscosity ratio reservoir has been 32% of OOIP, and final recovery is estimated at 45% of OOIP. He concluded finally that conventional gas injection is a practical heavy-oil secondary recovery application and should be considered as an alternative to thermal methods.

2.2.3 Gas Injection Process Studies

Based on the scaled model studies and numerical simulation of inert gas (CO_2 and N_2) injection with horizontal wells, Meszaros et al.[47] reported that about 70% oil in place may be recovered by gas injection from the top of a heavy oil reservoir of oil viscosities between 1000 and 4000mPa.s. Maintaining a stable gas front is very important for receiving high recovery. Moreover, CO_2 injection is likely to recover more oil than N_2 injection case for a higher oil viscosity deposit.

A gravity assisted immiscible gas injection process was investigated by Kantzas et al.[48] via the tests on 2-D glass micro-models, unconsolidated systems and reservoir cores. They concluded that gravity assisted immiscible gas injection can be very successful in oil-wet, mixed-wet or water-wet systems, but the success of gas injection process is closely related to the water-flood efficiency ahead of it. The lab test results showed that gas injection can result in an incremental recovery of up to 20% original oil in place (OOIP) even from a heterogeneous fractionally wet formation.

Islam et al.[49] studied the inert gas (CO_2 and N_2) injection processes at a constant injection pressure with horizontal wells in heavy oil reservoir. Using gravity-stabilization, they presented that the oil recovery may be as high as 70% of OOIP for moderately viscous heavy oil reservoirs. At higher injection pressures (34.47kPa and 68.95kPa) cases, CO_2 injection leads to a quicker response in oil production than N_2 injection cases. However, the production drops more quickly for CO_2 injection cases.

Butler and Mokrys[50] tested C_3H_8 (800-827kPa) and C_2H_6 injection processes on a large, scaled, physical model at 25-30℃. In 8 hours experimental time, oil recovery reached up to 55% for C_3H_8 injection and about 28% for C_2H_6 injection. Furthermore, the produced oil viscosity was dramatically reduced by C_3H_8 injection from 10000mPa.s to 2000mPa.s. That means the oil was in situ upgraded. But for the C_2H_6 injection case, the produced oil viscosity remained unaffected. They also concluded that C_3H_8 injection by itself results in high rates and recovery even compares to hot water-propane process-VAPEX.

Murray et al.[51] introduced a new approach to CO_2 flood; soak-alternating-gas (SAG). That is, inject CO_2 and shut in the well. Then, instead of producing as in the huff-puff process, inject CO_2 again. This process is a cyclic process like WAG. The mass transfer between CO_2 and oil during shut in period helps the mobility control. They reported that: "The goal of this new method is to optimize the CO_2 process by using periodic soak periods in a continuous flood to maintain the effectiveness of the transition zone at the flood front, and cause the oil mobilization behind the flood front to occur as close to the flood front as possible, thus forming an extended flood front. This would create greater mobility control in CO_2 flooding process without the use of WAG, reduce the travel distance needed to achieve optimal miscibility, and increase the mass transfer between CO_2 and oil without adding additional CO_2". Overall, SAG was developed conceptually to provide a mobility control method in CO_2 EOR processes where water injection is not feasible.

Dong et al.[52] investigated the methane pressure-cycling (MPC) process with horizontal wells for thin heavy-oil reservoirs by laboratory PVT, sand pack-flood and numerical-simulation studies. MPC process was intended to apply in some heavy oil reservoirs, particularly thinner ones, after termination of either primary or water-flood production. The goal of this process is the restoration of the solution-gas-drive mechanism. The restoration is accomplished by re-injecting an appropriate amount of solution gas (mainly CH_4) and then re-pressuring the gas back into oil by water injection until approximate original reservoir pressure is reached. After that, the system was shut in for soaking until pressures were steady, and then followed up by production. This process then can be repeated for cycling. The purpose of this process is to recreate the primary-production conditions. The sand pack used is 30.5cm (length) ×5.0cm (diameter), the dead oil viscosities were between 1700-5400mPa.s, API gravities were within 11.5-14.7, reservoir

temperatures were between 25-31℃, methane saturation pressure were within 1.1-8MPa (160-1160psi). From the solubility of CH_4 in heavy oils study, they concluded that oil exists in the liquid phase and CH_4 exists not only in the gas phase but also is dissolved in the oil phase in the pressure range of 2-8MPa. From the viscosity of heavy oil/ CH_4 mixture study, they reported that the viscosity of dead oils could be reduced greatly when they were saturated with CH_4. Viscosity reduction and volumetric expansion of the oil/gas system are the major displacement mechanisms of the MPC process. From the effect of oil viscosity study, they found that the MPC process for more-viscous oils was as effective as that for less-viscous oils at a low mobile-water-saturation. However, the process for more-viscous oils was far less effective than for less-viscous oils at high mobile-water saturation. When the mobile-water saturation was increased to a certain value, the cycle oil recovery declined to very low values (<1%IOIP). They also introduced that the gas injection rate during gas-recharging phase of a cycle is of substantial important to the performance of MPC process. At a higher gas injection rate, the greater amount of gas was absorbed and the higher rate of oil production was observed. To sum up, the principal of the pressure-cycling process is to restore situation of substantial amounts of gas being in solution for further primary production. A key step for this process is to make the gas contact the residual oil in the porous media. By releasing the solution gas from the oil and leaving the pore-scale gas channels everywhere in the reservoir, creating paths for recharged gas to finger into the remaining oil in porous media, MPC process can make this happen.

Enhanced solvent dissolution into the in-situ upgraded heavy oil under different pressures was studied by Luo et al.[53] When a solvent is dissolved into heavy oil under certain reservoir conditions, asphaltene precipitation may occur. Therefore, such in-situ upgraded heavy oil with lower asphaltene content is less viscous and easier to be recovered. Three heavy oil samples with different asphaltene contents of 0.0 wt. % (i.e., the maltenes), 7.0 wt. % (the reconstituted oil), and 14.5 wt. % (the original oil) were saturated with propane (C_3H_8) separately at five different equilibrium pressures ranging from 200 to 800kPa at 23.9℃. The detailed experimental results show that the asphaltene content in heavy oil strongly affects propane dissolution into the heavy oil. In general, if the heavy oil contains lower asphaltene content, the propane solubility is higher and the oil-swelling factor is larger, consequently, the viscosity of the heavy oil–propane system

is lower, whereas its molecular diffusivity is larger. They also reported that as the equilibrium pressure increases, the solubility, oil-swelling factor, and molecular diffusivity of each heavy oil–propane system increase, whereas its viscosity is dramatically reduced. Even at low pressures, viscosity of the heavy oil–solvent system can be significantly reduced by propane dissolution but it is strongly dependent on the asphaltene content in the heavy oil.

Wu et al.[54] experimentally investigated the propane (C_3H_8) flooding efficiency and applicability for Lloydminster heavy oil reservoirs. Both pure propane and mixtures of methane and propane (40% CH_4 and 60% C_3H_8) were tested. Horizontal and vertical mode injections were both studied during pure propane flooding processes at three different operation pressures to investigate the gravity effect. At a horizontal model (Figure 2.2), the oil recovery efficiency was very low for all tested pressures, and the SOR was high. However, at the vertical mode (Figure 2.3) injection, much more incremental oil recovery was obtained under all operation pressures, and the SOR dramatically decreased.

These results indicate that gravity force is more important than viscous force for solvent gas flooding. Gravity segregation accelerates the cross-flow mixing between solvent gas and heavy oil to increase the overall macro sweep efficiency. Maintaining gravity stable is crucial for solvent gas flooding success. Mixture gas injection at a vertical model was used to test the effect of injection rate. The results indicated that the performance of lower injection rate is much better because the gravity segregation effect could accelerate the cross-flow mixing between solvent gas and heavy oil around the “wall” of the penetrated finger or in the un-swept area.

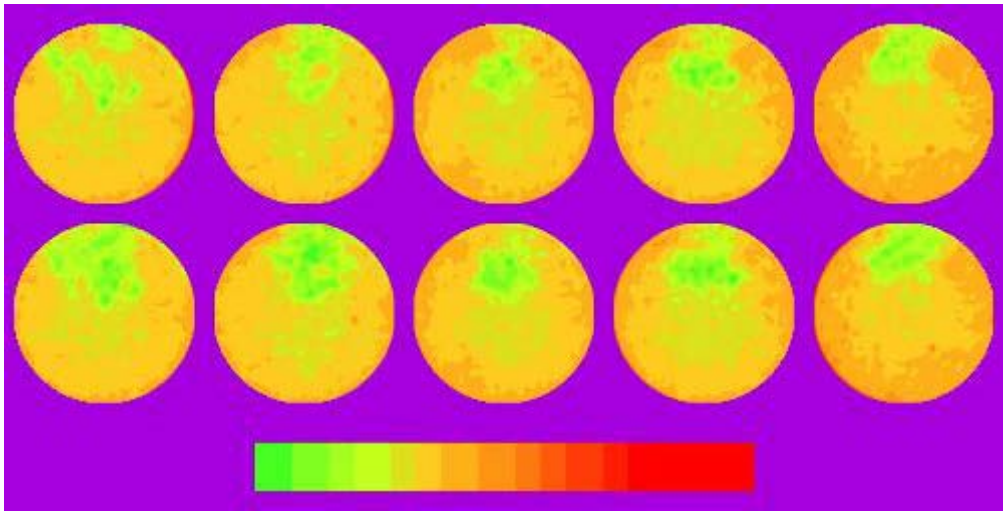

Figure 2.2 CT Images after horizontal flooding[54]

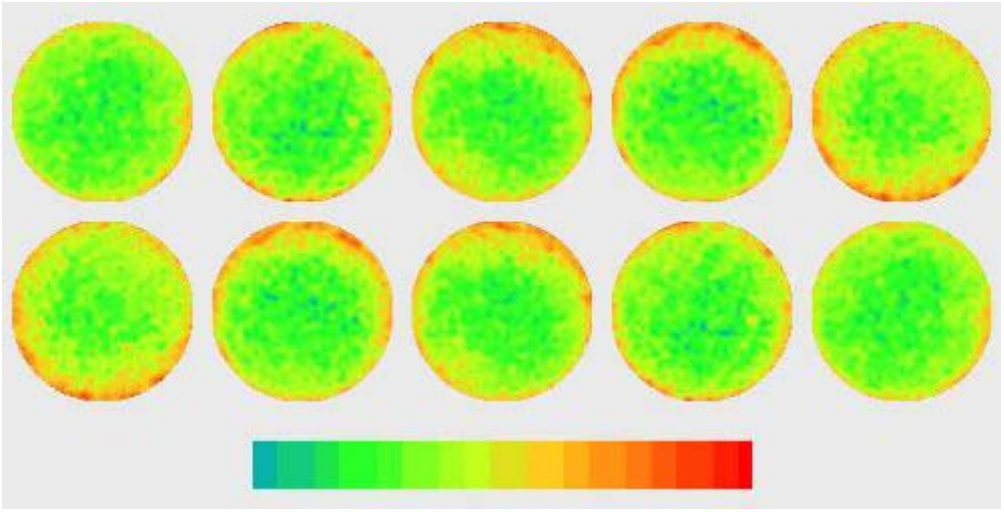

Figure 2.3 CT images after vertical flooding[54]

Yarranton et al.[55] studied the phase behaviour and physical properties of Athabasca bitumen, C_3H_8 and CO_2. He found a second dense asphaltene-rich phase at C_3H_8 contents above approximately 20 wt. % was formed in bitumen mixtures. CO_2 and bitumen mixtures also form a second CO_2-rich liquid phase at CO_2 contents above approximately 11 wt. %. Multiple liquid phases were only observed in a ternary mixture of 13.1 wt.% C_3H_8, 19.2 wt.% CO_2, and bitumen, but not showed for two other ternary mixtures: 13.5 wt.% C_3H_8 and 11.0 wt.% CO_2; 24 wt.% C_3H_8 and 6.2 wt.% CO_2. It is also observed that the mixed carbon dioxide and propane solvent is less likely to precipitate asphaltenes than pure C_3H_8. The author suggested that it is likely that the

CO_2 rich liquid phase will simply drain into the production well without extracting substantial oil components, thereby increasing the solvent consumption. Further studies should be addressed here for better understanding the behaviours of solvent based processes to recover heavy oil.

Luo and Gu[56] compared two situations of a heavy oil-propane system in the presence and absence of asphaltene precipitation. Totally five different saturation pressures in the range of P = 300–850 kPa and T = 20.8 ℃ were studied in a see-through windowed high-pressure saturation cell. The window was clean and transparent when P≤780 kPa. No observable asphaltene deposits occurred. Once the saturation pressure was increased to P = 850kPa (close to its vapour pressure), however, quick asphaltene precipitation was observed. The solubility and oil-swelling factor increase dramatically because of the asphaltene precipitation. In addition, de-asphalting makes the density, viscosity, asphaltene content, hydrogen and carbon aromaticities of the flashed-off heavy oil lower than those of the original heavy crude oil. These experimental results clearly show that asphaltene precipitation from the heavy oil tested in this study significantly alters its physicochemical properties and greatly improves its quality. The saturation time at 850kPa was also investigated. Figure 2.4 shows six sequential digital images of a small surface area (5.00mm×3.75mm) of the lower window. At t=0s and P=850kPa, the window was quickly covered with small asphaltene particles. Once the saturation pressure was suddenly reduced to P=780kPa, the precipitated asphaltene particles started to become liquid-like and mobile within t=30s. After t=1200s, all the precipitated asphaltene particles became liquid-like. On the other hand, if the saturation pressure was reduced several hours after the asphaltene precipitation, the precipitated asphaltenes were deposited as solid-like particles onto the visual window and did not become liquid-like afterwards (Figure 2.5).

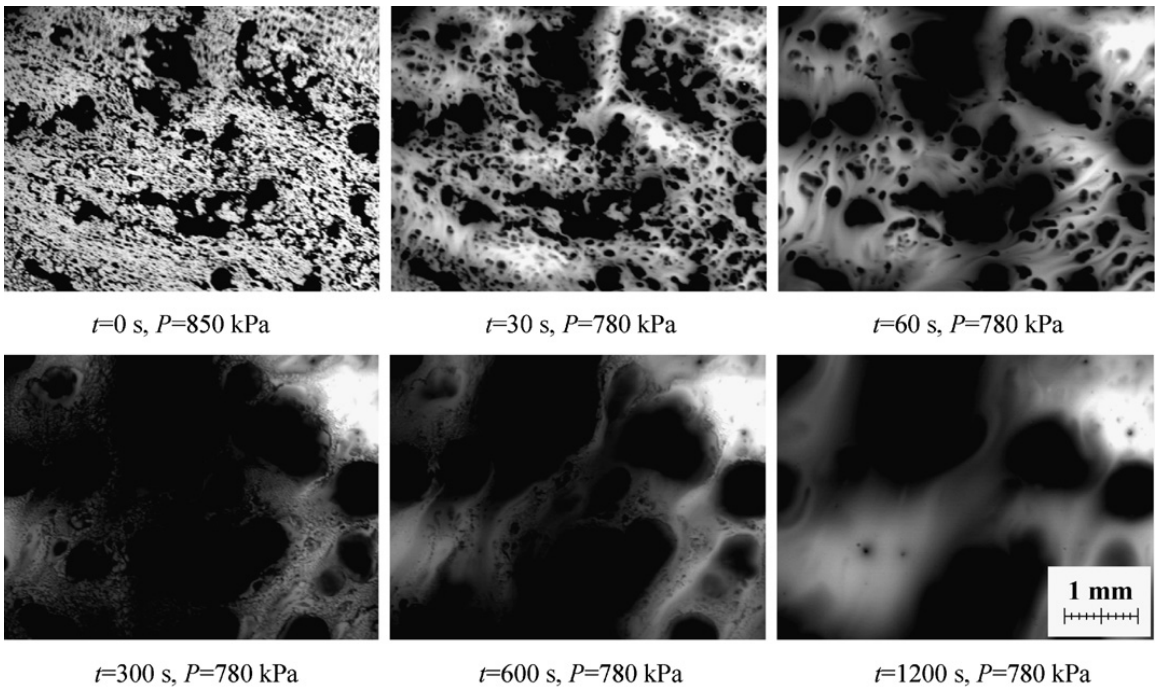

Figure 2.4 Six sequential digital images of asphaltene deposits[56]

On the acrylic window of the saturation cell at P = 850kPa and T = 20.8℃ and their state change from solid-like to liquid-like when the saturation pressure was suddenly reduced from P = 850kPa to P = 780kPa at T = 20.8 ℃.

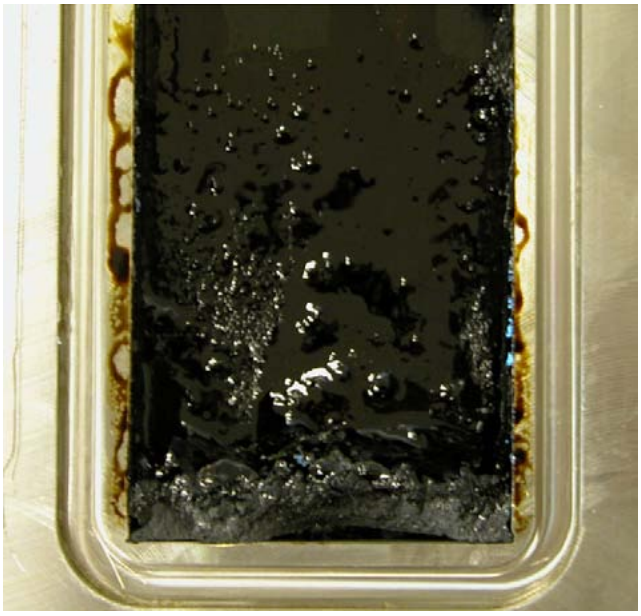

Figure 2.5 Asphaltenes and possible resins found[56]

At the bottom of saturation cell after the heavy oil–C_3H_8 system was equilibrated at P=850kPa and T=20.8 ℃.

Through a 3-phase-2D finely gridded compositional simulation model of considerably depleted saturated oil reservoir, Syed et al.[57] examined the feasibility of different gases (N_2, CO_2, or Enriched Gas) and Water-Alternating-Gas (WAG) to maintain pressure and optimize oil recovery.

N_2 injection can be used in deep light to medium oil reservoirs mainly containing C_1 to C_7 components. It is applicable in both the sandstone and carbonate reservoirs but need very high pressure to get miscible. The best pressure maintenance can be obtained by N_2 injection.

CO_2 injection is readily being adopted for the medium oil reservoirs, containing high percentage of C_5 to C_{12} components at significantly shallow depth. By getting miscible into the oil and causing to swell it, CO_2 makes the oil easier to flow to increase its relative oil permeability and hence reduces the amount of residual oil saturation (S_{or}). CO_2 injection may results up to 35% of more oil recovery of OOIP. It can be applicable in both sandstone and carbonate reservoirs. CO_2 injection provides the least pressure maintenance.

Water Alternating Gas (WAG) injection is a combination of water flooding and gas injection and it was found to be quite economical. Its first application was on North Pembina field in Alberta, Canada by Mobil in 1957. From the laboratory analysis it was calculated that simultaneous water/gas injection could have sweep efficiency up to 90% and only gas alone results in about 60%. But later alternate injection method of gas and water (WAG) was found more practical. WAG injection controls gas oil ration, thus, provides a stabilized oil production rate.

The hydrocarbon enriched gas injection mainly use the solvent composed of a mixture of hydrocarbon components (usually C_2 to C_5). The injected HC solvent is normally displaced with cheaper chase leaner or inert gas like Methane or Nitrogen. The Minimum Miscibility Pressure (MMP) plays the most major role to overcome the gravity over-ride problem during this process. Therefore, the solvent is to be injected at or above the MMP of the reservoir fluid. Once it becomes miscible then the sweep efficiency can be improved to achieve higher oil recovery. The enriched gas injection gives the highest recovery factor in the presence of thief zones.

Zheng et al.[58] presented the performance evaluation of CO_2 injection to heavy oil reservoirs for pressure maintenance purpose and effect examination of well configurations on pressure maintenance and oil recovery via two 3-D physical models (304mm×304mm×127mm). Model 1# is a five-spot well pattern-four vertical injectors and one vertical producer in center. Model 2# has a pattern of four vertical injectors with one horizontal producer lied down at the center of bottom layer (model 2#). For both models, after heavy oil saturated and aged, water flood was first conducted until no more oil produced out, then CO_2 injection was followed up, and blow down test was performed finally.

During water flooding, severe viscous fingering was observed in both models due to higher mobility ratio but the well configuration did not make obvious effect on oil recovery (14.9%-model 1# and 16.1%-model 2#).

With the CO_2 injection process, gas breakthrough occurs shortly after CO_2 injection due to the low resistance channel generated during water flooding and high mobility ratio between CO_2 and reservoir fluids (water and heavy oil). Such early CO_2 breakthrough indicates that viscous forces dominate the immiscible CO_2 injection and the effect of mass transfer between CO_2 and heavy oil was relatively small. It should be noticed that the oil recovery after CO_2 injection was quite different for both models (19.5%-model 1# and 32.2%-model 2#). That indicates that well configuration shows a considerable effect on pressure maintenance and oil recovery at CO_2 injection process in heavy oil reservoirs. Such a large difference is due to a better sweep efficiency resulting from the well configuration with a horizontal producer which controls a large area than that of a vertical well. The horizontal producer delayed early CO_2 production, leading to gas accumulating at the top of the model 2# and exerting an extra force to drive oil from the top to the bottom producer. Thus, higher oil recovery is achieved. From the comparison of top layer digital images for both models, the dark color of top layer for model 1# shows that much oil is still left there, which implies a bad sweep efficiency. On the contrary, light color of the top layer for model 2# indicates that the injected CO_2 accumulates at the top layer of the model, and then drive the oil to the bottom horizontal producer. The adverse effect of gas override in model 1# is alleviated by using the horizontal producer. It fully explains the advantage of well configuration with the horizontal producer that yields high oil recovery for model 2#.

Emadi et al.[59] also investigated the CO_2 injection process in a different manner to enhance heavy oil recovery via a series of micro-model and core flood experiments. The oil viscosity was 8670mPa.s at 50℃, API was 11.5, asphaltene content was 11.6%. There are totally two injection modes covered in this study. One is tertiary (post-water-flood) CO_2 injection (water flood-CO_2 injection-water flood), another is secondary (pre-water-flood) CO_2 injection (CO_2 injection-water flood). The micro-model (4cm×0.7cm) and sand pack (31.9cm×3.7cm×0.5cm) were both positioned vertically and the fluids were injected from the top ends. Therefore, the process of oil/brine displacement by CO_2 was gravity stable.

The tertiary CO_2 injection was conducted at the visible micro-model first (Figure 2.6). Oil is black, water is colorless and CO_2 is yellow in all images. The test started by injection of the heavy crude oil through micro-model which was initially fully saturated with DW water (Figure 2.6 a). The test then continued with an extended period of water flood (Figure 2.6 b), which was later followed, by an extended period of CO_2 injection to simulate tertiary injection of CO_2 (Figure 2.6 d). The test was concluded with a second period of water flood to displace the CO_2 diluted oil (Figure 2.6 e).

Some very important physical processes and mechanisms involved in tertiary injection of CO_2 at the pore scale were revealed via this test. First observation (Figure 2.6 c) was that the injected CO_2 flowed through oil-occupied pores rather than the water-occupied pores despite much higher viscosity of the crude oil compared to the water. In the high oil saturation area, a small oil bank formed and flowed ahead of the CO_2 front and hence, the advancement of the CO_2 front was associated with the movement of oil-water interfaces ahead of it (double displacement). In the low oil saturation area, a layer of oil covered the CO_2 front, which was indicative of a spreading system. At the image of CO_2 breakthrough (Figure 2.6 c), a thick oil layer around the CO_2 stream appears. This observation is quite important because without these oil spreading layers the injected CO_2 would flow through water occupied pores and the process of heavy oil recovery by tertiary CO_2 flood would be much less effective. Second observation (Figure 2.6 c and d) was the shielding effect of the water layers (red line) on the performance of the injected CO_2. This prevents the injected CO_2 directly from contacting the disconnected oil ganglia left after water flood period. Third observation (Figure 2.6 c and d) is that the injection of CO_2 resulted in

significant dilution of the crude oil. As can be seen, at the left of the red line, the colour of crude oil, which is directly in contact with CO_2, has changed from dark brown to brown. This is a good indication of the CO_2 dissolution in the crude oil and the subsequent dilution of the crude oil to a lighter mixture of the oil and CO_2. At the right of the red line, the colour of crude oil, which cannot directly contact with CO_2, also changes from light dark to dark brown. The dilution effect is not significant here. All these imply that secondary (pre-water-flood) CO_2 injection in which the oil phase is mainly connected and continuous would result in a more efficient process and hence, higher oil recovery. Although a small fraction of the diluted oil was produced through oil layers around the CO_2 stream during CO_2 injection period, a significant amount of this diluted oil was recovered during the second water flood due to the oil viscosity reduction brought about during the CO_2 injection period.

During the tertiary core test, as CO_2 injection progressed, brine was produced first until almost all the injected brine was displaced out, then an oil bank followed until CO_2 breakthrough, oil continuously produced at a low rate after the breakthrough. The oil bank strongly indicates the oil spreading behaviour at the oil-filled pores rather than water.

From the secondary CO_2 injection test results on visible micro-model (Figure 2.7), higher oil recovery after CO_2 injection was verified. Without the shielding effect by water injection at tertiary CO_2 injection, CO_2 directly contacts and dilutes oil at more area to enhance oil production.

At the secondary CO_2 injection on core test, oil was produced first. However, as the CO_2 injection continued, the effluent changed to foamy oil (mixture of CO_2 and oil). This foamy oil production was observed shortly before the CO_2 breakthrough. Similarly to the tertiary core test, oil production continued at low rates after the CO_2 breakthrough.

Based on Figure 2.8, the secondary CO_2 injection performs (29.1% OOIP) is somewhat better than the tertiary one (26% OOIP).

Finally the author summarized the mechanism for CO_2 injection process: direct displacement, fluid swelling (mainly oil), viscosity reduction and gravity drainage. Attention should be paid to

the CO_2 flow through the oil-occupied pore rather than water during tertiary CO_2 injection process.

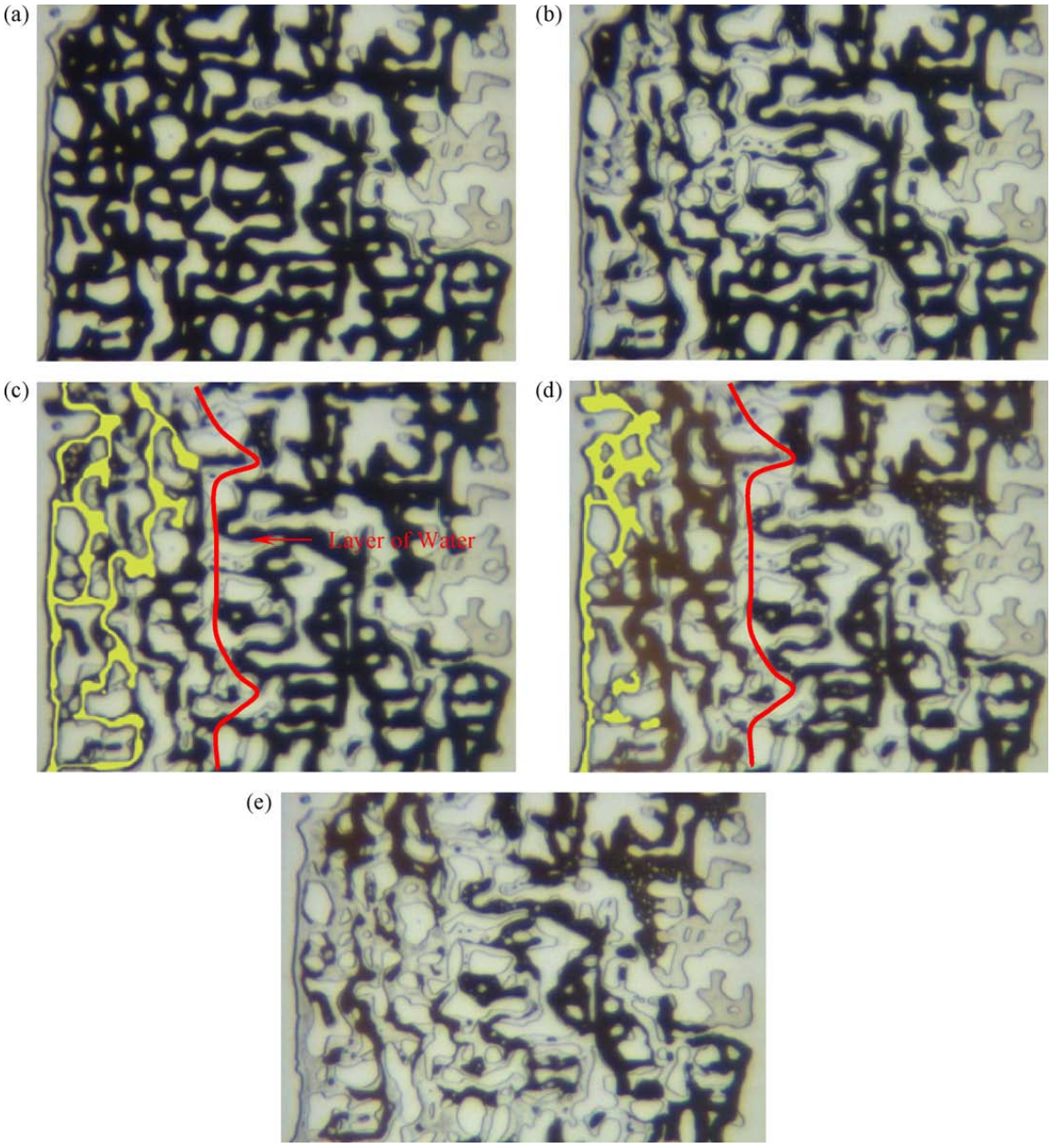

Figure 2.6 Oil recovery and fluid distribution in a magnified section of the micro-model at different stage of tertiary CO_2 injection test[59]

After (a) oil saturation (b) 1st waterflood (c) CO_2 breakthrough (d) CO_2 injection (e) 2nd waterflood

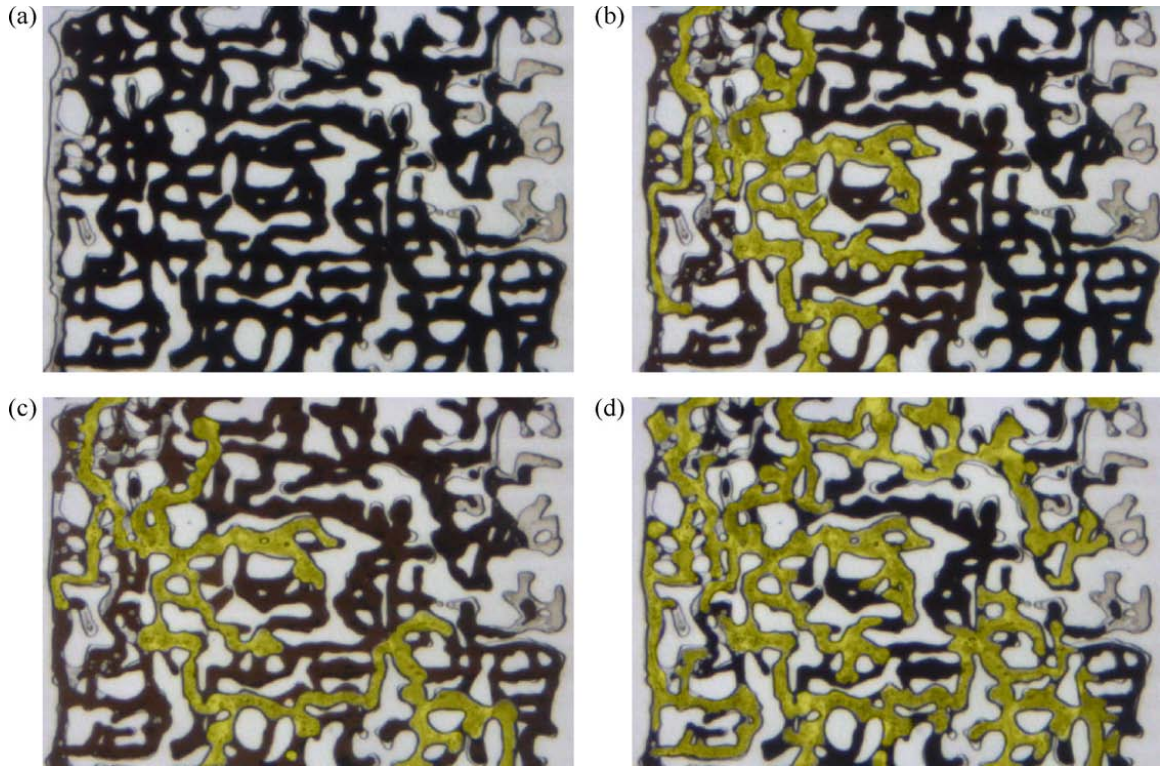

Figure 2.7 Oil recovery and fluid distribution in a magnified section of the micro-model at different stage of secondary CO_2 injection test[59]

After (a) oil flood, (b) CO_2 breakthrough, (c) 6 h of CO_2 injection, (d) 2 days of CO_2 injection

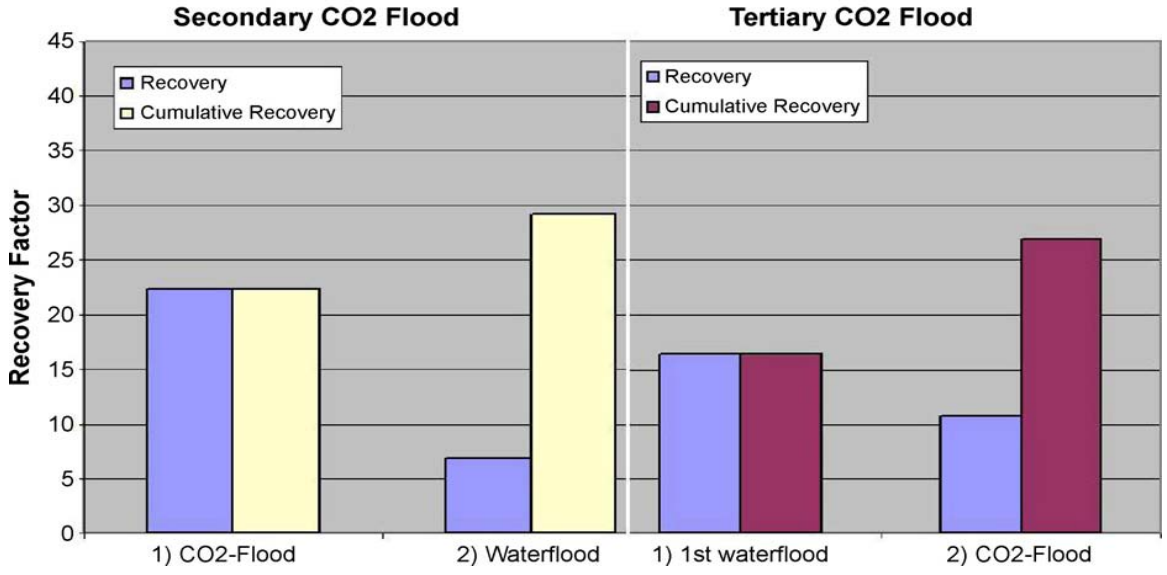

Figure 2.8 Comparison of the recovery factor at different stages of the 2nd and 3rd CO_2 injection experiments[59]

To sum up, solvent based post cold heavy oil production processes to recover heavy oil in thin zones are hampered by limited data and modeling capability for mixtures of heavy oils and solvents[55]. There are considerable data in the literature for mixtures of carbon dioxide and crude oils[9, 47, 49, 51, 57-59]. But less data was reported for mixtures of methane[52, 54] or propane[50, 53-56] with heavy oils. There are very little[55] data for mixtures of propane, carbon dioxide, and bitumen. This study intend to add methane recharging, propane and CO_2 huff-puff, and propane flooding experiments to contribute to further understanding of the post cold heavy oil production performance.

Chapter Three: Experiment Design

A series of gas recharging processes are designed in this study. Three cores will be used to perform these experiments. Two of them, a 18m in length glass beads packed core and a 18m in length sand packed core, were prepared for primary production by Goodarzi[29] and ready to be used for post-cold production. The third core is a 1.5m in length sand packed core, which was built for this thesis. The gas recharging processes were planned at different ways for the three cores. They are shown as follows:

Part 1-Two Long Cores:

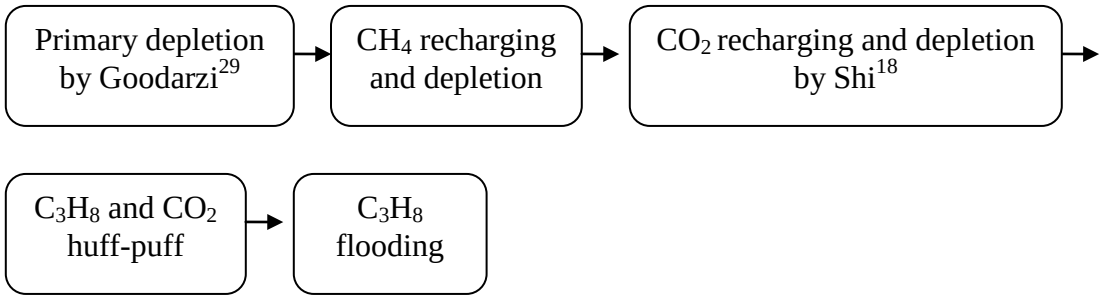

Part 2-1.5m Core:

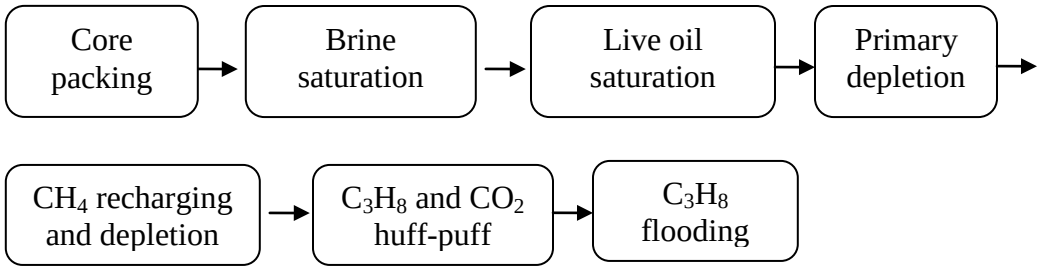

To better understand what happens at every process, CAT scanning was performed before and after each process.

Chapter Four: Experiments and Results: Part 1-Two 18m Cores

As we mentioned above, primary depletion tests have been conducted by Goodarzi[29] at these two 18m in length long cores, to help the understanding of what will happen later, these core conditions must be clarified before further study.

4.1 Core Situations after Primary Depletion

4.1.1 Core Preparation

As shown in Figure 4.1[29], the long core is set up by using 6 dural aluminum tubes of 3.05m in length connected together at the ends with welded tees. The dural aluminum is a high performance material that can withstand high pressures and is x-ray transparent. At the end of each tube is a pressure transducer that is plumbed into the welded tees. This provides pressure data at 12 locations along the experiment. The tubes have a 1.9 cm (0.75 inch) diameter and do not have applied overburden. Also, 2 heater and 5 thermocouples are placed along the core and wrapped to maintain and monitor temperature. The pressure and temperature variations are logged automatically during the experiment.

The differences for the two long cores are not only the packing material, but also the different locations of P_{12} pressure transducer (Figure 4.2 and 4.3). P_{12} is at the core outlet end for glass beads packed long core, but in the middle of P_{11} and core outlet end for sand packed long core.

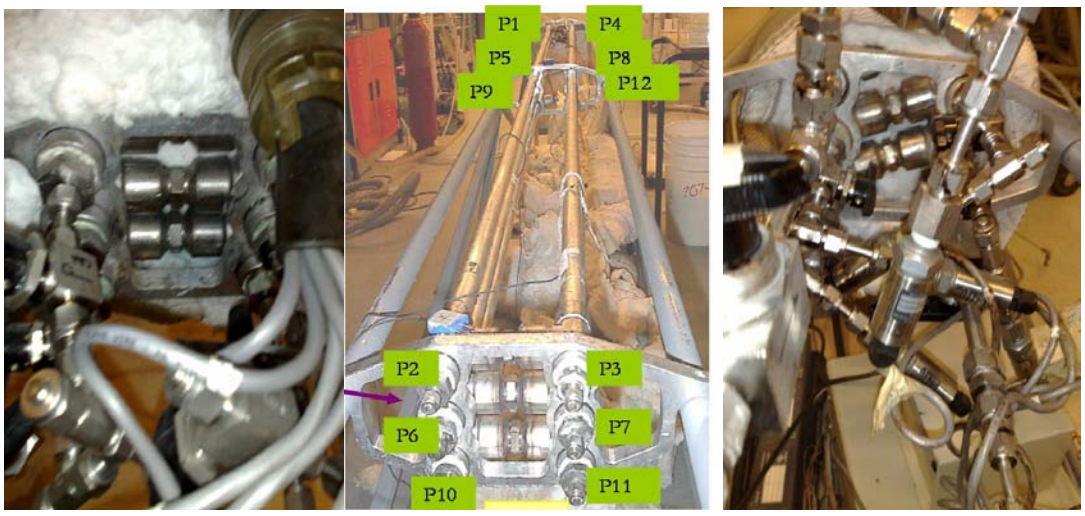

Figure 4.1 Photos of 18m in length core (Goodarzi[29])

Figure 4.2 Glass beads packed core (Goodarzi[29])

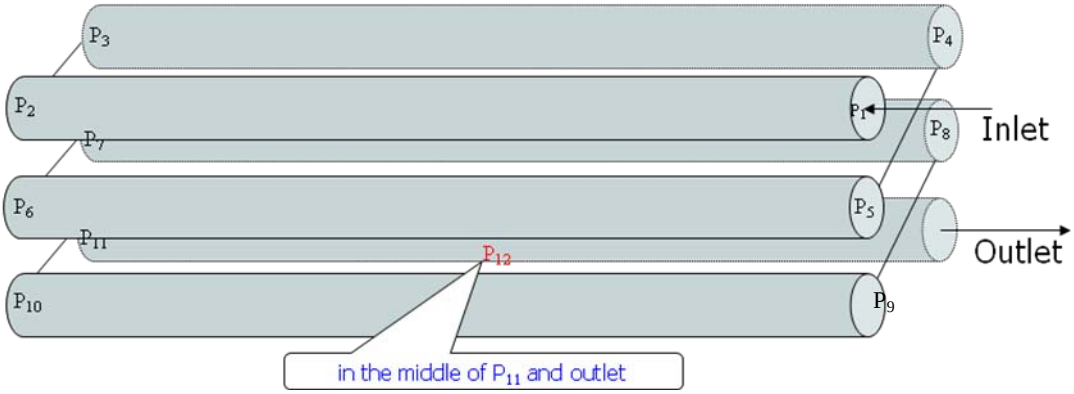

Figure 4.3 Sand packed core (Goodarzi[29])

4.1.2 Property Summary

Table 4.1[29] displays the dimensions of the core holder, the sand and the fluid properties of glass beads and sand packed 18m in length cores. It should be noted that the both core lengths are around 18m which are much bigger than the cores normally used in other studies[16, 20-28]. In addition, permeability difference between the two cores should be noticed as well; 11.8D and 1.9D for the glass beads and sand packed cores, respectively.

Table 4.1 Core and fluid properties (Goodarzi[29])

Type	Properties		
Core	Name	Glass beads	Sand
	Length	18.2m	18.55m
	Cross-sectional area	2.85cm^2	2.85cm^2
	Absolute permeability	11.81darcy	1.92darcy
	Pore volume	2099ml	2607ml
	Porosity	37.8%	36.4%
	Connate water saturation	7.6 %	9.21%
Fluid	Dead oil viscosity at 23℃	10711mPa.s	10695mPa.s
	Dead oil density at 23 ℃	982 kg/m^3	982 kg/m^3
	GOR at 23℃	14 m^3/m^3	14 m^3/m^3
	Live oil viscosity at 23℃	5688mPa.s	4837mPa.s
	Live oil density at 23 ℃	971kg/m^3	975kg/m^3
	Bubble point pressure	4102kPa	4647kPa

4.1.3 Core Status before Further Study

The recovery from primary production in heavy oil reservoirs may be as high as 20%[60, 61], but is usually lower. Therefore, there is still a significant amount of oil-in-place in the reservoir after primary depletion. Table 4.2 shows the results of Goodarzi[29]. There were 1939.48ml and 2366.9ml live oil saturated into these two long cores. After primary depletion, 22.2% and 10.2% oil was recovered. 77.8% and 89.8% oil were left in the glass beads and sand packed cores separately for further studies.

Table 4.2 Primary depletion results (Goodarzi[29])

Different stage	During Core Preparation	After Primary Depletion	
Properties	Live Oil Injected	Oil Recovery	Oil Left
Glass Beads Packed	1939.48ml	22.2%	77.8%
Sand Packed	2366.90ml	10.2%	89.8%

The reservoirs have been stripped of their natural energy after primary depletion. In order to recover additional oil, the reservoir energy has to be rebuilt up and oil has to be displaced to

production wells. Gas recharging technique as one of the important post-cold production methods is normally used to the heavy oil reservoirs which is not suitable for thermal recovery methods. CO_2 and hydrocarbon gas injection are the most widely applied processes.

4.2 Methane Recharging, Soaking and Depletion Processes

After primary production was conducted by Goodarzi, both long cores were shut in at ambient conditions and stayed alone for approximately one year. The oil recoveries during primary depletion process are 22.2% and 10.2% for glass beads and sand packed cores respectively. These are the starting points for the following gas recharging processes applied at both long cores. The first studied post-cold production method is methane recharging and depletion processes.

4.2.1 Demonstration and Methodology

The injection and production methodologies of this process are the same for both cores and demonstrated at Figure 4.4. Part A is for injection, part B is the long core and part C is for production.

Methane was continuously injected from the slightly opened methane cylinder at 6895kPa with the simultaneous shut-in of the producer well until the core inner pressures all reached around 6550kPa. This is similar to the process of methane pressure-cycling (MPC) which has been reported by Dong et al.[52] Instead of injecting water to build the pressure up, this study kept high pressure methane injection until the whole core pressures reach up to 6550kPa. The injection well was also shut in for a methane soak period to occur which is the same as MPC. When the core inner pressures were all stable, the core was ready for production. A back pressure regulator (BPR), pressure regulator and mass flow controller (MFC) were used to control the depletion rate of BPR same as primary production process, 2.34kPa/min. The gas-oil collection unit was used for monitoring the production fluid. Leak and DAS tests were performed before production. The gas release pressure was set at 34.47kPa, when one of the gas collection bottles reached this pressure, its bottom valve would be shut in and top valve would be opened to release gas automatically. Simultaneously, the BPR pressure was set just above the core inner pressure. The core outlet valve was opened for production. Pressure and temperature variations along the core

during the whole process, as well as oil and gas production data during production were all collected by DAS for further investigation.

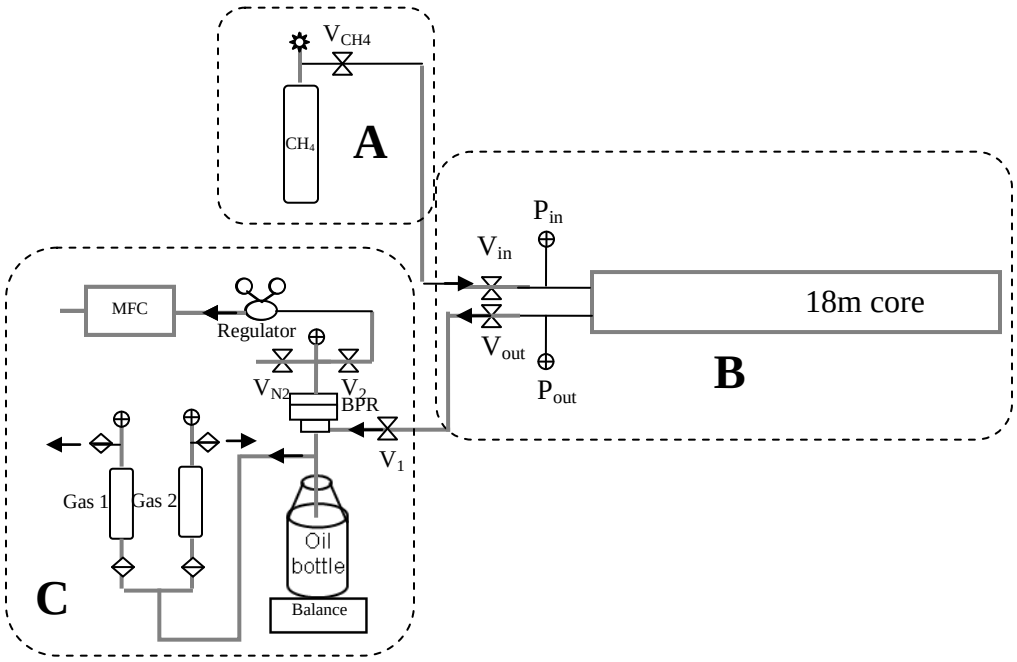

Figure 4.4 CH_4 recharging and depletion process at two 18m cores

4.2.2 Experiment Results

4.2.2.1 Injection and Soaking

4.2.2.1.1 Glass Beads Packed Core

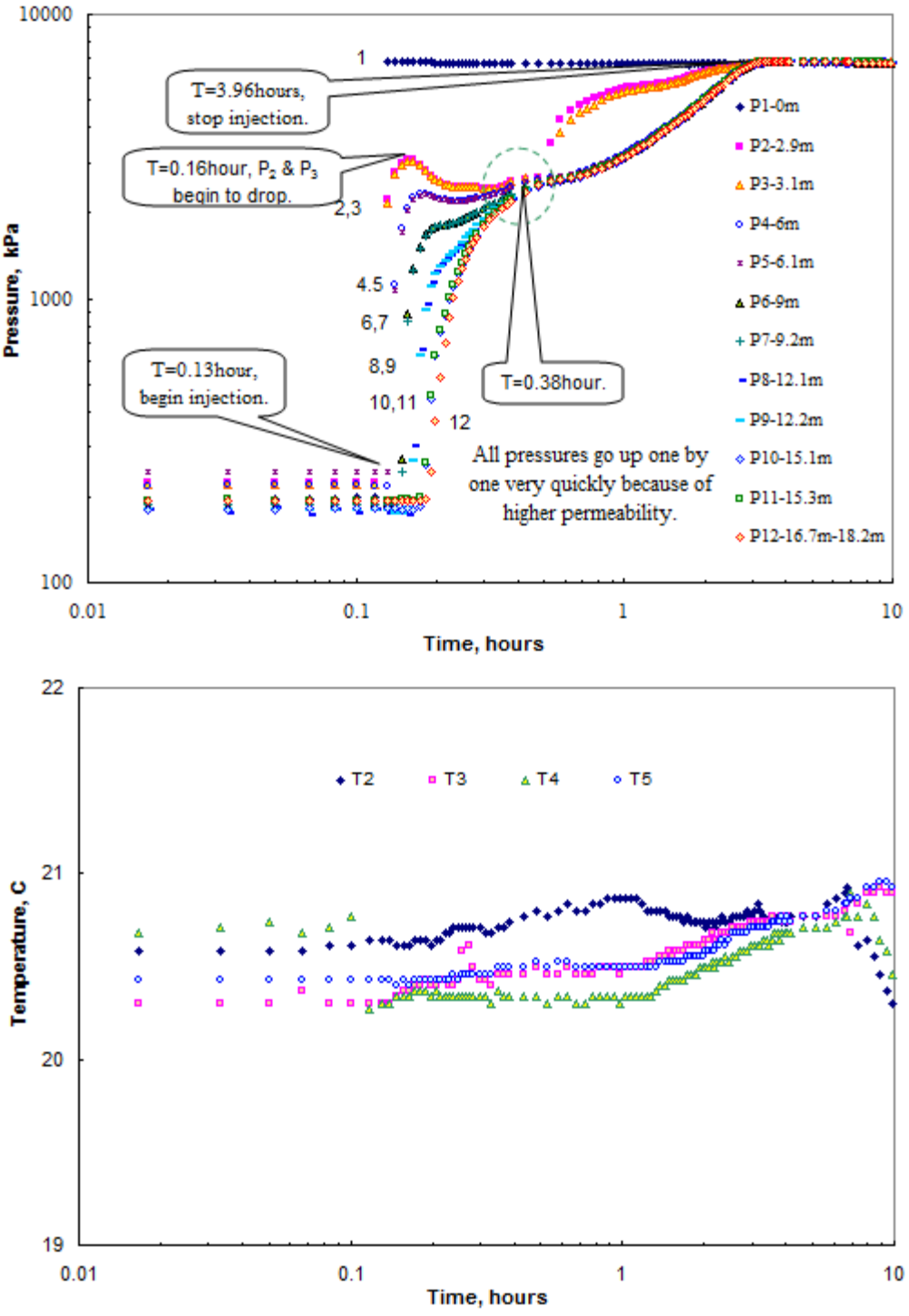

Figure 4.5 Early stages of CH_4 recharging process-glass beads

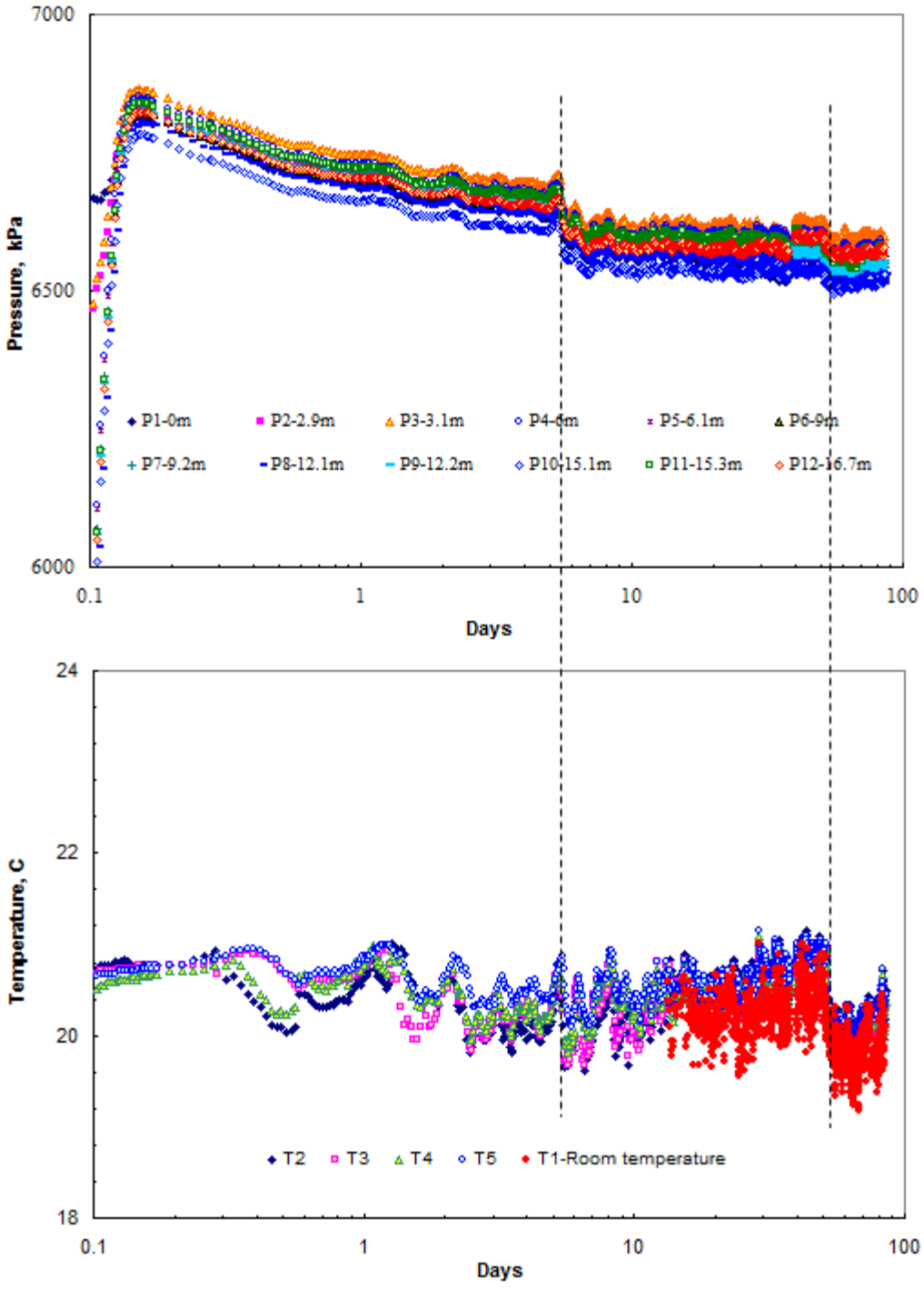

Figure 4.6 Soaking period of CH_4 recharging process-glass beads

Figures 4.5 shows the core pressure and temperature variations with time on early-stage of methane recharging process for glass beads packed core. All core inner pressures go up one by

one very quickly from P_1 to P_{12} (inlet to outlet) with the methane injection due to a higher core permeability. It only takes several hours for the whole core to reach pressure equilibrium. An abnormal phenomenon occurs here. At the very beginning, 0.16 hour, core pressures of P_2 and P_3 start to drop, then P_4 and P_5 follow the decrease tendency one after another, others delay their rise-up speed. At 0.38 hour, all pressures are closer to each other except P_1. After that, pressures of P_2 and P_3 begin increase quickly, but others shape the same way and rise up slowly. The possible reason for this phenomenon is the glass beads or oil migrations. At the very beginning of injection, due to the huge abrupt pressure difference, around 6550kPa, between the inlet and inner core, a sudden drive force can move and pack some glass beads or fluid to somewhere between P_1 and P_2. The following injection gas meets a resistance and has to accumulate more energy to go through. The packed stuffs are broken through later on and repack between P_3 and P_4 after 0.38 hour which slows down the pressure transmission rate after that position. Thus, curves of P_5-P_{12} show the same shapes after that. The temperature graph shows that the core temperatures were relatively stable but slightly varied during methane recharging process.

Figure 4.6 shows the core pressure and temperature variations with time during methane soaking process for glass beads packed core. All pressures decreased gradually until stable which showed that some of the gas methane dissolved into the residual oil to expand its volume. This phenomenon was also observed by Dong et al.[52] at MPC process. There are total two pressure sharp falls during soaking period which were caused by temperature decreases.

Figure 4.7 shows the core pressure gradient variations with time during injection and soaking processes. The curves of P_1-P_2 and P_3-P_4 shape themselves like "M"; these confirm the inference of pack-through-repack process by glass beads or fluid. No pressure gradients are built up from P_5 to core outlet.

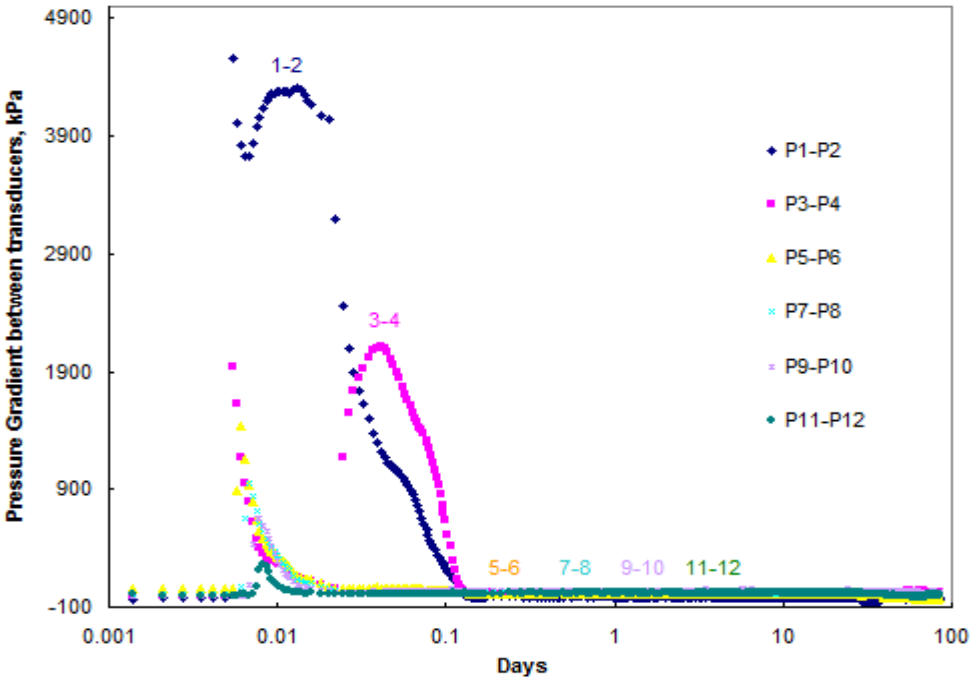

Figure 4.7 Pressure gradients of CH_4 recharging process-glass beads

4.2.2.1.2 Sand Packed Core

Figure 4.8 shows the core pressure and temperature variations with time on the early-stage of methane recharging process for sand packed core. Core pressures build up gradually from P_1 to P_{12}. Due to low permeability, it takes a longer time, 1.2 days, for the whole core to reach pressure equilibrium. At the very beginning of injection, there is also a migration and pack process by sand particle or oil between P_3 and P_4, but the pack was broken through very quickly by the following methane injection. After half day injection, the migration occurred between P_5 and P_6 again. Attention should also be paid to the two group pressure curves from P_1 to P_3 and from P_8 to P_{12} for shaping in the same ways. This infers that there probably are two free gas zones near both end of the core. One is between the core inlet to P_3 (3.2m), another is between 12.8m to core outlet. The temperature graph shows relatively stable curves.

Figure 4.9 shows the core pressure and temperature variations with time during soaking process for sand packed core. All pressures decreased gradually until stable. Some of the gas methane dissolved into the residual oil the same as that of the glass beads packed core and MPC process which reported by Dong et al.[52]. The pressure fluctuations after 70 days all caused by

temperature variations (the two temperature control boxes were shut down accidentally and turned on after approximate 15 days).

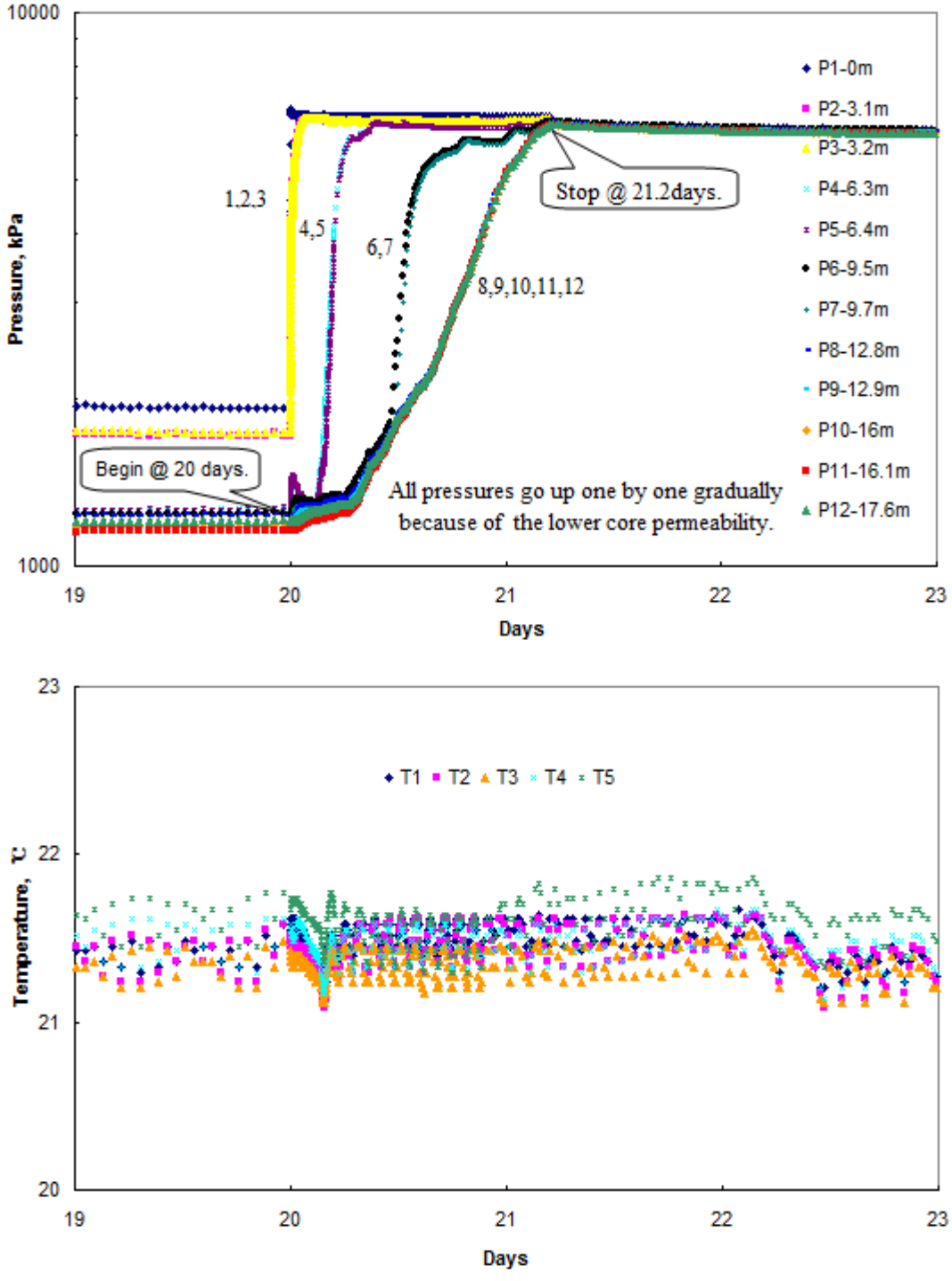

Figure 4.8 Early stage of CH_4 recharging process-sand packed

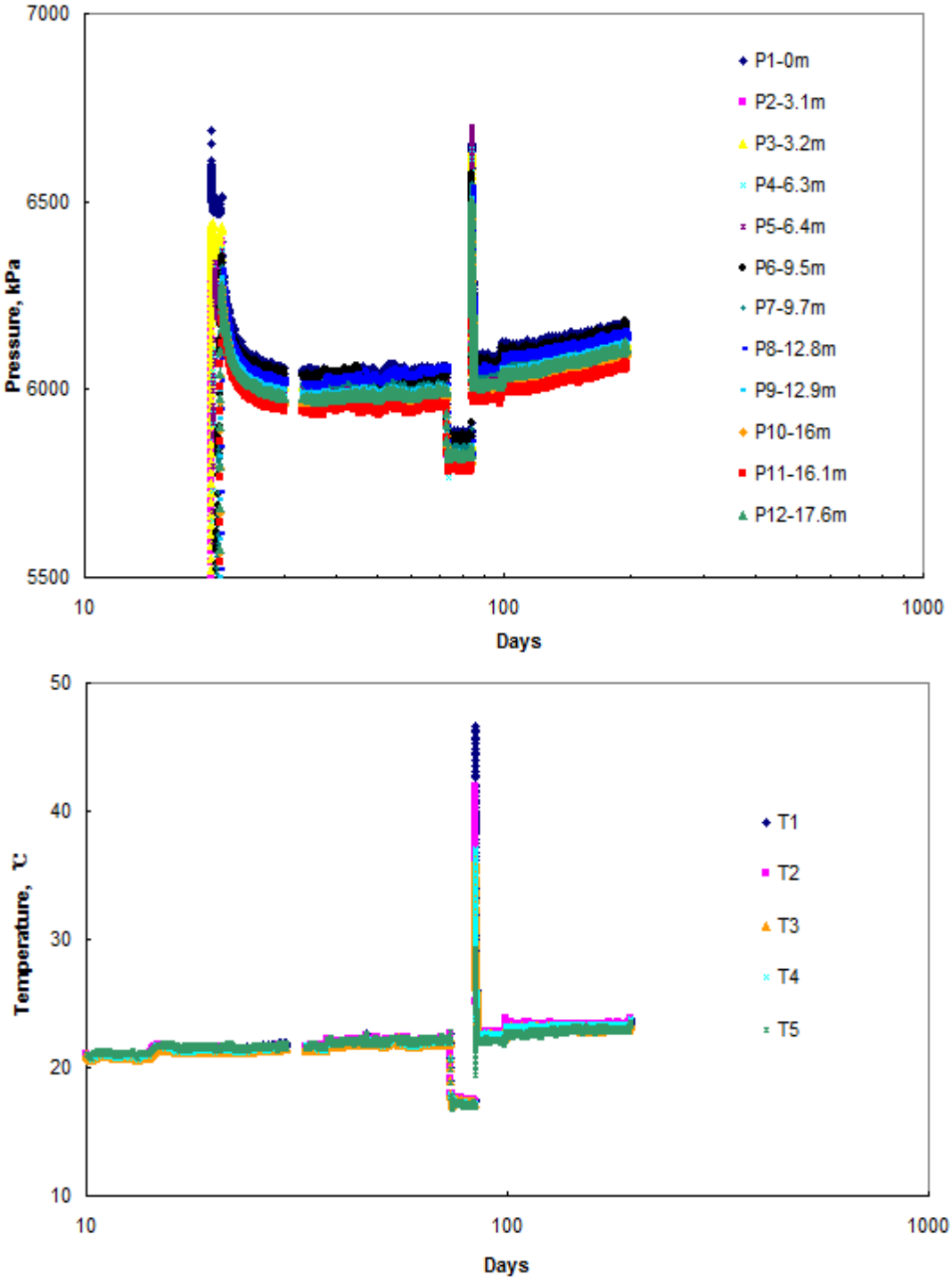

Figure 4.9 Soaking period of CH_4 recharging process-sand packed

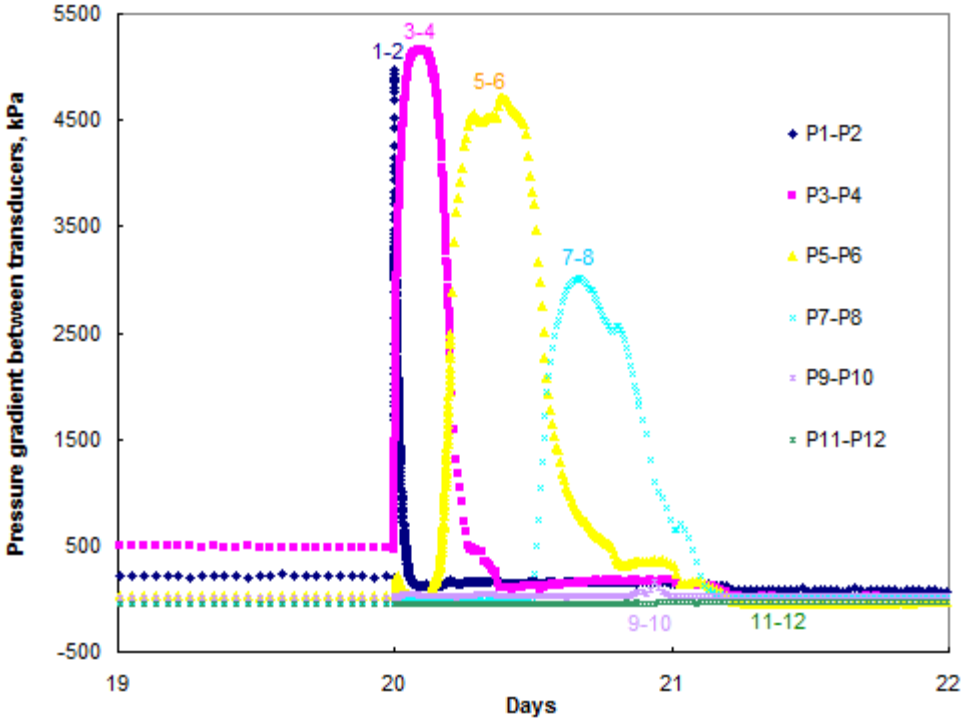

Figure 4.10 Pressure gradients of CH_4 recharging process-sand packed

Figure 4.10 shows the core pressure gradient variations with time during injection and soaking. The curve of P_1-P_2 shows a sharp peak, this confirms the first free gas zone between core inlet and P_3. A tiny peak shows up at the curve of P_9-P_{10}, no peak appears at the curve of P_{11}-P_{12}, these confirm the second free gas zone between P_8 to core outlet.

To summarize, core pressures and pressure gradients increase from inlet to outlet gradually for both cores. Pressure build up speed is affected by the core permeability. The faster the speed is, the higher the core permeability is. Phenomenon of particle or fluid movements is observed (Gas path is blocked first and reopened later).

4.2.2.2 Production

4.2.2.2.1 Glass Beads Packed Core

Figure 4.11 shows pressure variations with time during the depletion process for glass beads packed core.

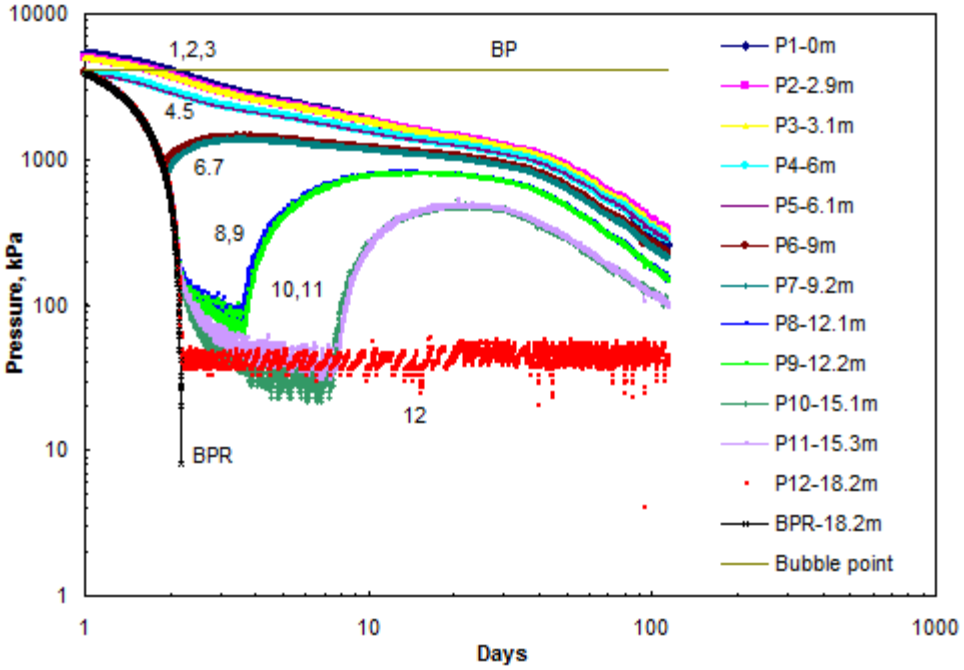

Figure 4.11 Pressure graphs of CH_4 depletion process-glass beads

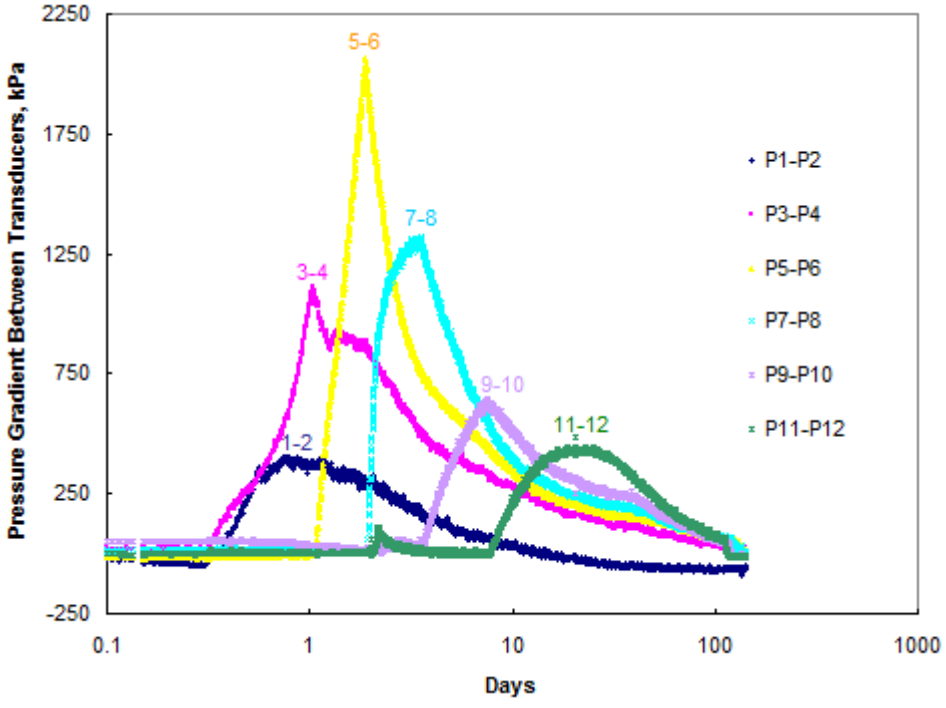

Figure 4.12 Pressure gradients of CH_4 depletion process-glass beads

First, the core outlet pressure P_{12} decreases promptly following the BPR declining tendency. After 2.2 days production, P_{12} drops to about 41.4kPa and keeps steady until the end. All the other pressures along the core follow the decline tendency one by one from the production end upstream, but the closer to the outlet, the bigger and the faster the pressure drop is.

Second, attention should be paid to the 3 pair of pressure curves (6 and 7, 8 and 9, 10 and 11), they all have two trend changes but they appear at different times. The first point, pressure tendency turns from down to up, the second point is the one where pressure decreasing tendency speeds up. The reasons for these are that two main physical processes occurred in the core during this depletion period. One is pressure drop with the production, another is the solution gas, which is dissolved into the oil during CH_4 recharging process, tends to come out of the oil when the core inner pressure drops under bubble point pressure. These two processes balance themselves with time and affect the curve shape. Between the first and second trends change points, the second physical process is dominant. On the other hand, before the first and after the second trend change point, the first physical process is dominant. Further, core properties, depletion rate and pressure transmission speed also affect the process. Therefore, all these factors together decide if the two trend change points appear or when they appear.

Figure 4.12 shows that the pressure gradients build up from inlet to outlet one by one during methane depletion process for glass beads packed core, foamy oil flow could happen here due to the big pressure gradients. Although the BPR depletion rate is constant during the whole depletion process, the pressure depletion rates throughout the core are quite different. The closer to the core inlet the position is, the lower the depletion rate is. An attention should be given to the peak show-up sequence of the 6 pressure gradient curves. The closer to the inlet the position is, the earlier the peak shows up. This infers the lower depletion rate is helpful for solution gas driver to form foamy oil flow. What is the best depletion rate to achieve the highest oil recovery? The relationship of depletion rate and the effect of solution gas drive should be further studied. The higher pressure gradient build-ups are in the middle of the core.

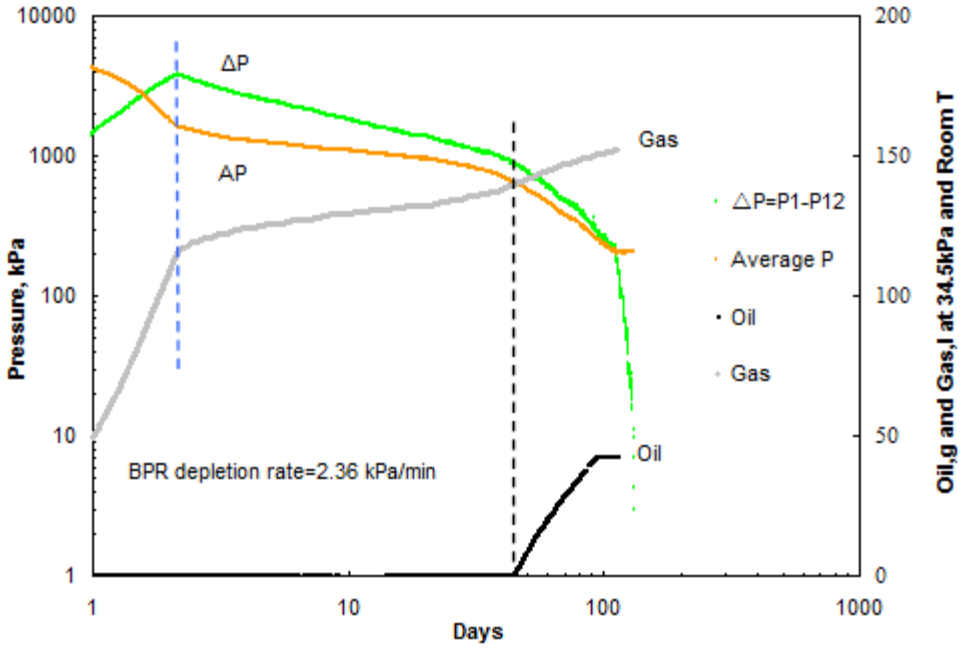

Figure 4.13 Pressure and production graphs of CH_4 depletion process-glass beads

Figure 4.13 is the pressure and production variations during methane depletion process for glass beads packed core. To better understand the relationship between pressure curves and production curves, average pressure and differential pressure are used instead of 12 pressure curves. Both two pressure curves have 2 trend change points during the whole process too.

First trend change point is at the dashed blue line. Gas production curve and both pressure curves happen to have a trend change point at the same time. This implies that before that point, produced gas is mainly free gas; after that point, a large quantity of gas bubbles form, swell the oil, block some gas pathways, thus slow down the gas production dramatically.

Second trend change point is at the dashed black line. Oil production occurs here too, and at this point, gas production also increases somewhat with oil production. That hints gas was produced together with oil. One thing should be paid attention to is that it takes more than 40 days for oil production to occur.

Based on the relationship of the two trend change points between pressures and production curves in Figure 4.13, the mechanism of this methane depletion process is foamy oil flow under solution gas drive, the same as primary production.

The oil curve is based on automatically balance reading, which drifts away a lot from the real weight during a long period of time. Therefore, the real oil production should be recalculated below.

The produced liquid (oil and water mixture) was collected in the oil collection bottle. Its weight was calculated by the weight difference before and after collection. The water in the produced fluid was measured by NMR technology. The oil produced equals the fluid weight minus the water weight. After recalculation, there was 97.87g, 5.14% OOIP oil recovered by this process totally.

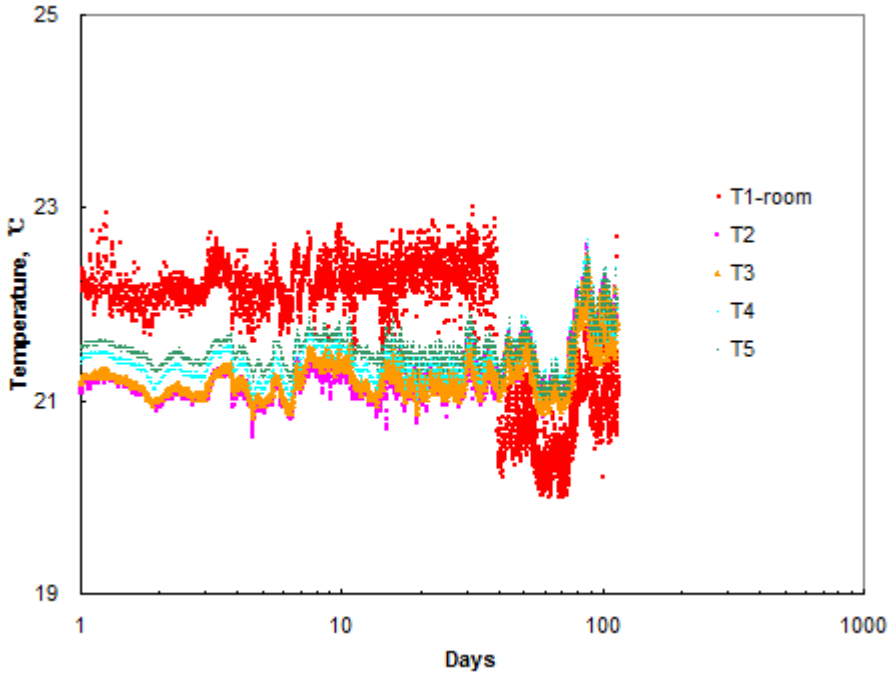

Figure 4.14 Temperature graphs of CH_4 depletion process-glass beads

Figure 4.14 shows that core temperatures were relative stable except room temperature T_1.

4.2.2.2.2 Sand Packed Core

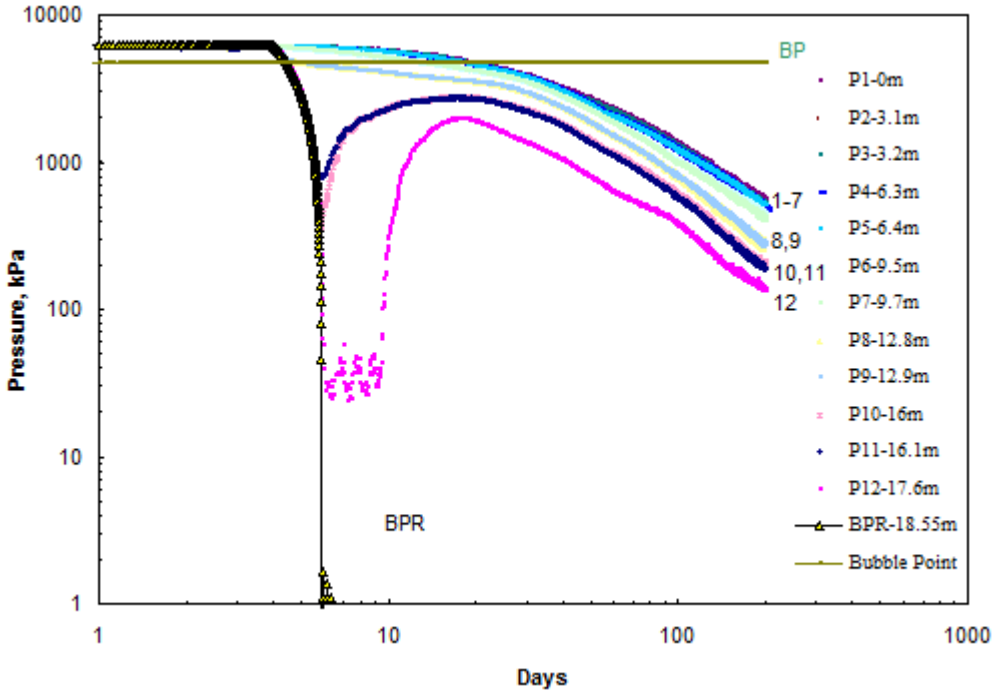

Figure 4.15 Pressure graphs of CH_4 depletion process-sand packed

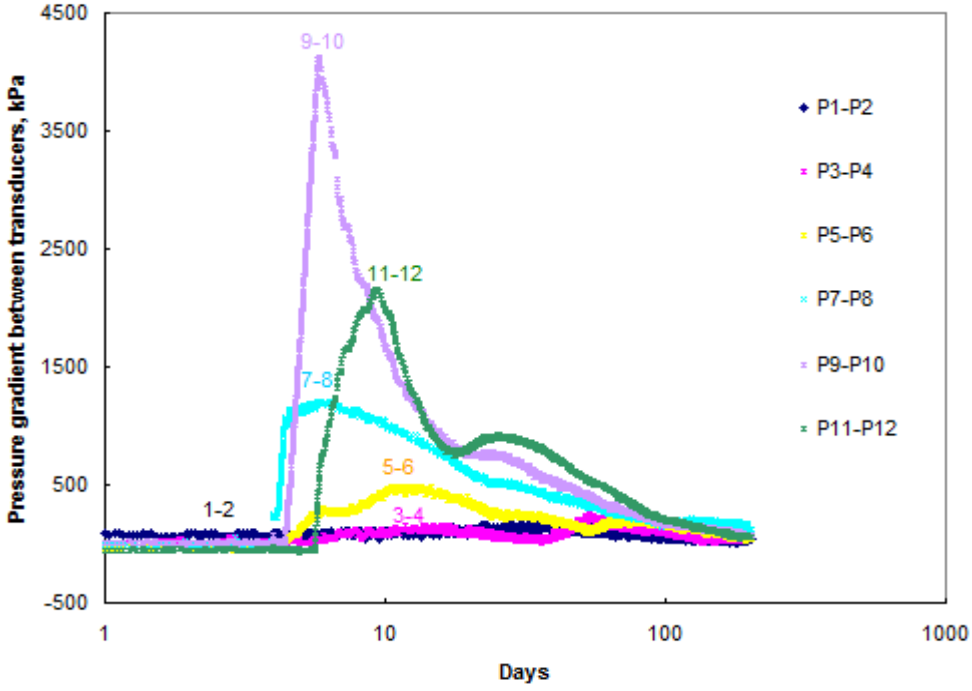

Figure 4.16 Pressure gradients of CH_4 depletion process-sand packed

Figure 4.15 is the pressure variations with time during depletion process for sand packed core. All curves show almost the same trend as the glass beads packed core except for the P_{12} pressure curve due to the location of P_{12} transducer is in the middle of the P_{11} transducer and core outlet which is not the same as glass beads packed core at the core outlet. Two trend change points also show up at several pressure curves from P_{10} to P_{12}. These infer that solution gas drive plays an important role in the methane depletion process.

Figure 4.16 shows that pressure gradients are built up irregularly which is different from glass beads packed core. No pressure gradient is built up from inlet P_1 to P_2. The heights and locations of other peaks vary a lot. The higher peaks are closer to core outlet (The length from P_{11} to P_{12} is only half distance of others-1.5m, therefore its pressure gradient build-up is not low). Foamy oil flow could happen here due to the higher pressure gradients. The lower core permeability affects the depletion process obviously. Its relationship should be further studied.

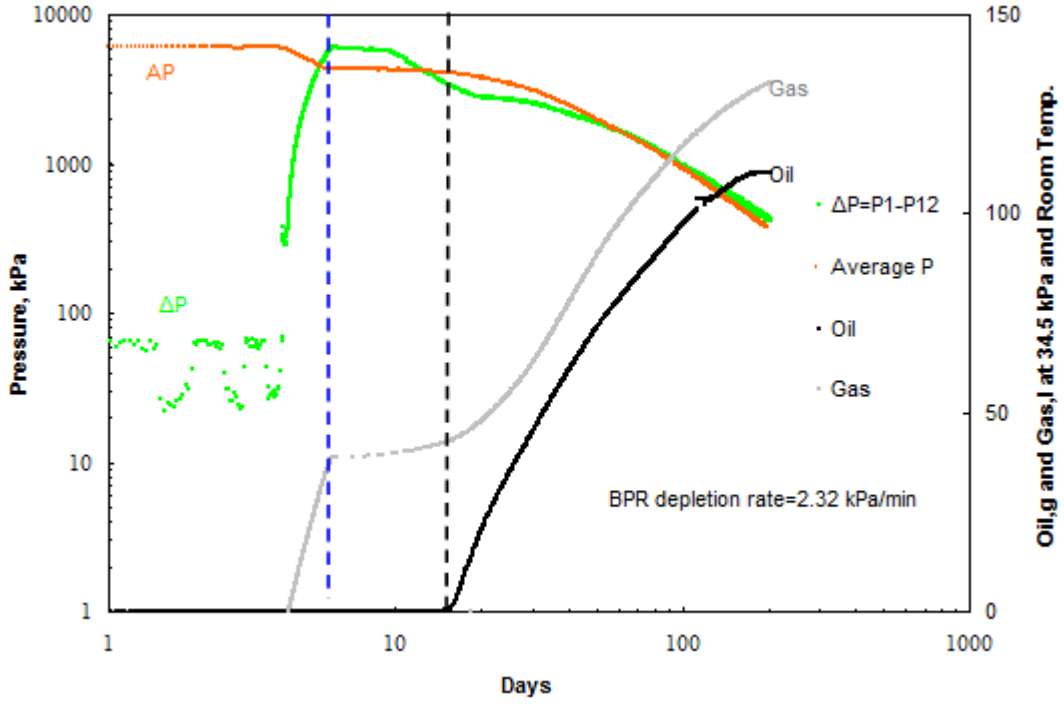

Figure 4.17 Pressure and production graphs of CH_4 depletion process-sand packed

Figure 4.17 is the pressure and production variations with time. It shows the same trend chart as glass beads packed core, but it only took 10 days for oil production to occur. The oil and gas

production periods after the second trend point last longer than the glass bead packed core. More details will be discussed later to compare with the glass beads packed core.

There was 110.33g, 4.75% OOIP oil recovered by this process totally.

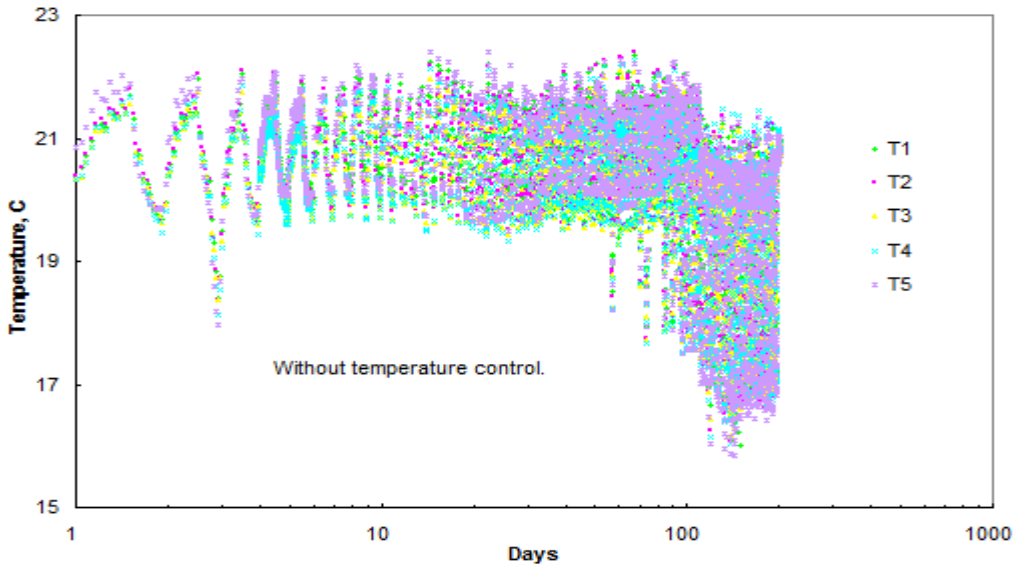

Figure 4.18 Temperature graph of CH_4 depletion process-sand packed

Figure 4.18 is the temperature variations with time. All the temperatures fluctuated regularly because the two heaters were not turned on during the whole production period by accident. All temperatures were affected by room temperature directly.

4.2.2.2.3 Comparison

To better compare depletion processes of these two long cores, four parts need to be taken into consideration. First, pressures dropped slowly in the lower permeability sand packed core. Second, in the glass beads packed core, the majority of gas is produced before the first trend change point due to high permeability. However, in the sand packed core, the majority of gas is produced after the second tendency change point. This indicates that gas bubbles were easily trapped at the low permeability core and produced with the oil together. Third, the slope of gas production curve between these two trend change point is higher in glass beads packed core than it in the sand packed core. This implied that gas paths were dramatically blocked during the formative period of foamy oil in sand packed core. Fourth, oil production in the sand packed core

occurred earlier and lasted longer than it in the glass beads packed core. This is probably because in the low permeability core, the swelled oil easily blocked more gas path quickly, thus, it forced the oil-gas dispersion to be driven out earlier by the following drive energy.

After methane depletion process, an additional 5.14% and 4.75% OOIP were recovered from glass beads and sand packed core respectively at a higher methane injection rate of 6550kPa. These further verified the conclusion of Dong et al.[52] at MPC process: "At a higher gas injection rate, the greater amount of gas was absorbed and the higher rates of oil production was observed."

In both of the 18m in long core systems, as in the primary depletion process, gas is not generated at the same time along the core. This demonstrates that nucleation is a localized phenomenon. However, higher permeability allows for rapid transmission of the pressure and nucleation occurs along the length quicker than in lower permeability sands[29].

To sum up, the principle of the methane recharging process is to make substantial amounts of gas methane to contact with and restore into residual oil in the porous media. The principle of its depletion process is a further primary production during which the solution gas is released from the oil and gas channels are left everywhere in the reservoir. This created paths are for the following recharged gas to finger into the remaining oil in porous media. All these match the mechanisms of MPC process[52].

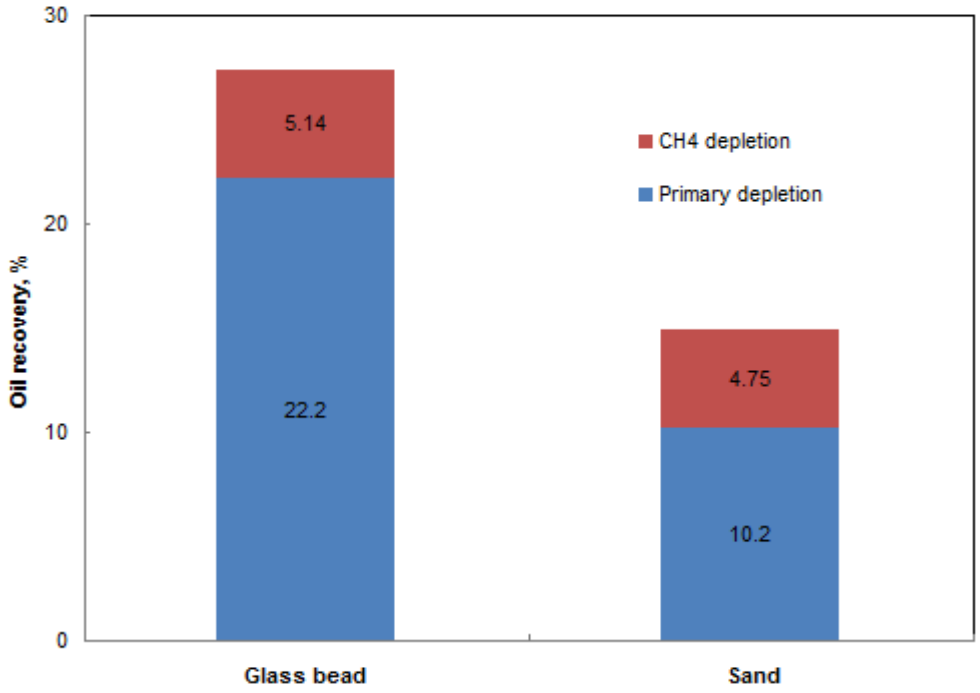

Figure 4.19 Oil recoveries after CH_4 depletion process

4.3 Core Situation after CO_2 Recharging and Depletion Process

After methane depletion, Shi[18] ran a carbon dioxide recharging and depletion test on these two long cores, 2.7% and 4.2% oil were recovered from glass beads and sand packed core separately as illustrated in Figure 4.20.

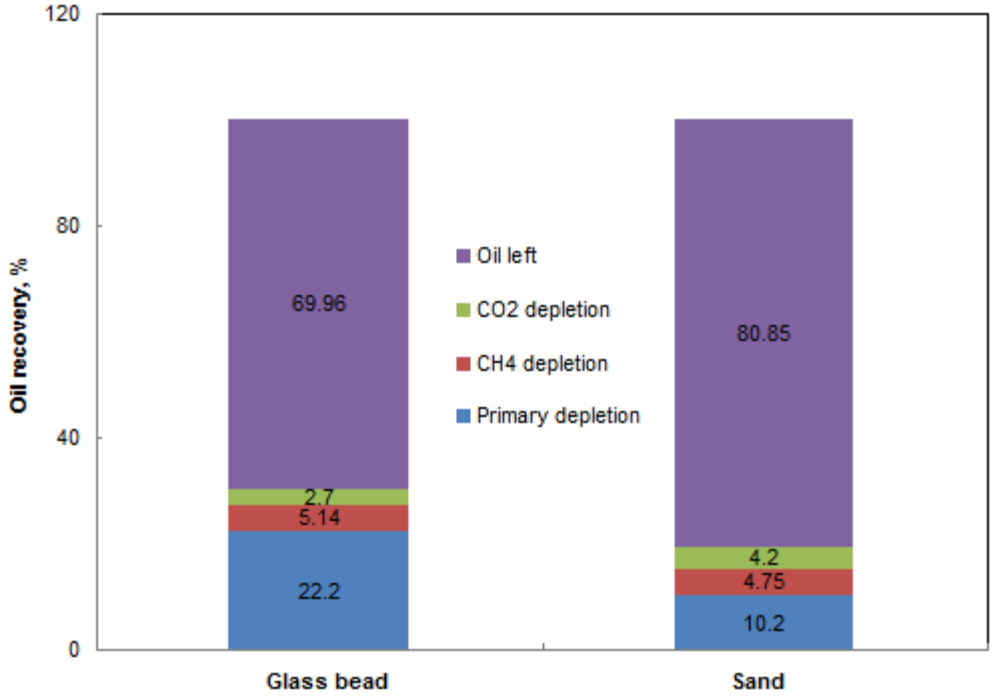

Figure 4.20 Oil recoveries before huff-puff process

4.4 Propane and Carbon Dioxide Huff-Puff Process

With 69.96% and 80.85% oil left in glass beads and sand packed cores separately, propane (C_3H_8) and carbon dioxide (CO_2) huff-puff process was performed next. The mixture fluid of C_3H_8 and CO_2 was designed to be a liquid phase for both injection and saturation periods. That is, the mixture stayed in liquid phase after being injected into the core.

4.4.1 Injection Preparation

4.4.1.1 Propane and Carbon Dioxide Transfer

Liquid C_3H_8 and CO_2 piston cylinders are needed for running huff-puff injection experiments. Figure 4.21 and 4.22 illustrate how the two hydrocarbons are transferred from their cylinders to their piston cylinder separately at liquid phase.

Figure 4.21 Picture of propane transfer rig

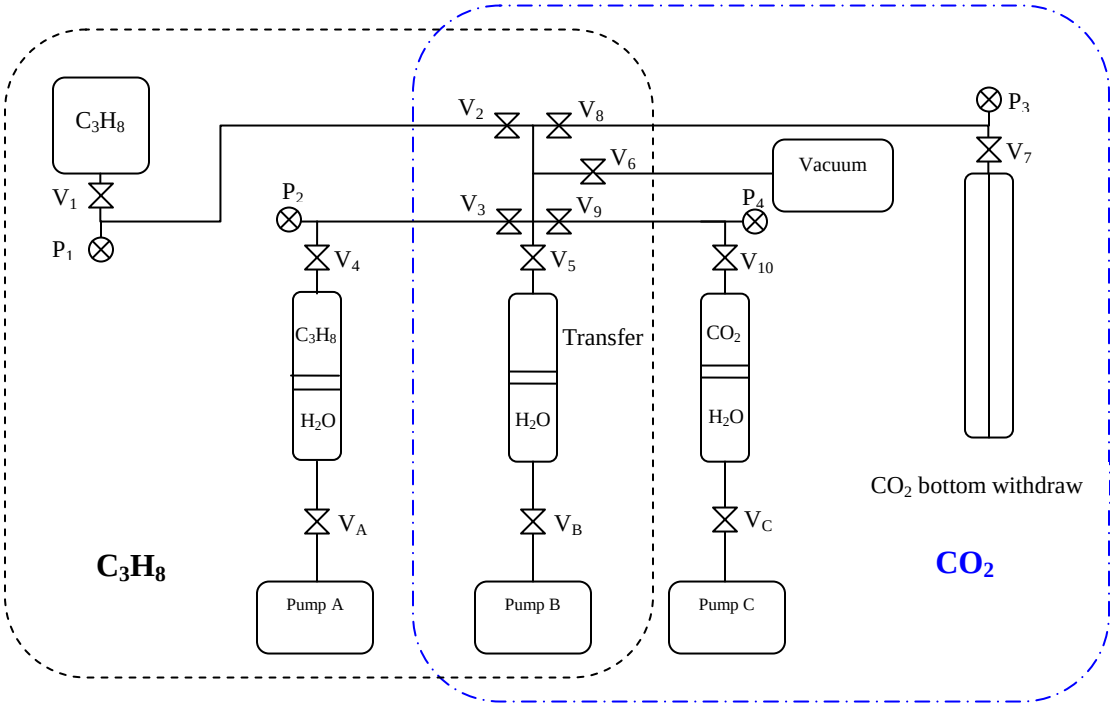

Figure 4.22 Propane and carbon dioxide transfer rig

Propane cylinder is placed bottom up at a higher position than transfer piston cylinder to make sure liquid propane to be transferred. For the same purpose, the bottom withdraw cylinder is used to ensure liquid carbon dioxide to be transferred. Before the test, make sure 3 pistons are at the top of 3 6L piston cylinders.

4.4.1.1.1 Propane Transfer

From propane cylinder to transfer piston cylinder:

- ✧ Open valve 2-6; close all other valves, vacuum top area for 10 minutes, close valve 3, 4 and 6.
- ✧ Set a very low water volume in pump B, run pump B at constant pressure 965kPa (From Table 4.3), and open valve B.
- ✧ Open valve 1, slightly decrease pump B constant pressure step by step until this pump begins to refill water, record that pump pressure (P_B).
- ✧ Keep running pump B at P_B to let liquid propane transfer from its original cylinder to the transfer piston cylinder until pump B is full.
- ✧ Close valve B, empty pump B to a very low water volume, run pump B at P_B, and open valve B. Repeat the above step 4 and 5 until enough liquid propane is transferred.
- ✧ Close valve 1 and 2.

From transfer piston cylinder to propane piston cylinder:

- ✧ Increase pump B injection pressure to a higher valve (P_B') than 965kPa and keep running until pump injection rate is near zero to make sure only liquid propane is in the top of transfer piston cylinder.
- ✧ Set pump A at a lower water volume value.
- ✧ Run pump A at a constant pressure P_B', open valve A, valve 3 and 4, run pump B at a higher constant flow rate to transfer liquid propane from transfer piston cylinder to the propane piston cylinder until pump A is full.
- ✧ Close valve A, empty pump A to a lower water volume. Close valve B, refill pump B.
- ✧ Repeat step 9 and 10 until all propane is transferred.

✧ Close valve 3, 4 and 5, valve A and B, stop pump A and B, liquid propane transfer is finished.

Table 4.3 Propane properties at 23℃

No.	Temperature ℃	Pressure kPa	Density kg/m^3	Liquid density kg/m^3	Vapour density kg/m^3
1	23	4826	0.50593	0.50593	Subcooled
2	23	4137	0.5042	0.5042	Subcooled
3	23	3447	0.5024	0.5024	Subcooled
4	23	2758	0.50055	0.50055	Subcooled
5	23	2068	0.49863	0.49863	Subcooled
6	23	1379	0.49663	0.49663	Subcooled
7	23	1034	0.49561	0.49561	Subcooled
8	23	965	0.4954	0.4954	Subcooled
9	23	896	0.019365	Superheated	0.019365
10	23	827	0.017536	Superheated	0.017536
11	23	758	0.015787	Superheated	0.015787
12	23	689	0.01411	Superheated	0.01411

Table 4.4 Carbon dioxide properties at 23℃

No.	Temperature ℃	Pressure kPa	Density kg/m^3	Liquid density kg/m^3	Vapour density kg/m^3
1	23	4826	0.12671	Superheated	0.12671
2	23	5516	0.16309	Superheated	0.16309
3	23	5861	0.18891	Superheated	0.18891
4	23	5998	0.20238	Superheated	0.20238
5	23	6136	0.21949	Superheated	0.21949
6	23	6205	0.74166	0.74166	Subcooled
7	23	6274	0.74514	0.74514	Subcooled
8	23	6550	0.75725	0.75725	Subcooled
9	23	6895	0.76963	0.76963	Subcooled

4.4.1.1.2 CO_2 Transfer

Carbon dioxide is transferred the same way like propane, using a liquid withdraw carbon dioxide cylinder instead of the bottom up propane cylinder, and 6205kPa (Table 4.4) instead of 965kPa.

4.4.1.2 Final Core Inner Pressure Design after Injection

To ensure the mixture hydrocarbon is in liquid phase in the core after injection at 23℃, the final core inner pressure is the key point. Figure 4.23 shows the dew and bubble point pressures vs. a series ratios (C_3H_8/ (C_3H_8+CO_2) in mass of the mixture hydrocarbon at 23℃. At the ratio of 0.5, the mixture is all in liquid phase when pressure is above 4000kPa. Figure 4.24 shows density and compress factor vs. pressure for a ratio of 1:1 (C_3H_8/CO_2) in mass mixture at 23℃. The mixture fluid is in liquid phase when pressure is beyond 4000kPa too. Therefore, the final core inner pressure is designed beyond 4000kPa at the ratio of 1:1 (C_3H_8/CO_2) in mass.

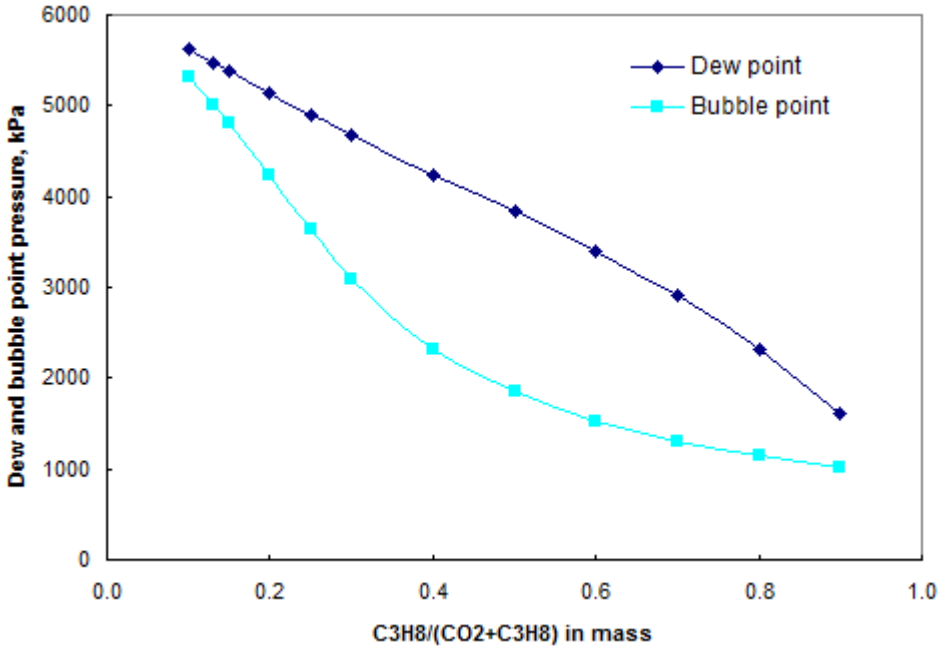

Figure 4.23 Dew and bubble points vs. ratio of CO_2 and C_3H_8 mixture at 23℃

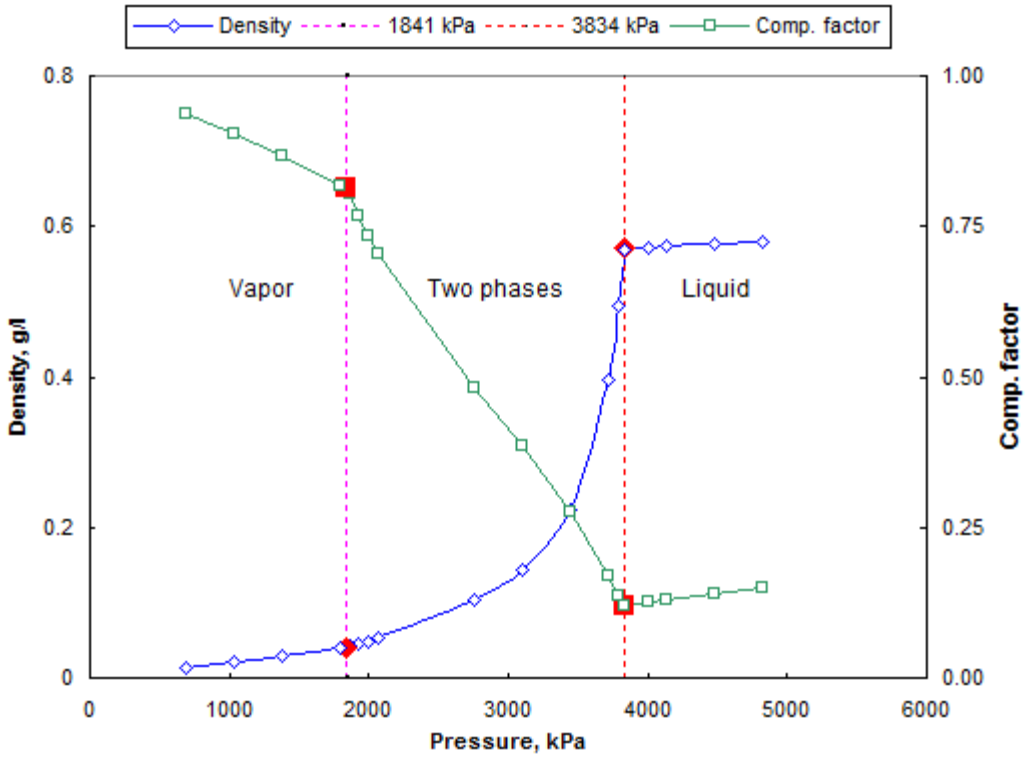

Figure 4.24 Pressure vs. density and comp. factor at 1:1 in mass of CO_2 and C_3H_8 at 23℃

4.4.2 Demonstration and Methodology

4.4.2.1 Demonstration

To keep injecting the liquid mixture hydrocarbon at a constant ratio and in liquid phase; the injection system is designed and set up as shown in Figure 4.25. The production system is shown in Figure 4.26. The injection and production were both from the core outlet end for huff-puff process.

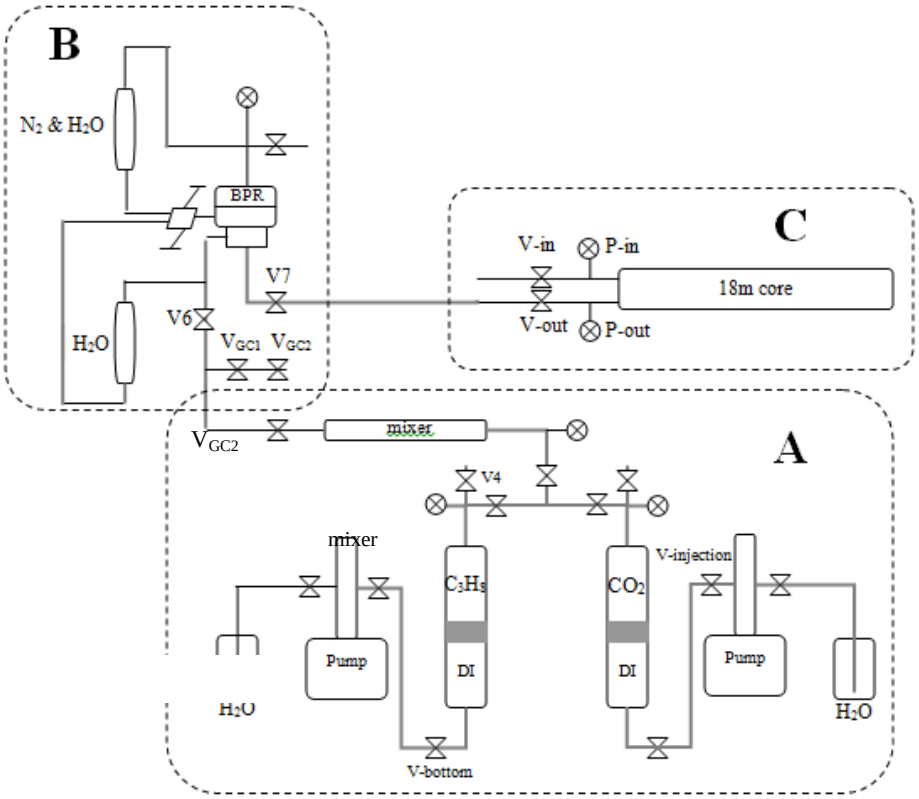

Figure 4.25 Injection system of huff-puff process

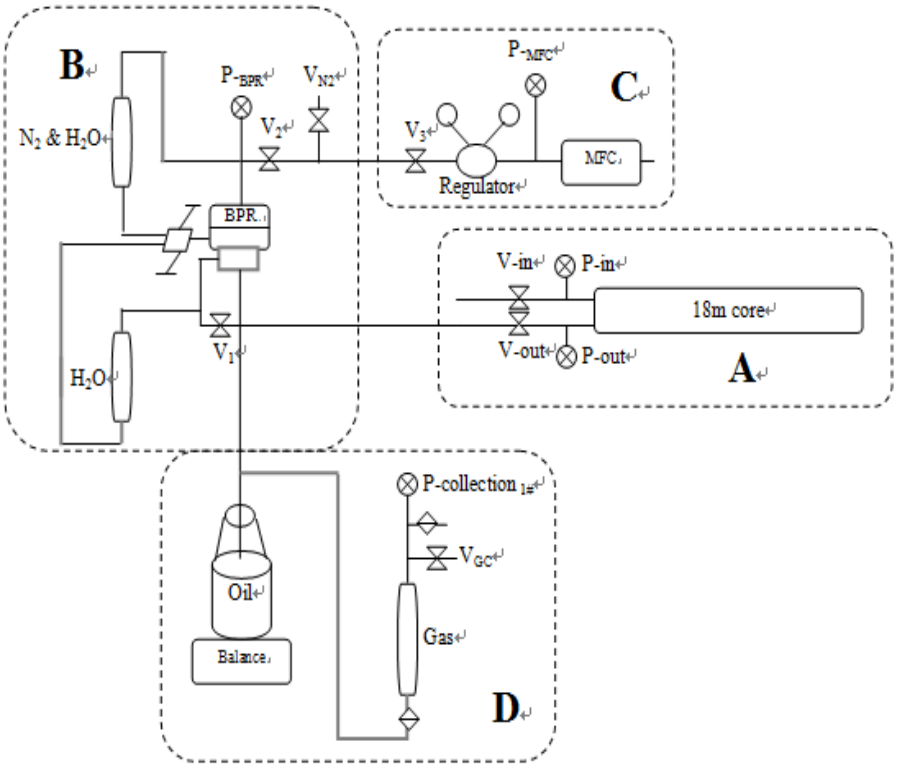

Figure 4.26 Production system of huff-puff process

4.4.2.2 Methodology

As shown above in Figure 4.25 and 4.26, following the steps below, huff-puff injection and production processes were conducted in the same way for the two long cores at different injection rate due to their permeability difference.

4.4.2.2.1 Injection and Soaking

Glass beads packed core:

- ✧ Built part A and B as shown in Figure 4.25.
- ✧ Set up BPR pressure at about 6619kPa which is far beyond 4826kPa to ensure liquid mixture hydrocarbon would be injected into the core.
- ✧ Run both pumps to pressurize their related piston cylinders of carbon dioxide and propane.

- ✧ Run pump A at 0.9ml/min and pump B at 0.6ml/min when both piston cylinder pressures were not far from BPR pressure. Stopped both pumps one by one until their related piston cylinder pressures were very close to the BPR pressure separately.
- ✧ Kept core inlet valve closed.
- ✧ Run both pumps at their constant flow rates, then quickly opened valves of 2, 4, 3, injection, 6, 7, and core outlet valves in sequence. The two injected fluids could be better mixed when they went through the tube mixer (1/4" OD 27 ELEMENT 316SS).
- ✧ Set up GC sample location before BPR.
- ✧ Kept valve GC_1 closed, open valve GC_2, and vacuumed the very short, 1/8” in diameter GC sample tube for a few minutes, then closed valve GC_2, stopped vacuum.
- ✧ Opened valve $GC_1$and waited for a few minutes, then closed it.
- ✧ Opened valve GC_2 to take GC sample, then closed valve GC_2.
- ✧ While core pressure P_{12} was close to BPR pressure, closed valve 2 and 4, and stopped both pumps immediately.
- ✧ Waited for core inner pressures to equilibrate themselves.
- ✧ Repeated the above steps except the first and second steps many times until the core inner pressures were all above 4826kPa.
- ✧ Closed core outlet valve, stopped injection process.
- ✧ Collected pressure and temperature variations datum, measured GC samples.
- ✧ Waited for pressure equilibrium-soaking period.

Sand packed core:

- ✧ Repeated all the steps for glass beads packed core. Due to the permeability difference, the two pump flow rates were set at: A-0.12ml/min, B-0.08ml/min.

4.4.2.2.2 Production for Both Cores

- ✧ Built part B, C and D as shown in Figure 4.26.
- ✧ Set BPR pressure at about 5516kPa far beyond 4826kPa to maintain the liquid phase in the core.
- ✧ Tested and set MFC at the same depletion rate of 2.34kPa/min as before.

- ✧ Waited until the BPR pressure is a little bit higher than the core inner pressure, opened core outlet valve to produce.
- ✧ Set up GC sample location after gas collection bottle.
- ✧ Took GC sample occasionally.
- ✧ Collected pressure and temperature variations datum, as well as oil and gas production datum during the whole process.
- ✧ Measured the viscosity and density of produced oil, GC of the produced gas.

4.4.3 Experiment Results

During the process interval of CO_2 depletion and huff-puff injection, the two long cores remained shut-in. One heater controller of the sand pack core did not work properly for 3 months by accident.

As Figure 4.27 shows, thermocouples T_4 and T_5 were controlled by the malfunctioning heater which was closer to the core outlet. The other 3 temperature increases were caused by heat transfer. The extent of temperature increase depended on the distance to the control area of the malfunctioning heater. Even though the temperatures of T_4 and T_5 were below 80℃, the temperature at the heating area controlled by the malfunctioning heater could be much higher than them because there were distances between T_4 and T_5 to the heating location.

Figure 4.28 indicates all core inner pressure went up gradually from 138-207kPa to 896-965kPa along with the core temperature increase. Even though the temperatures of T_1-T_5 were relatively stable after 1 day, the core pressures kept going up quickly until the heater got fixed. Furthermore, all the pressures after the temperature got controlled were much higher than those before the temperature abnormal. This infers that some gases must have come out of the fluid at the abnormally heated area to rise up the core pressures. After the heater was fixed, the pressure curves of P_{11} and P_{12} (near the core outlet) showed different ways from others. P_{11} went up quickly and dropped down later, but it was still higher than others. P_{11} showed an obvious peak and P_{12} jumped up at some points and stayed at higher pressure level like P_{11}. That probably shows that some gas was trapped near the core outlet during core cooling down process. The type of the produced gas will be discussed at the puff process later.

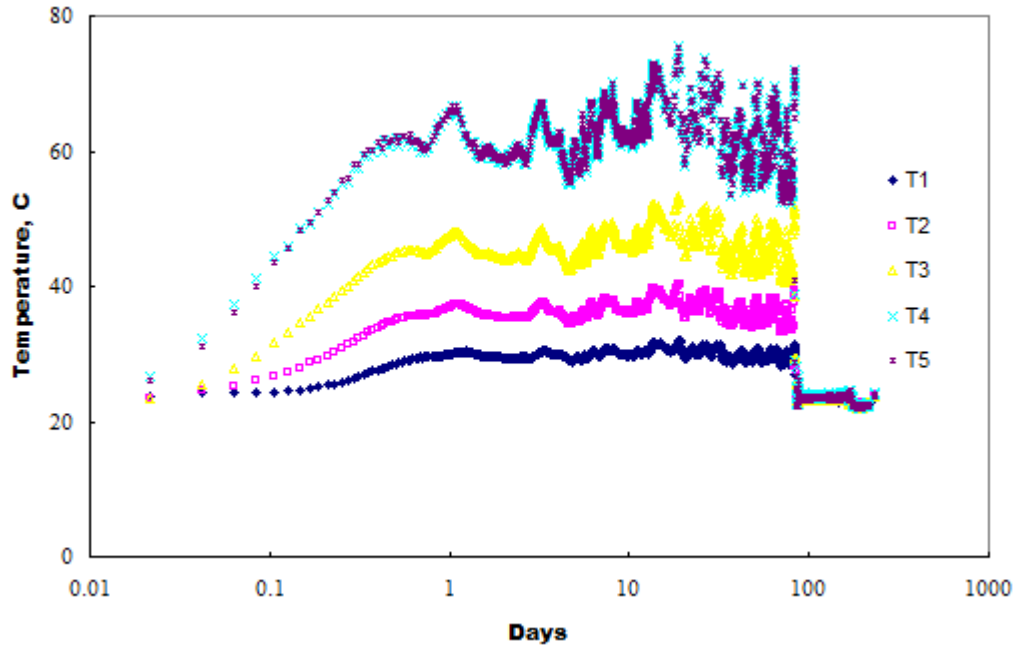

Figure 4.27 Temperature effects of the malfunctioning heater-sand packed

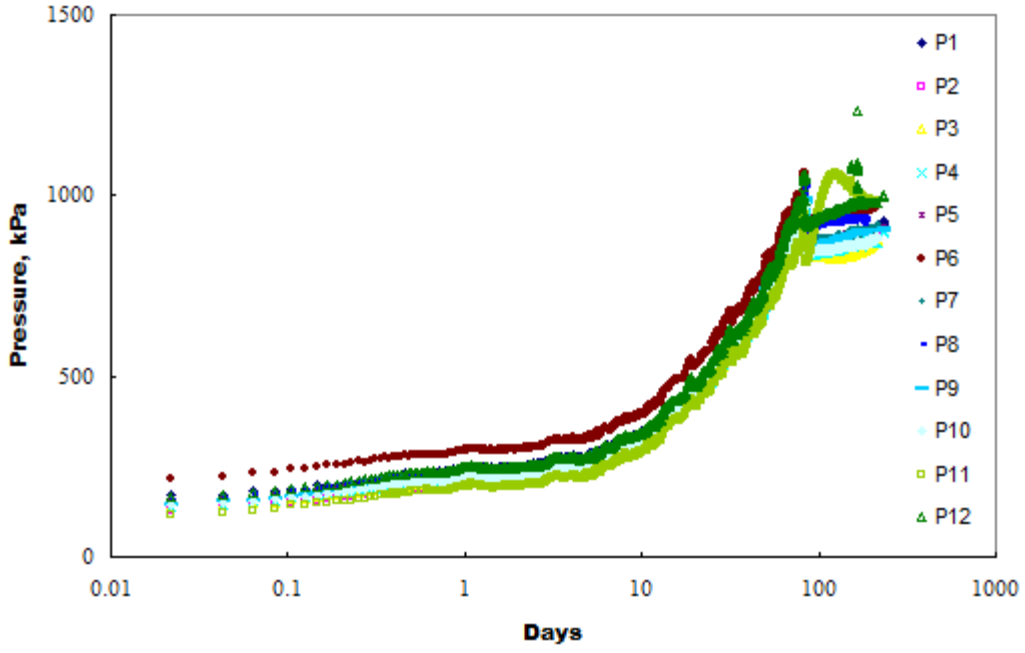

Figure 4.28 Abnormal pressure file-sand packed

4.4.3.1 Injection and Soaking

4.4.3.1.1 Glass Beads Packed Core

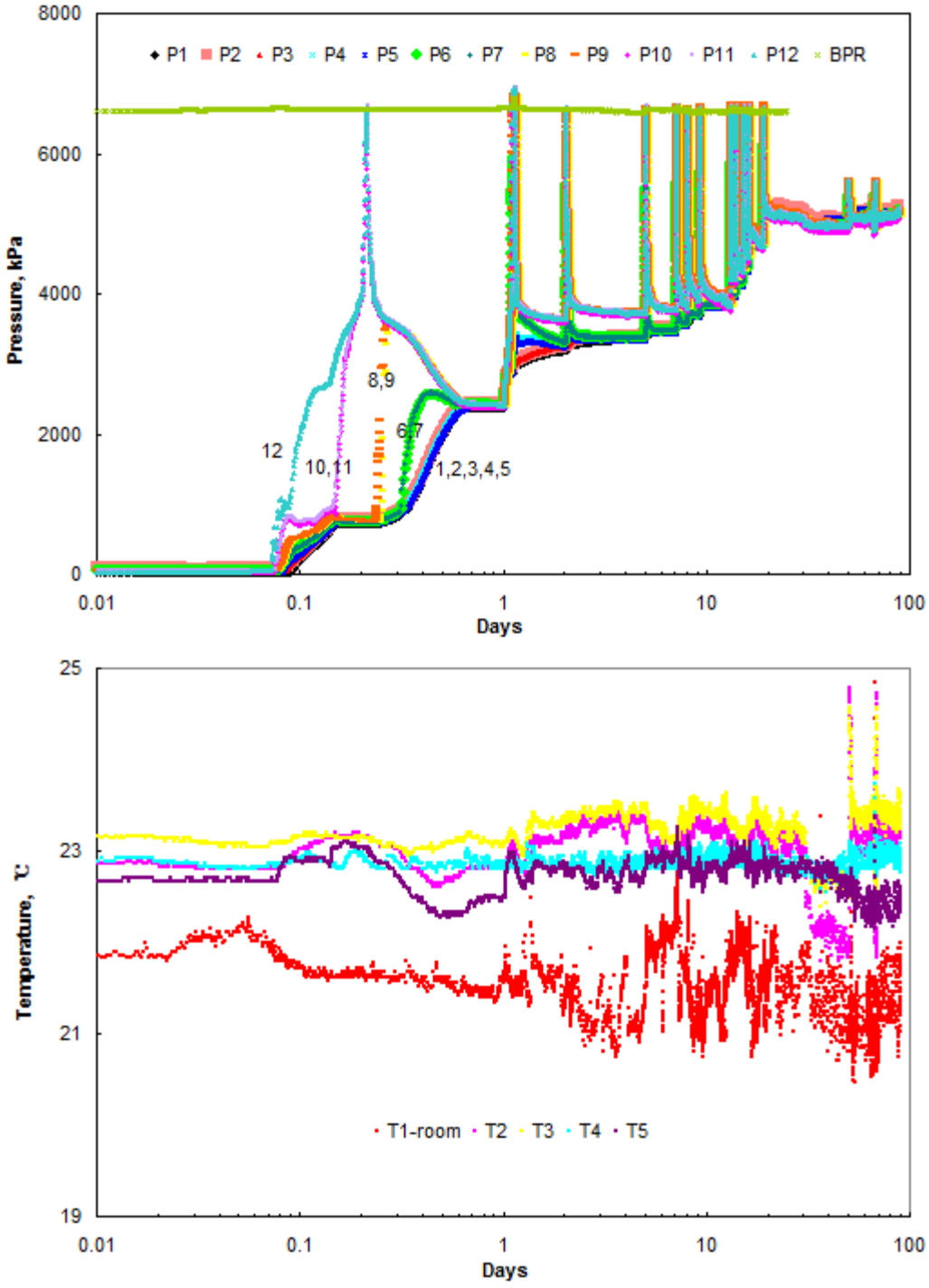

Figure 4.29 Injection and soaking period of huff-puff process-glass beads

Figures 4.29 shows the variations of core pressures and temperatures with time during the periods of injection and soaking for the glass beads packed core. To achieve liquid mixture fluid

in the core after the huff process, a series of injections were performed. At the first injection, it can be clearly seen that pressures increased in sequence from P_{12} (outlet) to P_1 (inlet). Due to higher permeability, it only took about 20 days for the whole injection process to finish. Pressure decrease can be seen after each inject. The last two pressure increases during the soaking period were caused by temperature changes. The heater which controlled T_2 and T_3 was power off by unknown reasons and restarted twice. The room temperature was somewhat lower than the core temperatures during the periods of injection and soaking. The final core inner pressures were around 5171kPa, which is over 4000Kpa, to ensure a liquid phase mixture fluid in the core.

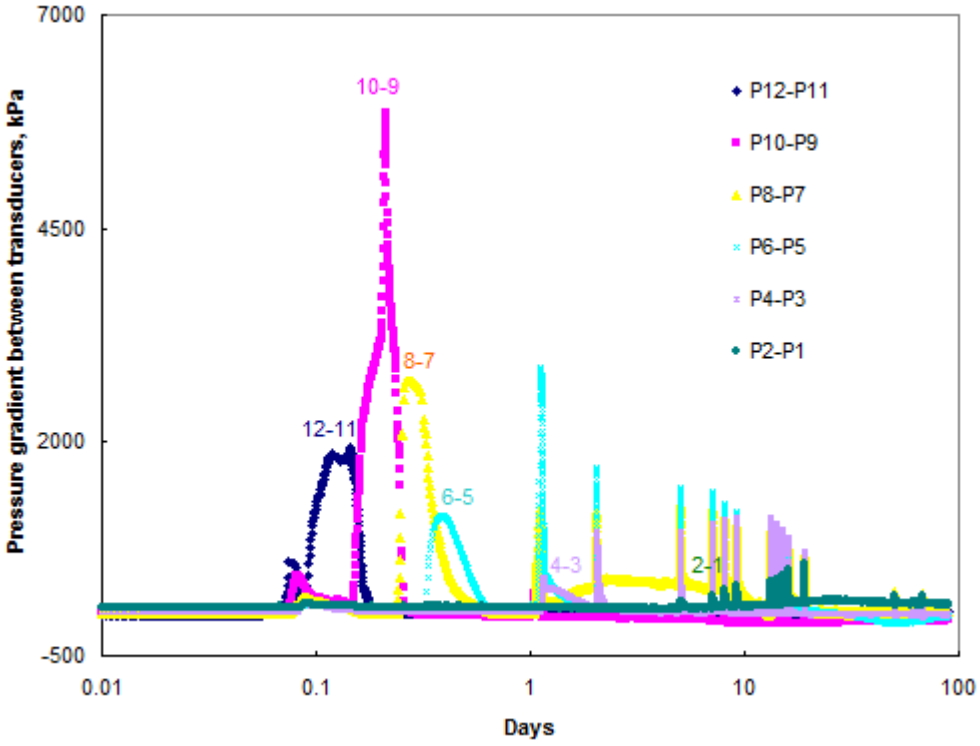

Figure 4.30 Pressure gradients of huff process-glass beads

Figure 4.30 shows the pressure gradients during the injection period. During the first injection period, the blue and pink curves showed more than one peaks. This infers that pack-through processes or oil movement occurred to affect the waves of core pressures.

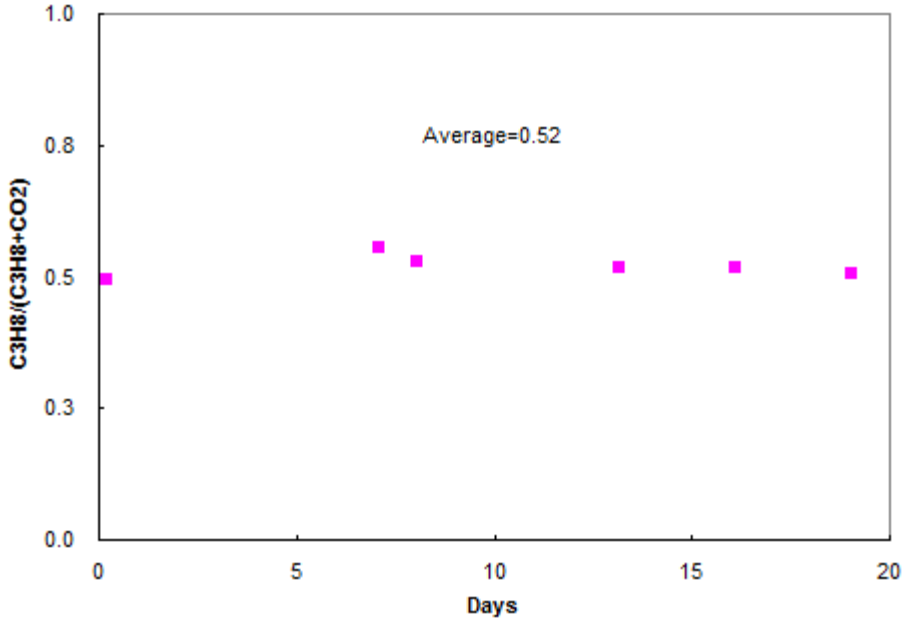

Figure 4.31 GC results of injection mixture fluid-glass beads

Figure 4.31 shows GC results of injection mixture fluid, it can be clearly seen that the propane and carbon dioxide were injected at the ratio around 1:1. The tiny variations among the points were caused by changes of room temperature and air pressure during the series of injection periods.

4.4.3.1.2 Sand Packed Core

Figure 4.32 shows the variations of pressures and temperatures with time during the periods of injection and soaking for the sand packed core. Due to lower permeability, not only the number of injection days was longer, but also the core inner pressures increased one by one more clearly from core outlet-P_{12} to inlet-P_1 compared to the glass beads packed core. The last three pressure increases were not caused by injection. They occurred at the soaking period due to temperature jump-up similarly to what happened for the glass beads packed core. The final core pressure is above 4000kPa to ensure liquid fluid in the core.

The temperature graph shows that the core temperatures were relatively stable until 50 days. The temperatures of T_1, T_2 and T_3 dropped down from 50 to 78 days due to the power off of their related heater. After that, there were still several restarts of the heater by the unplanned power off.

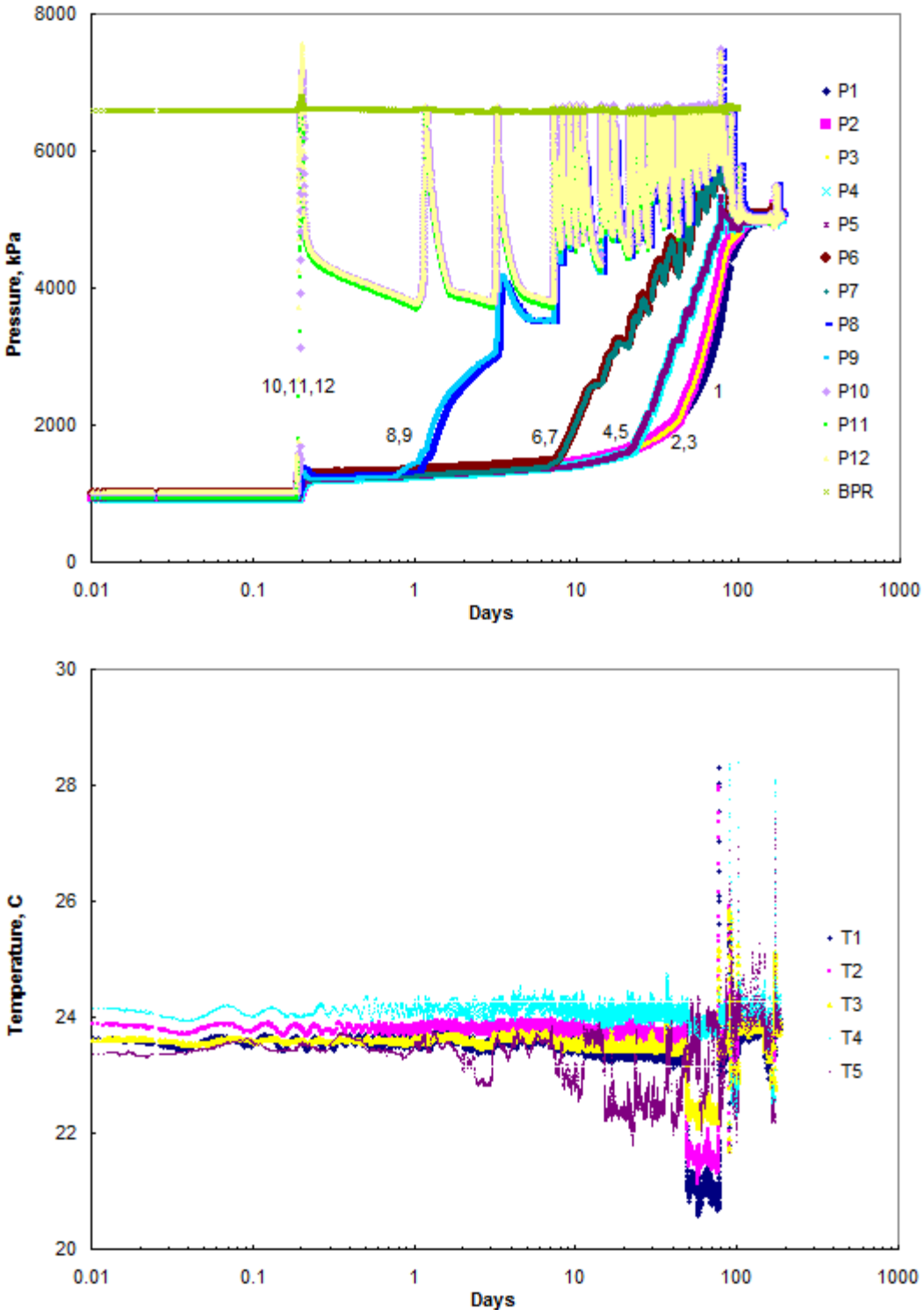

Figure 4.32 Injection and soaking period of huff-puff process-sand packed

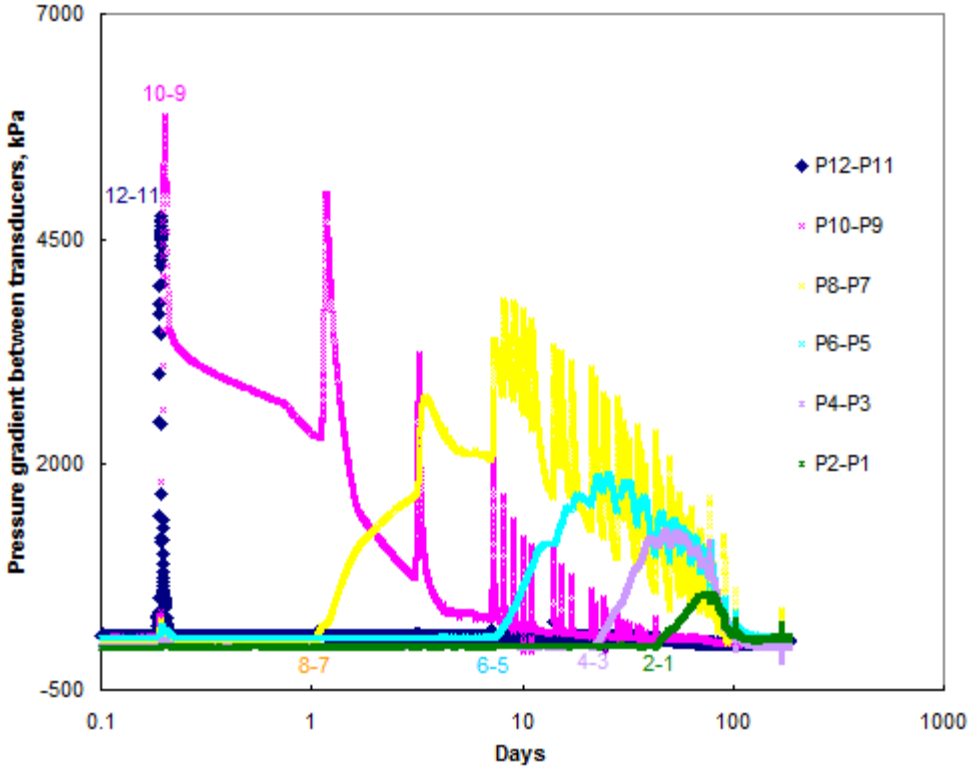

Figure 4.33 Pressure gradients of huff process-sand packed

Figure 4.33 shows the pressure gradients in sand packed core during the periods of injection and soaking. Pressure transmissions appear from outlet to inlet one by one like glass beads packed core, but this phenomenon is clearer here than the higher permeability core.

Figure 4.34 shows that the propane and carbon dioxide were injected at the same ratio around 1:1 as glass beads packed core. The tiny variations among the points were caused by the changes of room temperature and air pressure during the series of injection periods, which is the same as glass bead packed core.

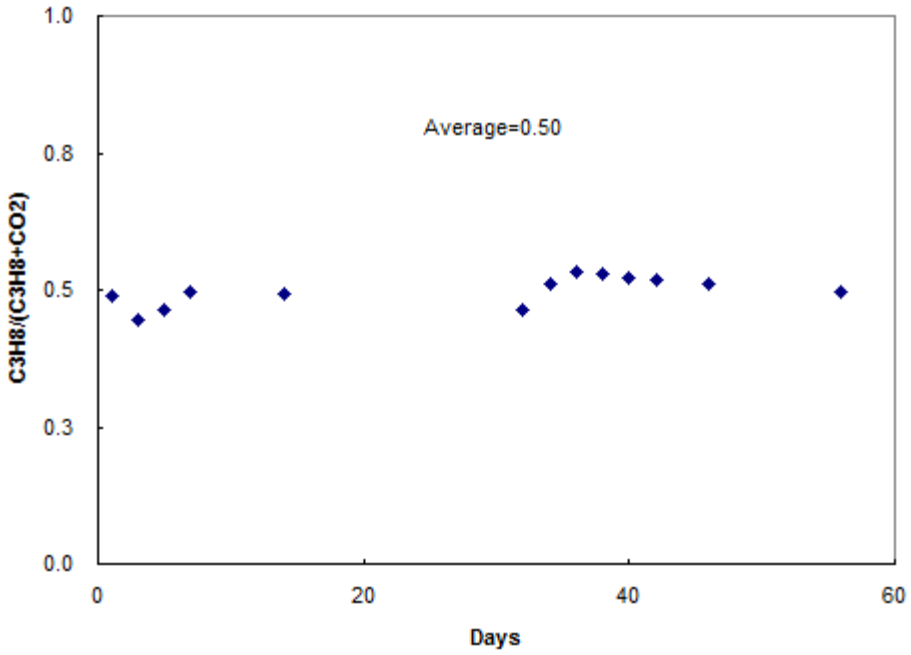

Figure 4.34 GC results of injection mixture fluid-sand packed

4.4.3.2 Production

4.4.3.2.1 Glass Beads Packed Core

Figure 4.35 shows pressure variations with time during the huff-puff production process for the glass beads packed core. All the core inner pressures dropped a little bit from outlet to inlet one by one in a short period of time due to the higher permeability after the core outlet valve was opened. Once the BPR pressure decreased lower than core inner pressures, all pressures began to drop following the BPR depletion rate from outlet to inlet one after another. There was only one trend change point at some pressure curves which is different from methane depletion process.

Figure 4.36 shows pressure gradients was built up throughout the core from inlet to outlet. This is similar like the CH_4 depletion process. The highest peak appeared between P_7 and P_8, which is one step closer to the core outlet than the CH_4 depletion process (The highest peak was between P_5 and P_6).

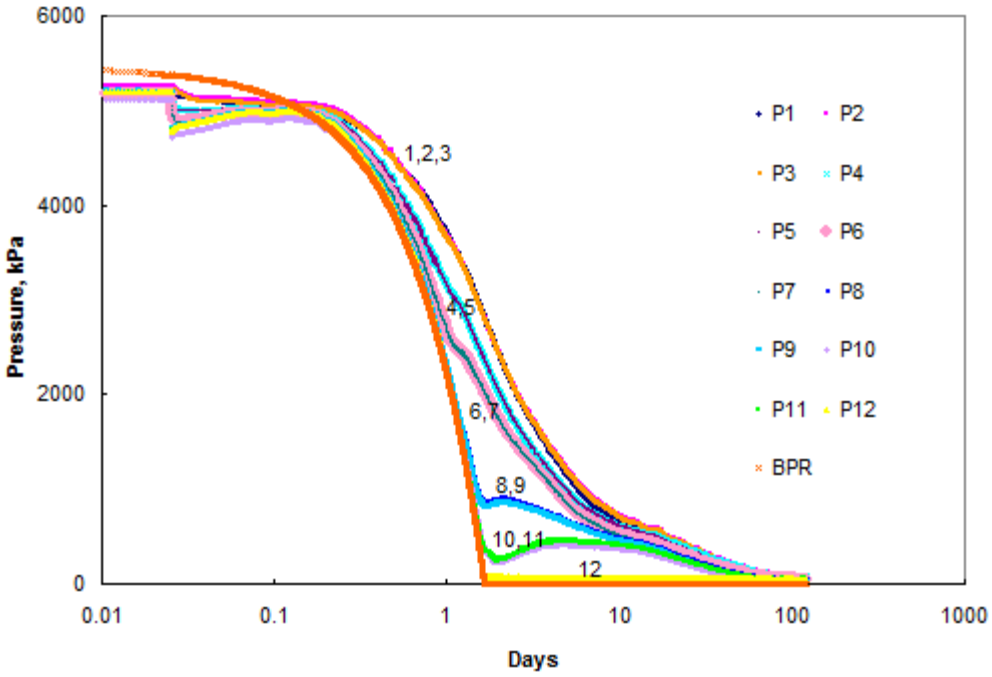

Figure 4.35 Pressure graphs of puff process-glass beads

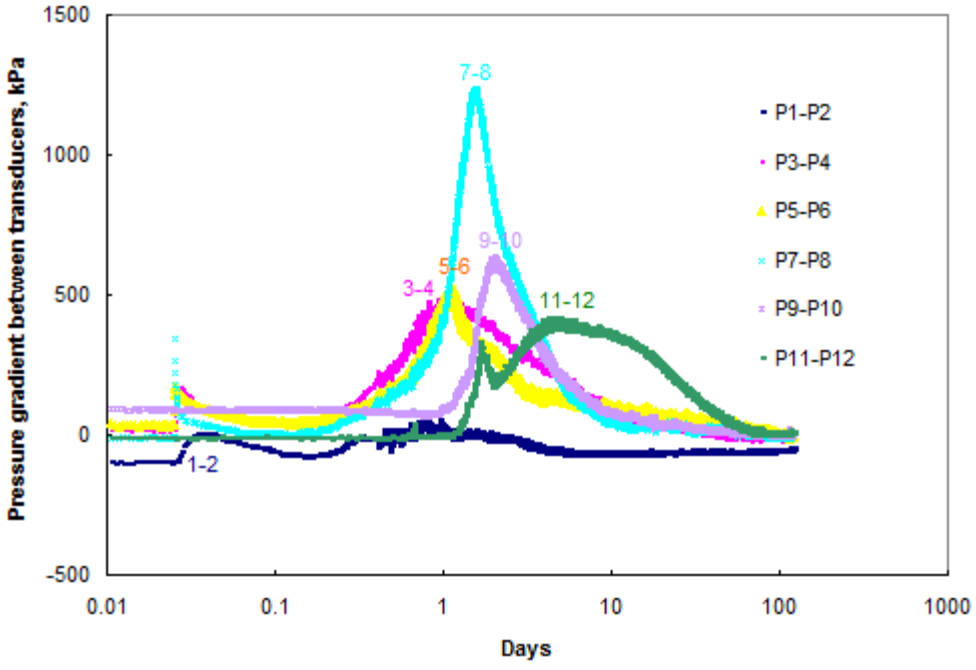

Figure 4.36 Pressure gradients of puff process-glass beads

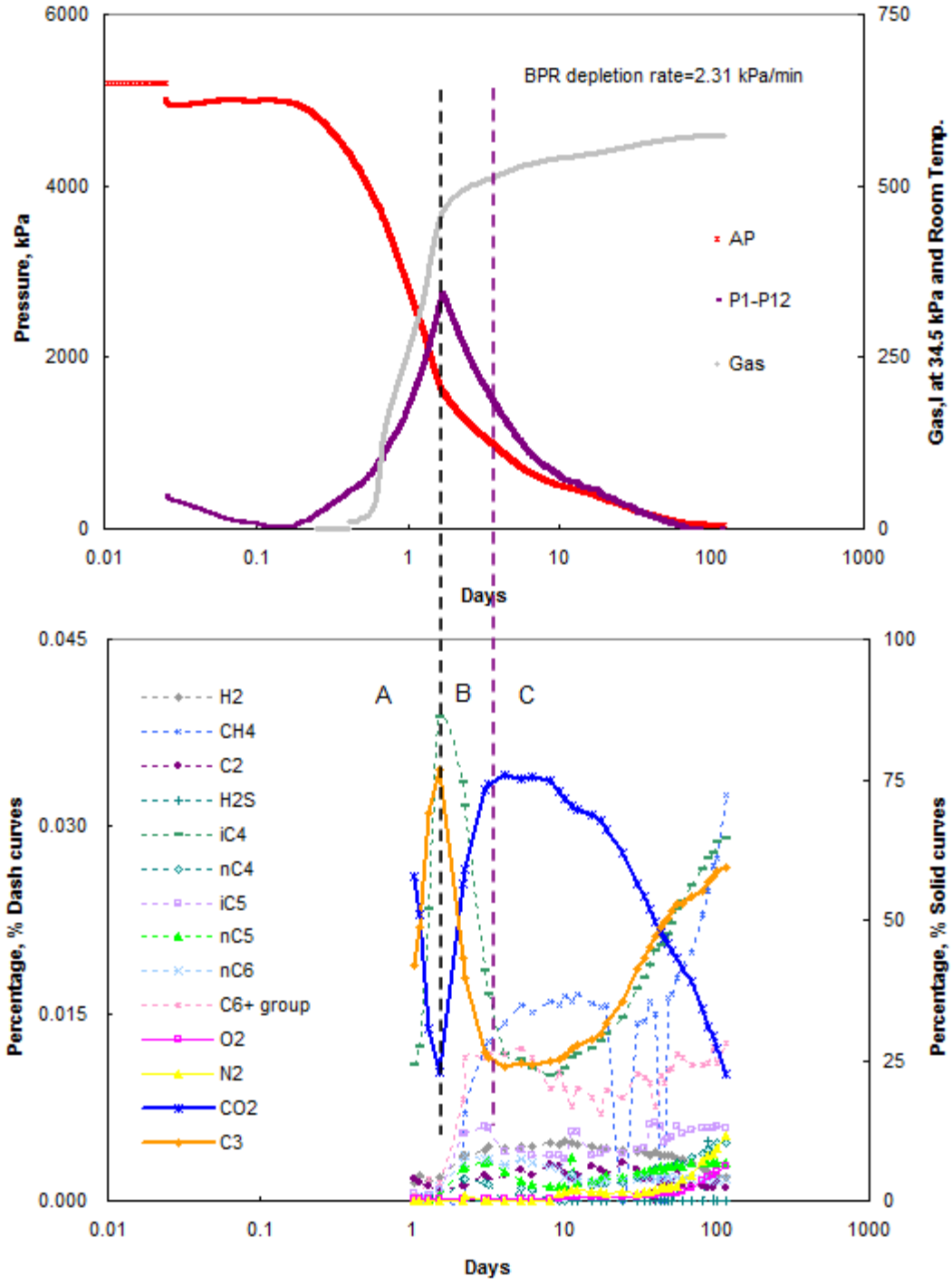

Figure 4.37 Production graphs and GC results of puff process-glass beads

Figure 4.37 shows production graphs of huff-puff production process for glass beads packed core. The same as the methane depletion process, average pressure and differential pressure were

used instead of 12 pressures to better understand the relationship between pressures and production curves. Both pressure curves and gas production curve only have one trend change point at the position of black dashed line. This implies that before that point, production gas was mainly free gas; after that point, solution gas evolved from the oil within the pore space and trapped within the oil due to high viscosity, thus reduced gas mobility, swelled the oil, blocked the free gas zone to some extent, decreased the gas production. The second trend change point did not show up, therefore, no oil was produced out during this process.

The GC results graph is divided into three parts by the black and purple dashed straight lines to better explain the varied curves. Before analysis, the vaporizing pressures of related fluids should be introduced in Table 4.5.

Table 4.5 Vaporizing pressure of fluid at 23℃

Fluid	Vaporizing pressure, kPa
CO_2	6144
C_3H_8	905
50% CO_2+50% C_3H_8	1841

To analysis the GC result during puff process, it is closely related to how the mixture is injected. The huff process needs to be clarified first.

At the section of 4.2.2.2.3, it has been discussed that the gas channels are left everywhere in the reservoir after methane depletion process which creates paths for the following recharged gas to finger into the remaining oil in porous media. At the beginning of injection, the core inner pressure was around 69kPa which is lower than propane vaporizing pressure 905kPa. Therefore, the liquid mixture, CO_2 and C_3H_8, both vaporized immediately and occupied the gas channels after passing through BPR until the C_3H_8 vaporizing pressure is reached. After that, C_3H_8 tended to liquefy; CO_2 in the gas phase is higher than C_3H_8. High content of gas CO_2 should be trapped near outlet with the following liquid propane and gas CO_2 injection. After the vaporizing pressure of mixture fluid was reached, the liquid mixture was driven into the core until the end of injection. Along the movement towards inlet, pressure decreased, therefore, CO_2 still vaporized along the way until the lowest pressure was above the vaporizing pressure of mixture fluid. The soaking period lasted for 2.5 months to let the injection fluid dissolve into the oil. After soaking,

average pressure was lower than the vaporizing pressure of CO_2 but higher than the one of mixtures. There should be gas CO_2, liquid propane and liquid mixture existing throughout the core. The liquid propane and mixtures were easily dissolved and trapped in the oil than gas CO_2.

Part A (6144kPa>P>1841kPa)

At the beginning of production, differential pressure at outlet was very low; most of injected liquid fluids were still trapped there. Produced gases were mainly from the easily moved high content of gas CO_2, trapped there during huff process, together with a tiny amount of free liquid mixture and propane at outlet. Therefore, CO_2 should be higher than C_3H_8. With the production continuing, differential pressure increased gradually. The increasing drive force could displace large amount of free liquid mixture and propane to outlet and produced out. Component of C_3H_8 was higher than the one of CO_2 in these liquid phases; Furthermore, the effect of trapped CO_2 gas could be ignored since liquid phase started to vaporize and produce because trapped CO_2 quantity was very small comparing to the one in liquid phase; therefore, C_3H_8 curve increased together with CO_2 curve decreasing.

Part B (1841kPa>P>905kPa)

When pressure dropped down to vaporizing pressure of mixtures but still higher than the one of C_3H_8, liquid mixtures started vaporizing. Gas propane intended to be liquefied again during the way out, mainly CO_2 was produced. Therefore, CO_2 increased together with C_3H_8 decreasing. Some solution gas came out of the oil and moved towards outlet.

Part C (P<905kPa)

When the core inner pressure dropped to the propane vaporizing pressure 905kPa (at the purple dashed straight line point) more propane vaporized out of the free liquid mixture and free liquid propane. Some solution gas, in which the content of C_3H_8 was higher than the content of CO_2, came out of the oil too as Figure 4.35 shown. Therefore, propane increased together with CO_2 decreasing.

iC_4 curve shaped the same way as propane curve based on the similar compatibility principle. Tiny amount of CH_4 and C_6^+ group increases were also observed.

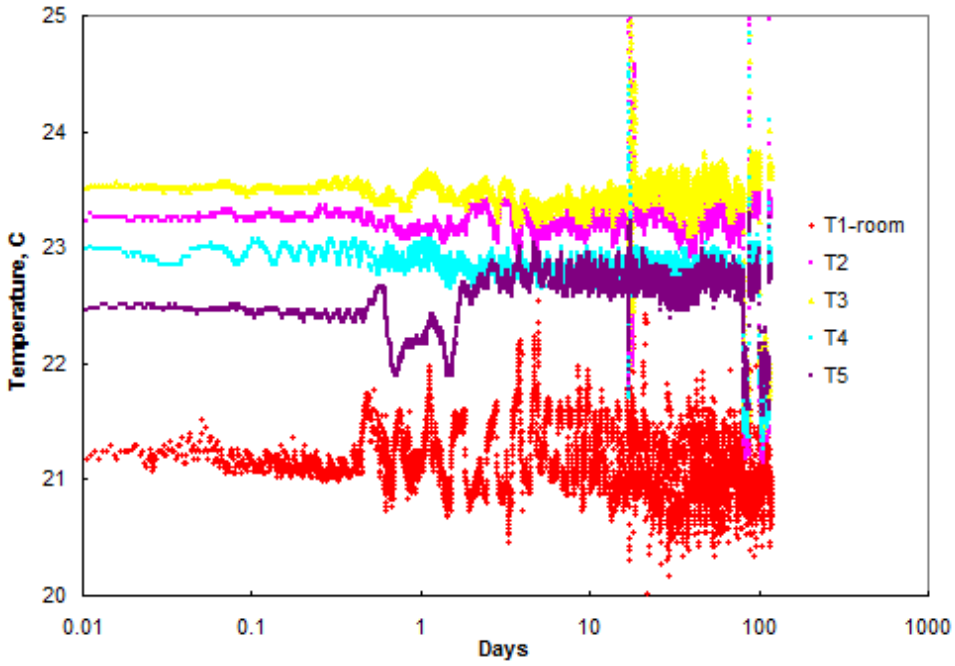

Figure 4.38 Temperature graph-huff-puff production-glass beads

Figure 4.38 shows that the core temperatures are relatively stable during the whole production process except several jumps due to temporarily power off. Room temperature is a little bit lower than core temperatures.

4.4.3.2.2 Sand Packed Core

Figure 4.39 shows pressure variations with time during huff-puff production process for sand packed core. All curves are similar to the glass beads packed core, the differences are that core pressure decreased slower and production period takes a longer time due to lower core permeability.

Figure 4.40 shows that pressure gradients appeared irregularly. The highest pressure gradient was at the core inlet and the second higher one was far from the core inlet. These were totally different from glass beads packed core. Further study should be performed later.

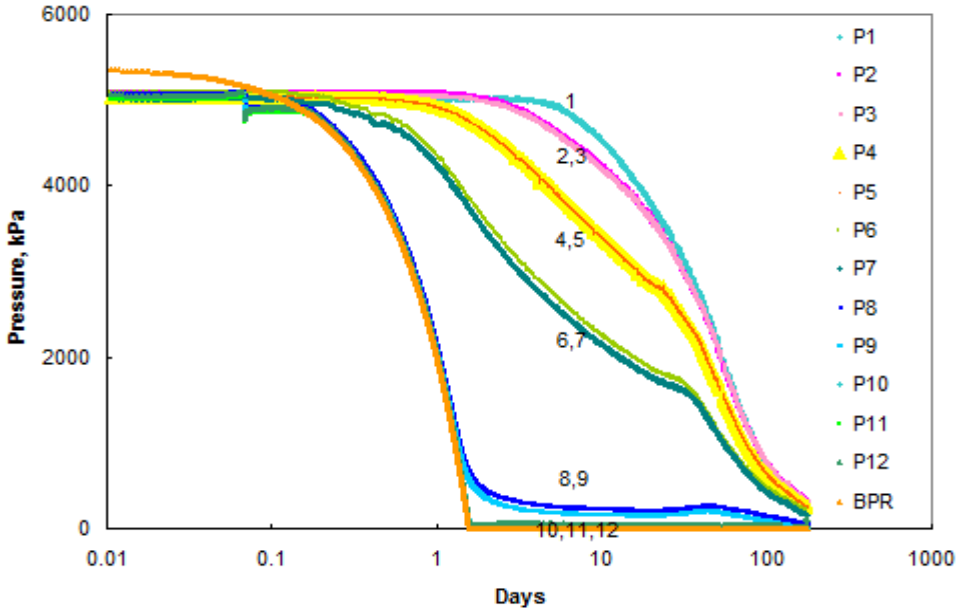

Figure 4.39 Pressure and production graphs-huff-puff production-sand packed

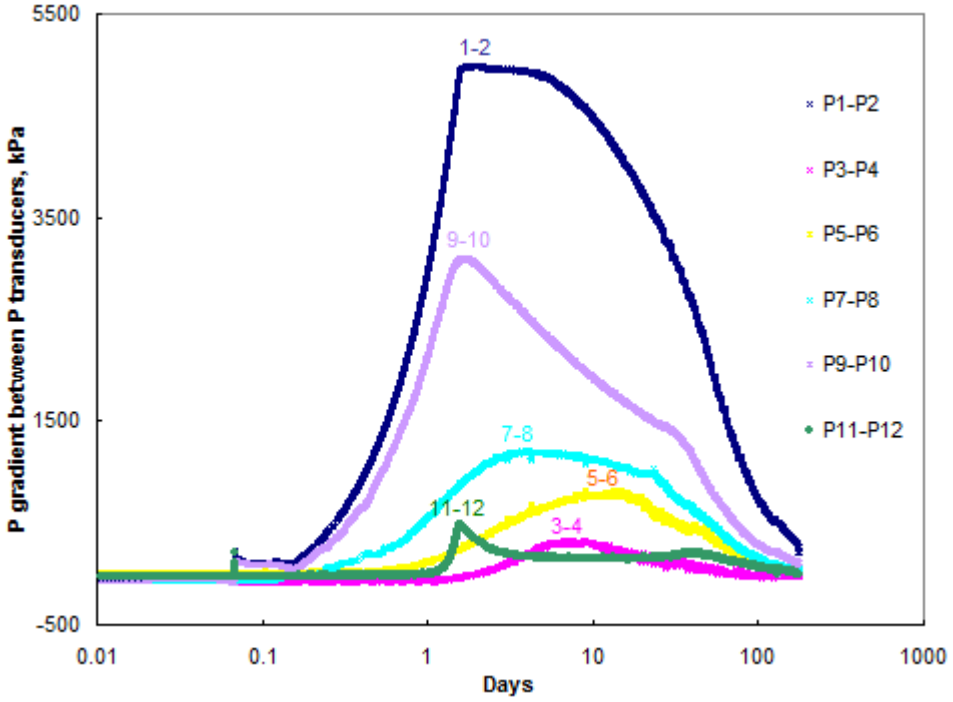

Figure 4.40 Pressure gradients of puff process-sand packed

Figure 4.41 shows pressure difference, average pressure and production graphs of huff-puff production process for sand packed core. Comparing to the glass beads packed core, the average

pressure and pressure difference in sand packed core both decreased slowly after the first tendency change point. The slope of gas production curve in sand packed core was obviously lower than it in glass beads packed core. These above differences were caused by gas paths block greatly in sand packed core during forming the foamy oil period due to lower permeability. Only one trend change point showed up and no oil was produced out during this process too.

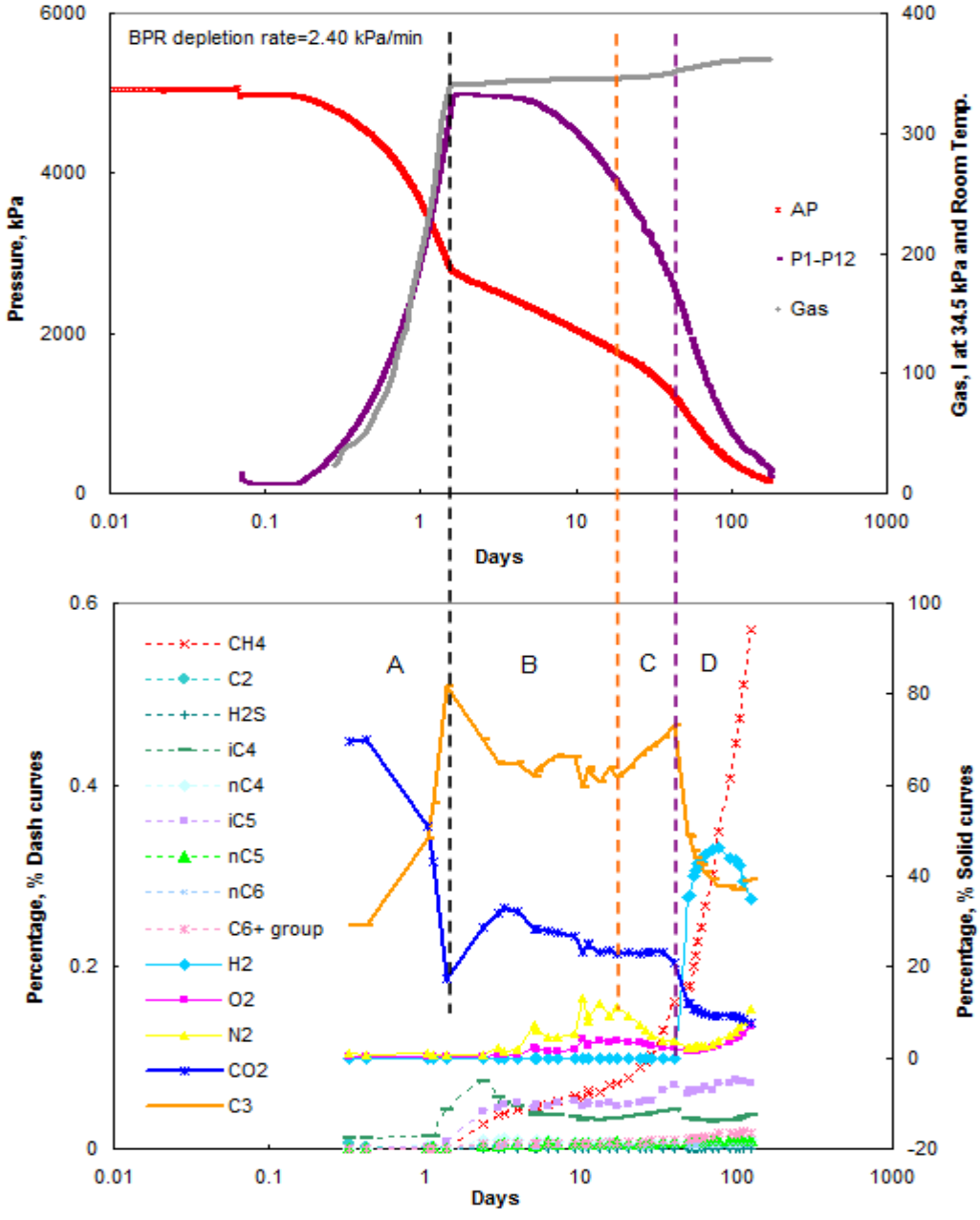

Figure 4.41 Production graphs and GC results of puff process-sand packed

The graph of GC results was divided into four parts by the black, orange and purple dashed straight lines for a detail discussion.

The same as glass beads core, huff process needs to be clarified first. They are similar except: First, the trapped gases due to malfunctioning heater in sand packed core were pushed away from outlet to inlet by huff process. Second, the start core inner pressure is around 931kPa, which is beyond the maximum vaporizing pressure of C_3H_8, only CO_2 vaporized immediately until the mixture fluid vaporizing pressure was reached.

Soaking period lasted for about 4 months to let the injection fluid dissolve into the oil. The final average core pressure was around 5033kPa which is beyond the vaporizing pressure of mixture fluid but lower than the one of CO_2. There should be gas CO_2, liquid propane and liquid mixture existing throughout the core. The liquid propane and mixtures were easily dissolved and trapped in the oil than gas CO_2.

Part A is the same as glass beads packed core.

Part B is similar to the glass beads packed core.

Due to the lower permeability, with pressure decreasing, dissolved gas evolved from and trapped within the oil, swelled the oil, thus closed the gas channel dramatically. Core pressure decreased very slowly, the increasing of CO_2 and decreasing of C_3H_8 were both slowed down. No crossover point showed up and a relative stable period appeared.

Part C is the same as glass beads packed core

When the core inner pressure dropped to propane vaporizing pressure 905kPa (at the orange dashed straight line point) more propane vaporized out of the free liquid mixture and free liquid propane. Some solution gas, in which the content of C_3H_8 was higher than the content of CO_2, came out of the oil too as Figure 4.39 shown. Therefore, propane increased together with CO_2 decreasing.

Part D only exists in sand packed core

The produced gas due to malfunctioning heater during the interval period of CO_2 depletion and huff-puff injection processes is H_2 based on GC results. It was pushed far away from outlet towards inlet by huff process, produced out at around 40 days of production. One phenomenon should be mentioned was that the content of CH_4 increased with the content of H_2 increase. This methane probably was the one trapped in the oil after the methane depletion process. During the huff-puff process, together with the help of the trapped gas-H_2, the oil was not only relocated but also diluted by the additional dissolved gases. A small amount of trapped methane probably was released during these complicated processes. The contents of CO_2 and C_3H_8 both decreased due to the content of H_2 increase.

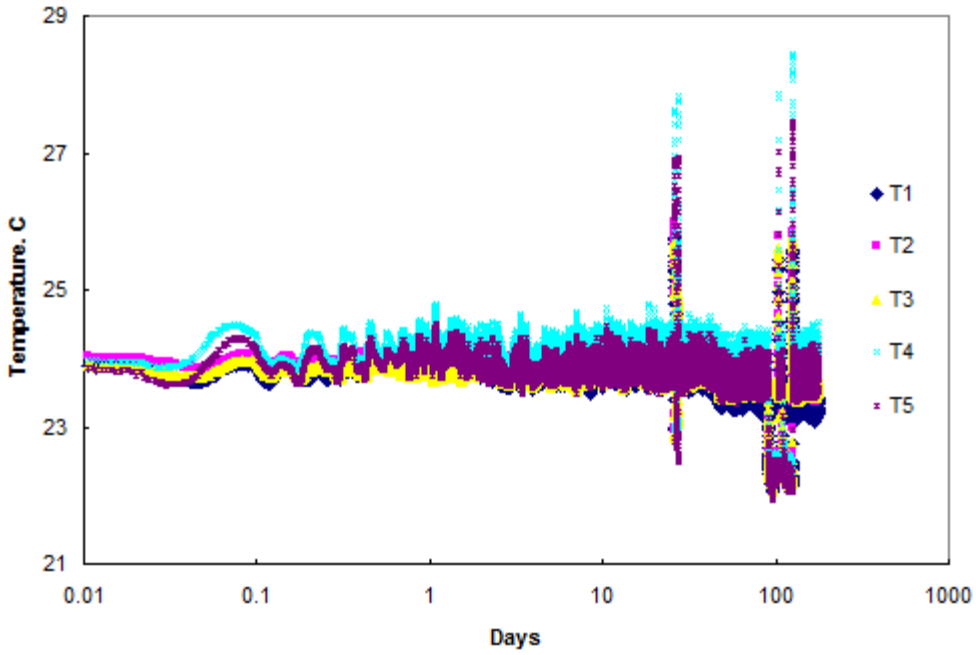

Figure 4.42 Temperature graph-huff-puff production process-sand packed

Figure 4.42 shows that the core temperatures were relatively stable during the whole puff process except jumping sometimes due to the restart of the heater after the temporary power loss.

4.4.4 Analysis

During the huff-puff process, no oil was produced out for both long cores. The possible reason for this is that the residual oil near the core outlet was pushed far away towards core inlet during the multiple huff processes due to the strong dissolving ability of the liquid mixture fluid and

liquid propane into the oil. On the contrary, during the puff process, the driving energy in the core was not big enough to overcome the effect of core length and permeability to drive the foamy oil out, but it did move the foamy oil towards production end at a certain extent. To verify this hypothesis, propane flooding was planned to carry out at these two long cores next to provide driving force.

4.5 Propane Flooding

During the whole propane flooding, propane was planned as a gas phase. The injection part A (as shown in Figure 4.44) was placed in room temperature (between 20℃ to 25℃). Figure 4.43 indicates that propane is in gas phase if the pressure is below 800kPa at that temperature range.

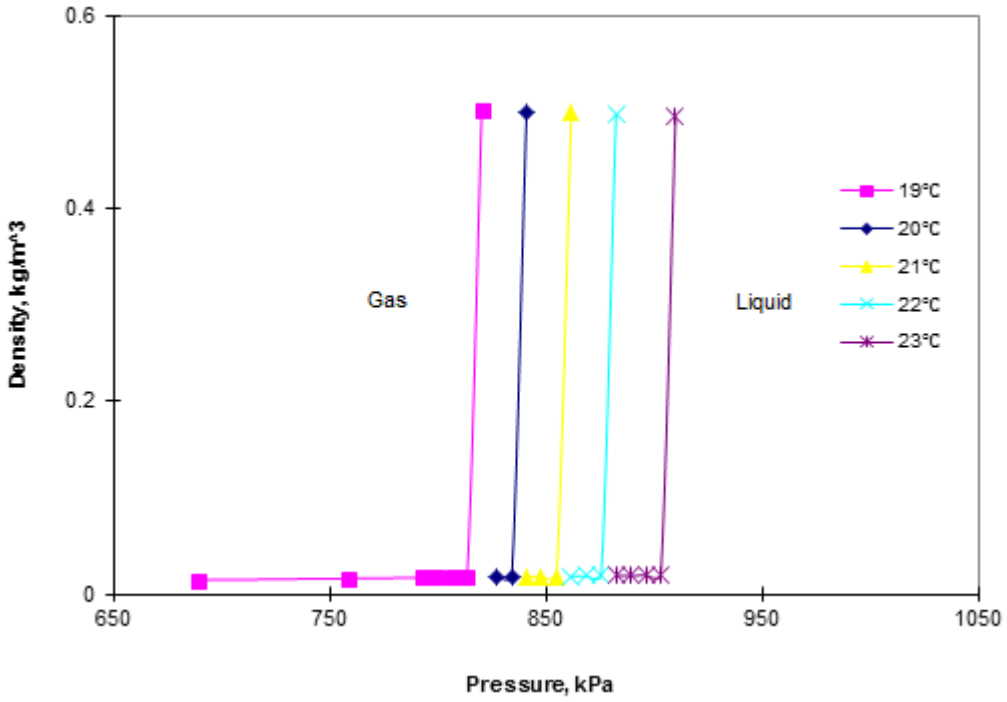

Figure 4.43 Pressure vs. density of C_3H_8 at different temperatures

4.5.1 Demonstration and Methodology

4.5.1.1 Demonstration

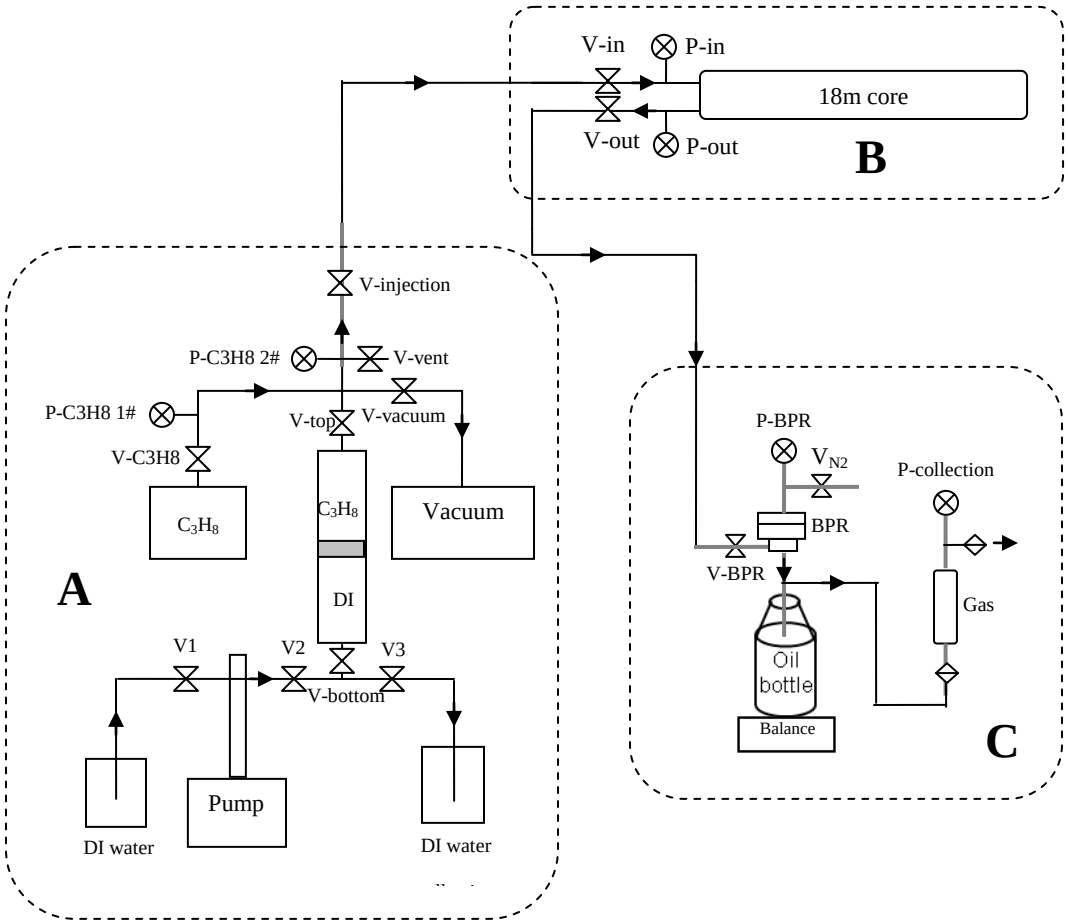

Figure 4.44 Demonstration of propane flooding process for both long cores

4.5.1.2 Methodology

4.5.1.2.1 Glass Beads Packed Core

As Figure 4.44 shows, part B indicated propane was injected from the core inlet and produced from the core outlet.

At injection part A, after vacuuming the connection tubes, gas propane was charged into the piston cylinder from a propane tank. In order to maintain propane in gas phase at varying room

temperature, the related valves were closed quickly to control the propane pressure in the piston cylinder between 689-758kPa. At the beginning of injection, the core outlet valve was closed and the inlet valve was opened slightly. Gas propane was slowly charged in to increase core inner pressure to around 689kPa, and then the core outlet valve was opened for the real propane flooding to occur. During the whole flooding process, propane needed to be refilled to the piston cylinder many times to maintain injection, pump injection rate needed to be adjusted momentarily to maintain a slow injection.

At production part C, a plastic bottle was used for oil production, a stainless steel bottle was set for gas collection. When its inner pressure reached to 34.5kPa, gas would be released automatically. At this flooding process, the production mode was different from previous processes. First, the BPR pressure was set just above the core inner pressure. Second, when production began, it was slowly released for several steps until atmosphere pressure was reached, Third, it was maintained stable for a period of time after each step.

4.5.1.2.2 Sand Packed Core

All methodology was the same as glass beads packed core except for the following:
First, due to the lower core permeability, to maintain a gas propane injection for the pressure build-up process in the core was impossible, the flooding process started earlier than the glass beads packed core. Second, at 46.9 days which was just before production, the core outlet pressure was around 207kPa, which was too low to set a suitable BPR pressure. Therefore, the BPR pressure was set at the atmospheric. Third, due to the impossibility of continuing gas propane flooding, the injection pump pressure was set above the propane vaporizing pressure after 72.8 days. That means liquid propane flooding occurred since then. Fourth, the flooding process was terminated after around 3 months due to zero production.

4.5.2 Experiment Result

4.5.2.1 Glass Beads Packed Core

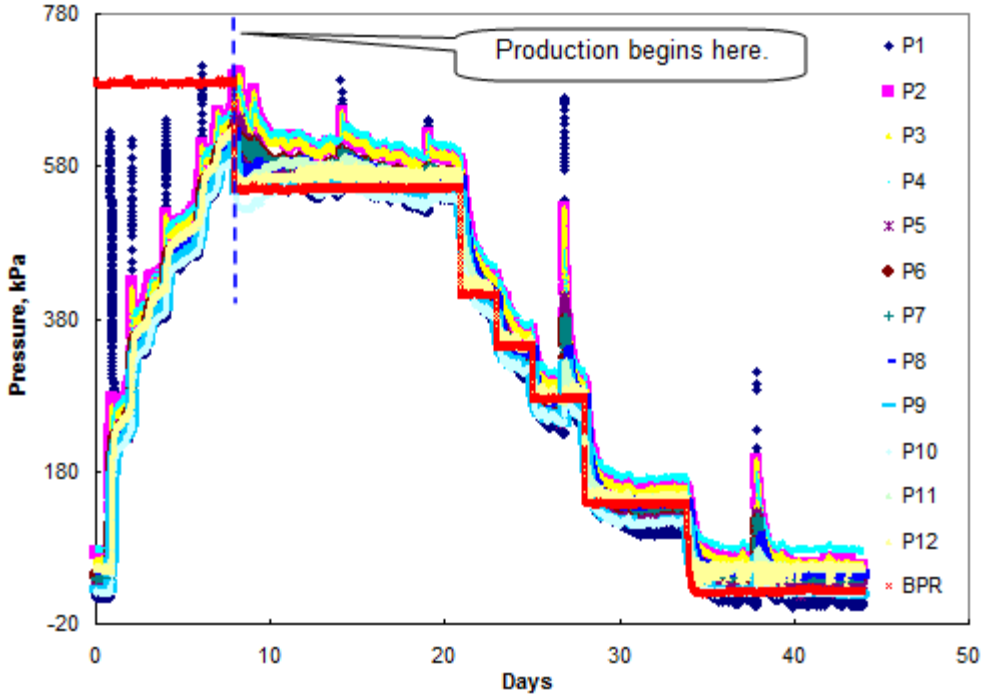

Figure 4.45 Pressure curves of C_3H_8 flooding process-glass beads

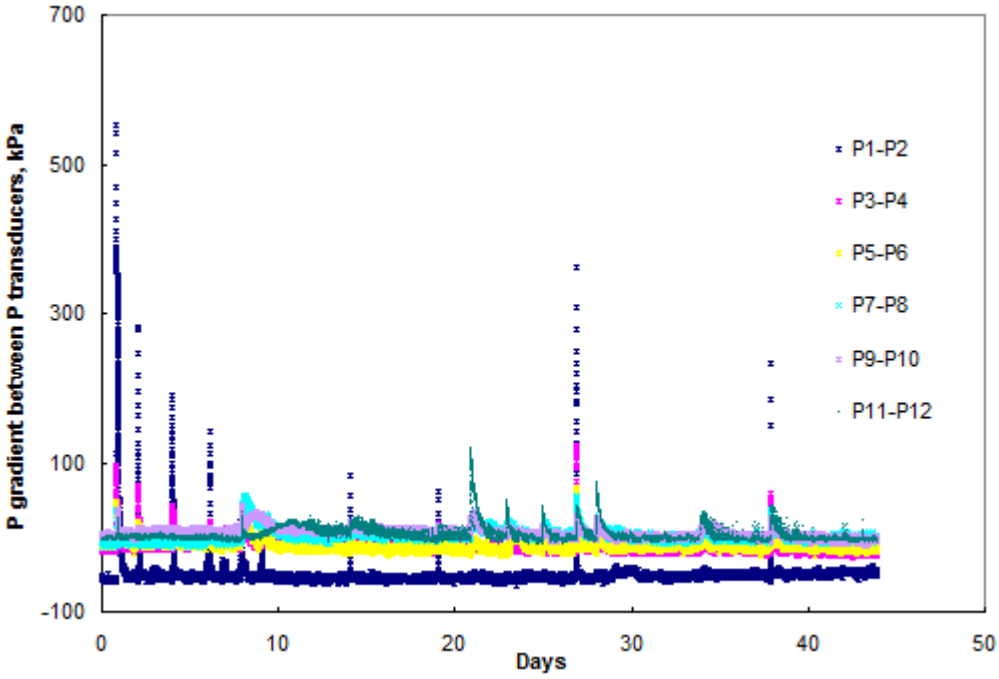

Figure 4.46 Pressure gradients of C_3H_8 flooding process-glass beads

Figure 4.45 presents the pressure variations during the flooding process. At the left of the dashed blue line area, core pressures raised up gradually in the core. At the dashed blue line point, when the core inlet pressure is around 689kPa, production started. At the right of the dashed blue line area, the real flooding process began. The BPR pressure was released at 6 steps to the atmospheric. The core inner pressures transmitted quickly at the whole flooding process due to the higher core permeability. Pressure peaks here were caused by propane piston cylinder refilling.

Figure 4.46 indicates that the pressure gradients did not build up throughout the core due to the higher permeability.

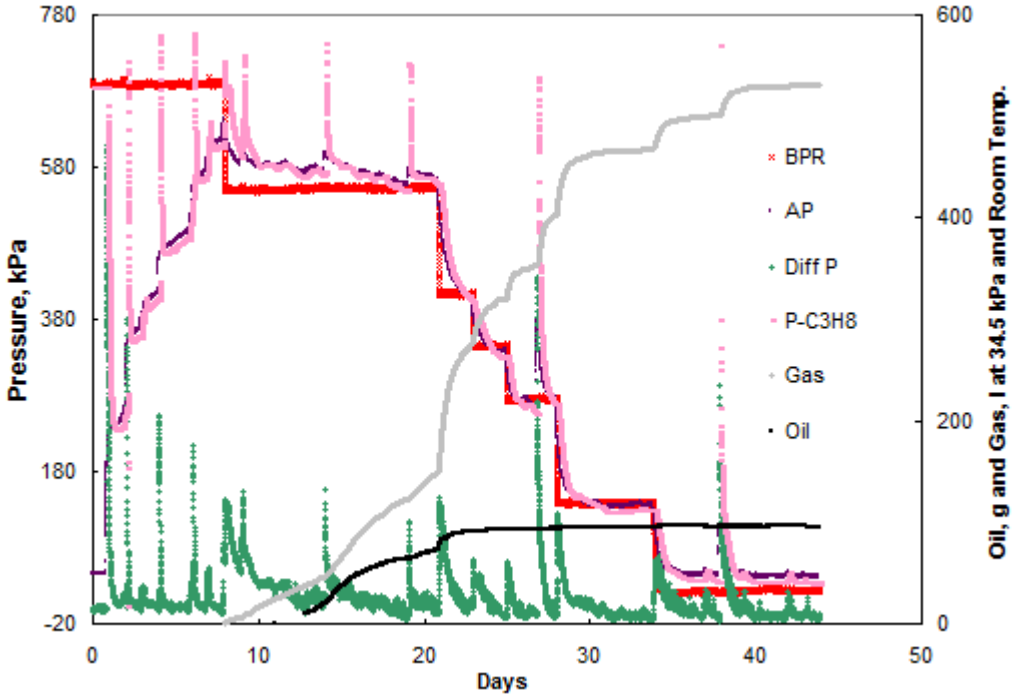

Figure 4.47 Production curves of C_3H_8 flooding process-glass beads

Figure 4.47 shows the relationship of average and differential pressures and production curves. First, core average pressure built up gradually to 641kPa. Second, BPR pressure was released from 689kPa to 552kPa to begin flooding. Due to free gas in the core, partially miscible flooding and solution gas drive both occurred, average pressure decreased slowly at the first BPR pressure releasing process. Gas production began at the same time when BPR pressure was equal to core

outlet pressure. The continual oil production started after 4.8 days. The oil production rate was high for several days, and then slowed down. This oil bank probably formed during huff-puff process and was moved closer to the core outlet after huff-puff production process. This verified the hypothesis made after the huff-puff process.

At the second BPR pressure releasing step, from 552kPa to 414kPa, core average pressure decreased quickly and gas and oil productions increased fast. These indicated that solution gas played an important role during this process. Not too much oil was produced out at the following BPR pressure releasing steps. The BPR pressure releasing rate and level should be further studied later to get more oil out.

The propane piston cylinder was refilled to the many times to continue flooding. Each sudden increase of gas production was related to BPR pressure release and propane piston cylinder refill. The change of differential pressure was affected by the changes of propane piston cylinder pressure and BPR pressure closely, but the peak shapes were different. The peak of differential pressure related to BPR pressure drop had gentle slopes, especially at first two steps of BPR pressure drops. These indicated there was solution gas coming out of the oil.

After recalculation, there was 98.15g oil, or 5.15% OOIP that was produced.

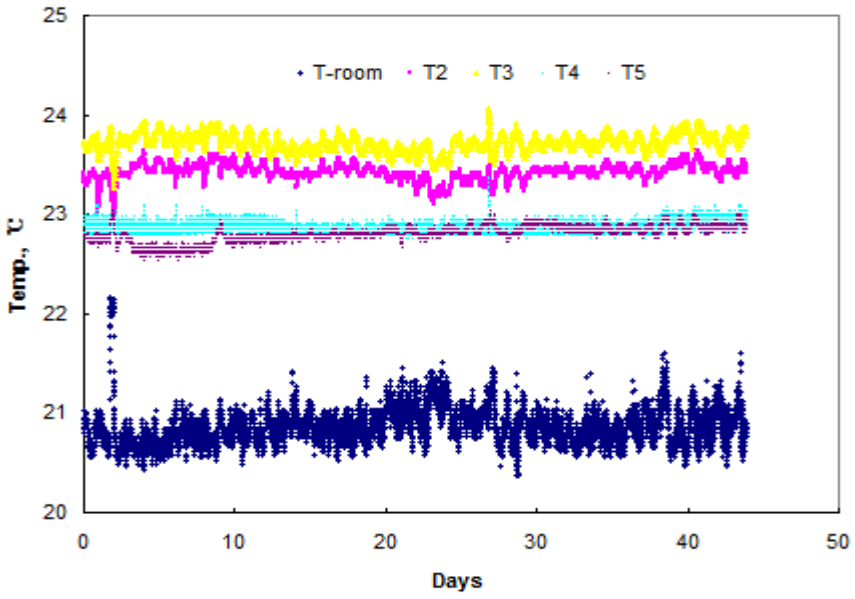

Figure 4.48 Temperature curves of C_3H_8 flooding process-glass beads

Figure 4.48 was temperature curves during the whole propane flooding process. All temperatures were relatively stable except the room temperature was a little bit lower than others.

4.5.2.2 Sand Packed Core

Figures 4.49 and 4.50 demonstrated the whole propane flooding process for sand packed core. This flooding process can be discussed into 4 parts from beginning to the end.

Part 1

Figure 4.50-split graph shows that gas propane was slowly injected to the core inlet at 3.8 days. All core inner pressures went up from P_1 to P_{12} one by one. After that, P_2 and P_3, P_4 and P_5 together with P_6 and P_7 decreased, others kept going up slowly. This phenomenon indicated that gas path between P_1 and P_2 was shut off after the fluid redistribution by gas propane injection.

Part 2

At 11.4 days, P_2 and P_3 began to increase slowly. There were two possible reasons for that. First, pump pressure was raised up gradually thus broke through the shut-in path again; Second, the injection gas propane dissolved into the oil and change its property, the fluid distribution was reset, gas path was reopened between P_1 and P_2.

Part 3

At 46.9 days, the core inlet pressure was close to the liquefied pressure of propane. To maintain a gas flood, we opened the core outlet valve to start production. Core pressures dropped slowly from P_{12} to P_4 one by one. Gas production began at the same time but slowed down very quickly. That meant the gas movement in the core was extremely slow. P_4 and P_5 began to increase sluggishly. This was caused by fluid redistribution after production. Gas path between P_3 and P_4 was opened, but gas path between P_5 and P_6 was shut off.

Part 4

To speed up the flooding process, the propane piston cylinder pressure was increased three times at 72.8, 75, and 75.8 days, therefore, P_1 to P_5 all jumped up with them. With the pressure rise-up

beyond the propane liquefied pressure, propane began to liquefy. The pressure transducer of the propane piston cylinder was closed at the third rise-up because the pressure was beyond its range limit.

There was not too much gas production (totally 10 gas purges-1500ml) until the flooding process was terminated. This indicated that the gas channel was closed at a large extent by the swelled foamy oil which formed at huff-puff process.

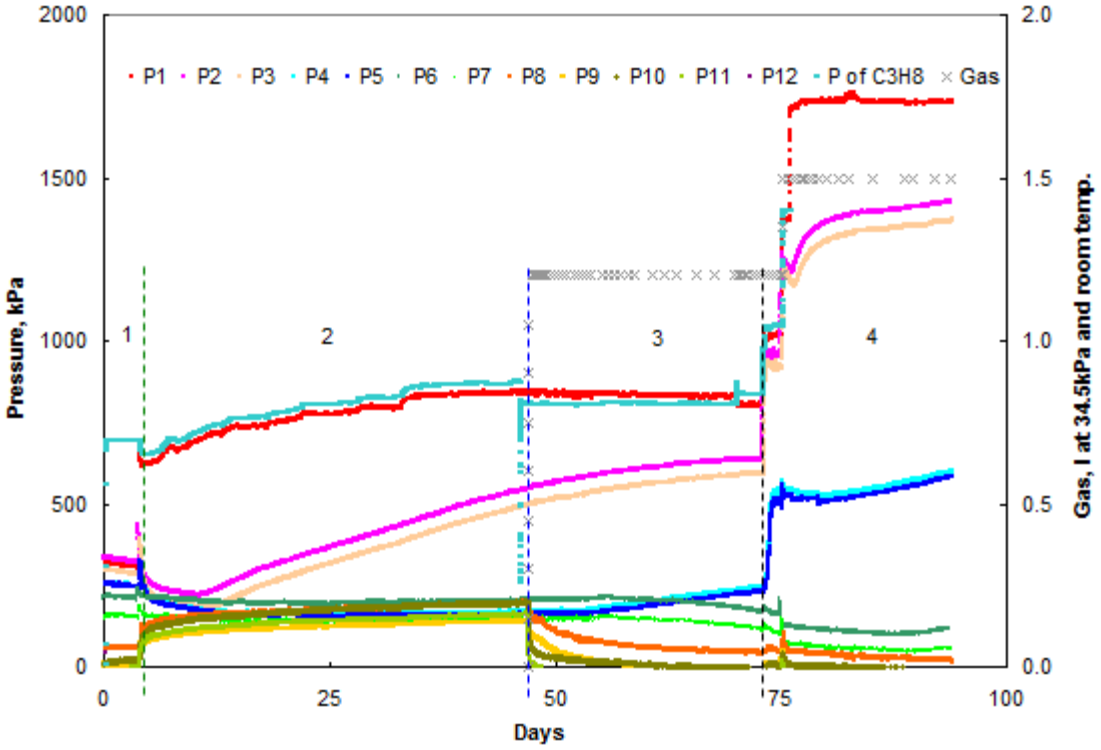

Figure 4.49 C_3H_8 flooding process-sand packed

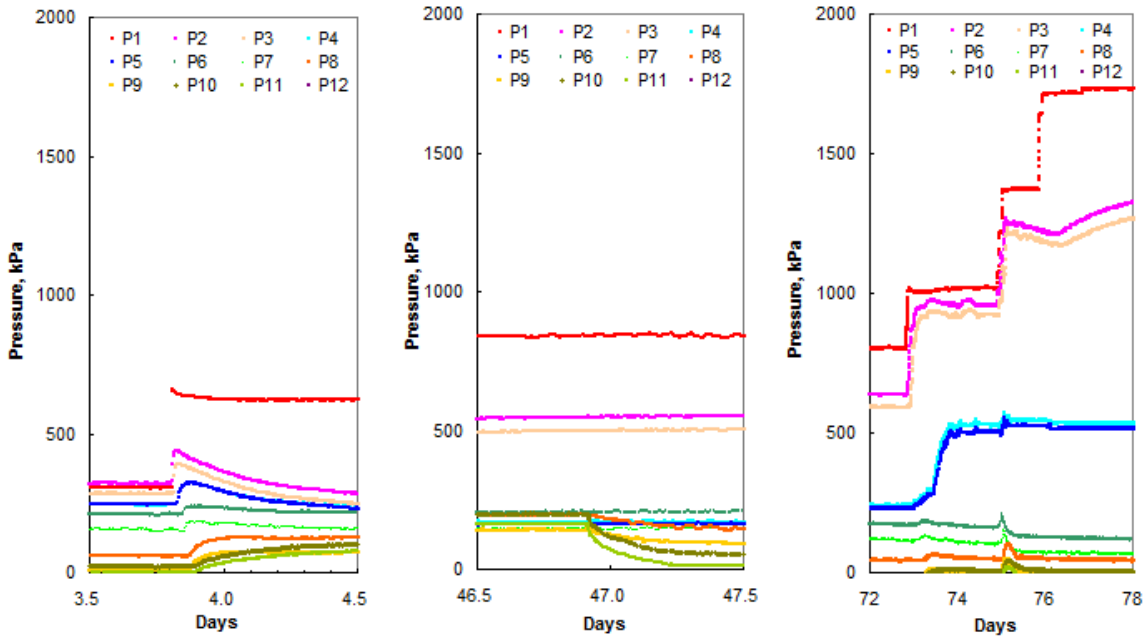

Figure 4.50 Split graphs C_3H_8 flooding process-sand packed

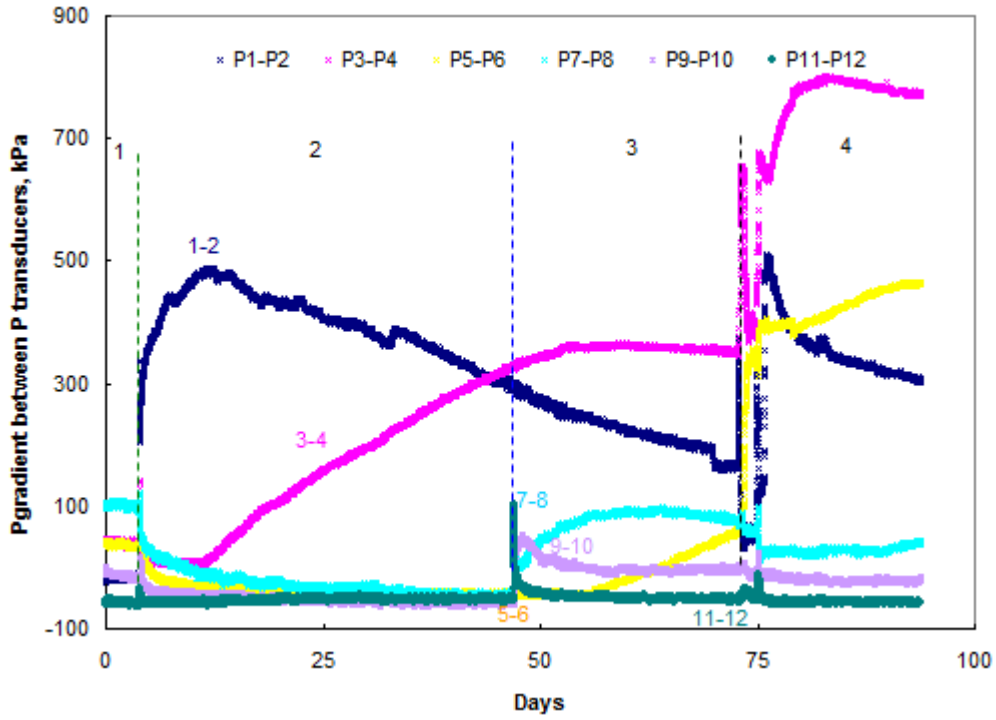

Figure 4.51 Pressure gradients of C_3H_8 flooding process-sand packed

Figure 4.51 shows that the pressure gradients were mainly built up from core inlet to the middle of the core (P_6), the other half core was less affected by propane flooding, thus it limited the core production dramatically.

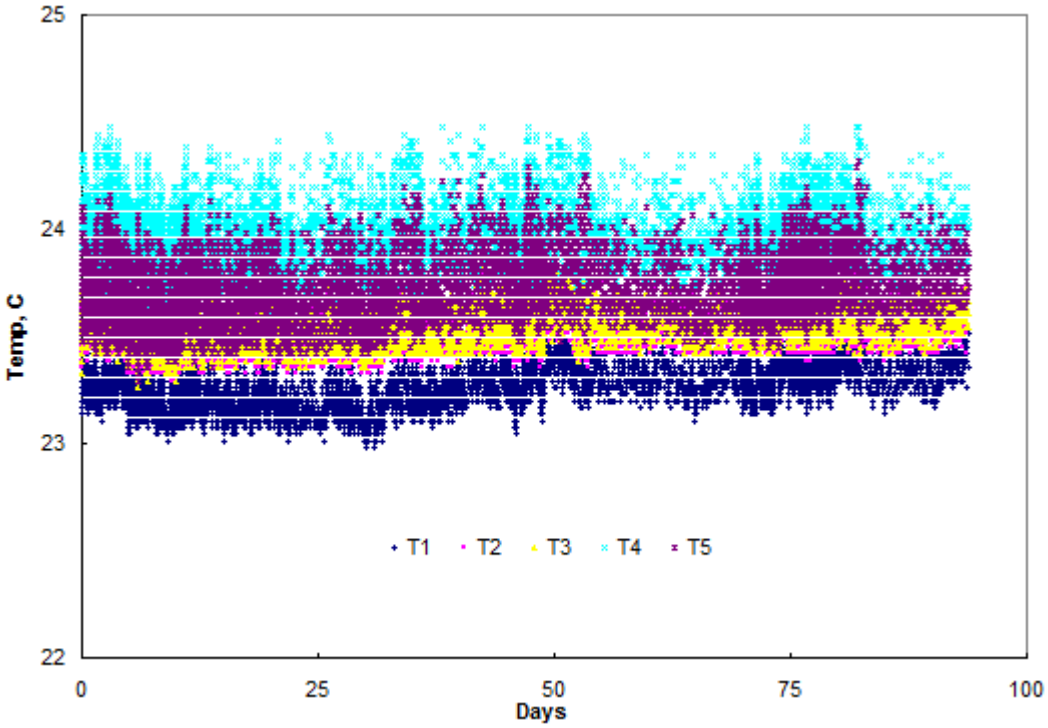

Figure 4.52 Temperature curves of C_3H_8 flooding process-sand packed

As shown in Figure 4.52, all temperatures stayed stable during the whole propane flooding process.

Chapter Five: Experiments and Results: Part 2-1.5m New Core

5.1 Purpose

All the three gas recharging processes were tested at these two long cores. From the relationship of core pressure variations and production graphs, core permeability difference, and the composition analysis of produced gas, gas recharging mechanisms have been revealed. But in order to know better about the oil and gas movements in the core during each process, a 1.5m in length core was designed to repeat all the processes performed at both long cores. This time, a CT scan was conducted to capture oil and gas migration information at each process before and after.

5.2 Preparations

Before the experiment, some preparations need to be performed. Core, related saturation fluids, gas recharging rig set up and data acquisition system (DAS) are necessary and will be introduced as follows.

5.2.1 Core Preparation

A ready to use core preparation includes sand selection, core holder design, core packing, and packing results check. All these will be described below.

5.2.1.1 Sand Selection

To get a better packing core, Ottawa silica sand F-62 was selected for core packing. Ottawa sand[62], so called because it is mined in Ottawa, Illinois, is used in many experimental situations because the individual sand particles are uniform in size and spherically shaped. Its rounded grains of clear colorless quartz, diamond-like in hardness, are pure silica (silicon dioxide) uncontaminated by clay, loam, iron compounds, or other foreign substances. Consequently, the behaviour of this material may be modeled as a group of uniformly sized spheres and considered theoretically.

How to estimate if the core is packed well or not? It is assumed that the particle spheres are all in contact with one another. This condition is referred to as "close packing". In the least efficient

close packing form, simple cubic packing (SCP), it can be shown that solids fill 52% of the total volume of a sample. In the most efficient close packing arrangement, cubic close packing (CCP), solids fill 74% of the total sample volume.

The sand particle distribution of Ottawa silica sand F-62 is shown below:

Table 5.1 Sand particle distribution of ottawa silica sand F-62

Mesh size.		Result tested				Result from U.S. Silica	
		Sand weight, g		Ind%	Cum%	Ind%	Cum%
No.	mm			Retained	Retained	Retained	Retained
+40	420	20.61	799.87	2.6	2.6	6.7	6.7
+50	297	156.00		19.5	22.1	21.5	28.2
+60	250	119.71		15.0	37.0	/	/
+70	210	/		/	/	27.4	55.6
+80	177	213.63		26.7	63.8	/	/
+100	149	124.42		15.6	79.3	27.9	83.5
+120	125	70.78		8.8	88.2	/	/
+140	105	60.55		7.6	95.7	14.3	97.8
+200	74	32.28		4.0	99.8	2	99.8
<200	<74	1.89		0.2	100.0	0.2	100.0

5.2.1.2 Core Holder Design

To be used for CT scan, the core holder was made from an x-ray transparent aluminum tube-1.866mm in inner diameter and 150cm in length. To prevent sand out, two cylinder-shaped stainless steel slices were designed and placed at both ends of the tube inside the tube fittings. As shown below, 13 axial distribution small holes were designed at one side of the slice for fluid flowing, three crossed axial lines and two round circles in different diameters were designed at another side. A mesh size 200 sieve was welded at this side to prevent sand out. In order to do a better comparison, no overburden was added which is the same as two long cores.

Figure 5.1 Photos of two slides

5.2.1.3 Core Packing, Leak Testing, Vacuum, and CT Scan

Fixed the core holder upright and attached it to a vibrator, the F-62 sand was slowly poured into the core holder along with isopropyl alcohol (IPA). The initial volume of core holder (bulk volume) and the weight of the sand poured into the core were measured to estimate of the pore volume. The core was also softly hit with a rubber mallet to remove all the air bubbles and generate a uniform pack. Wet packing the sand created a uniform pack and IPA was used since it is volatile and rapidly evaporated.

After the sand was packed in the core holder, air was continuously injected and flowed through the core for 72 hours to completely dry the porous medium. Then, to ensure that all the fittings, valves, lines and pressure transducers were not leaking, nitrogen gas was used to pressure up the core. The core was shut in; the pressures at both ends of the core were monitored for several days. At constant temperature, if there was no pressure drop with time, the core was considered to be leak free.

After leak test, nitrogen gas was released and carbon dioxide was injected into and vacuumed out of the core for 3 times to remove all the nitrogen from the sand and ensure no trapped gas remained in the system. Nitrogen was displaced by carbon dioxide because unlike nitrogen, carbon dioxide is soluble in water, so if there was any remaining gas it would most likely dissolve in the brine, as it was flooded.

After the third vacuum, the core was CT scanned to ensure the sand pack was uniform and tight. It was scanned axially at small intervals; if there were any cracks or pockets in the sand, this could be reflected from the core density distribution. As shown in Figure 5.2, the core density was almost uniform except core inlet and outlet areas. The higher density at inlet area was caused by manually packing tightly there. The core was considered uniformly packed except both end areas. Furthermore, the average core porosity is 32.78%, this shows that solids fill 67.28% of the total volume of the core, which is between 52% (simple cubic packing) and 74% (cubic close packing), this indicates the core was efficient close packing.

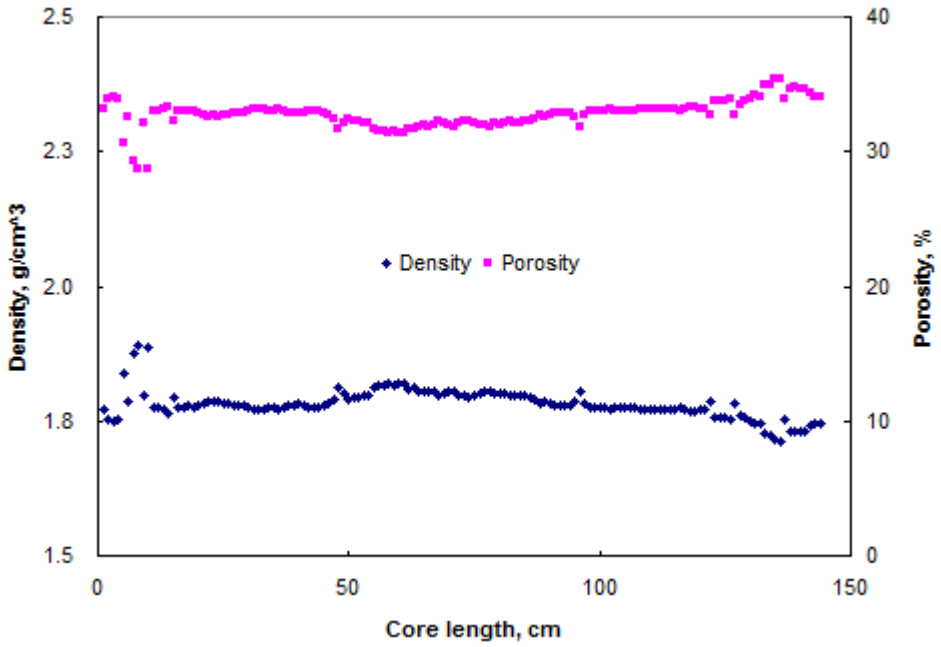

Figure 5.2 Evacuated core density and porosity distributions by CT scan

5.2.2 Fluid Preparation

After core preparation, the saturation fluids (brine and live oil) should be prepared too.

5.2.2.1 Brine

Brine was a 2 wt% sodium chloride and water solution. Solid sodium chloride was added to deionised water. Covered and mixed with a magnetic mixer until the solid all dissolved. Afterwards the brine was poured into the top of a piston cylinder to fill it up and attached the top to a vacuum pump to vacuum for 0.5hour until brine came out of the cylinder to the glass

container which was connected to vacuum pump. Closed the top valve of the brine cylinder and the valve to vacuum pump, stopped vacuum and removed the vacuum pump. Now the brine was ready to be injected to the evacuated core.

5.2.2.2 Dead Oil

To better compare results between the 1.5m in length core and two 18m in length cores, Luseland dead oil was chosen to make live oil for the 1.5m in length core, which was the same as Goodarzi[29] did for the two long cores.

5.2.2.3 Live Oil Making

As shown in Figure 5.3, a 6L piston cylinder (mixer) was chosen to make the live oil. The piston was placed at the mixer's bottom end (right side). Let the mixer top end (left side) up, the Luseland dead oil was filled in. Then, two small stainless steel balls were put into the mixer from the top end either. Closed the top end and let mixer lay down as the figure showed. A methane cylinder was connected to the top end for charging methane in later. An ISCO pump was connected to its bottom end to control pressure. A pressure transducer was set up at both ends to monitor pressure change. A thermocouple was stuck on the mixer outside surface near the top end to monitor room temperature change. This mixer was held in the middle but a little bit closer to the bottom end. An air pump was used to automatically rock the mixer up and down. The rock speed could be controlled by the air flow rate. The two small balls rolled inside the oil and methane to mix them better during rocking. The temperature and top and bottom pressures of the mixer were monitored. If the top pressure drops, it indicates that insufficient gas is in the mixer (some gas dissolved into the oil). Methane was recharged in and the mixer was rocked again. Repeated this step until the top pressure was stable for 48 hours. This was assumed that oil was saturated at that pressure.

Before using the live oil, the free gas in the top end of the mixer needed to be released. Set the mixer vertically with top end up. Injected water at bottom end of the mixer at 138kPa to overcome the resistant force of piston, which was higher than the top end pressure. A tube was connected to the top end valve. Another end of the tube was put into a water cup and a flexible vent duct was placed above the water cup to capture the escaping gas. The top end valve was

opened just a little bit to try the best to maintain the constant oil pressure. Kept constant pressure injection from the bottom of cylinder by pump as the top free gas escaped. If the pump could not maintain the set-pressure, the top outlet valve was closed. Once the pump pressure increased again to the set-pressure, the top outlet valve was opened less than before. Kept doing this until live oil came out of the tube end to the water. Closed top end valve. There was no more free gas cap left in the top, the live oil was ready to be used.

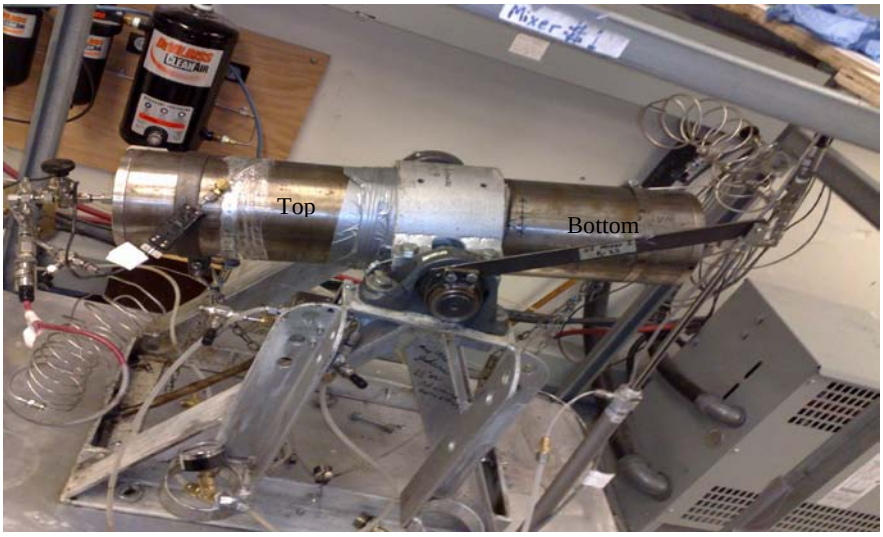

Figure 5.3 Photo of live oil mixer

5.2.3 Gas Recharging Rig

As Figure 5.4 shows, the gas recharging rig was designed the same way as the two long cores except the shorter core length and temperature control method.

5.2.3.1 Design and Set up

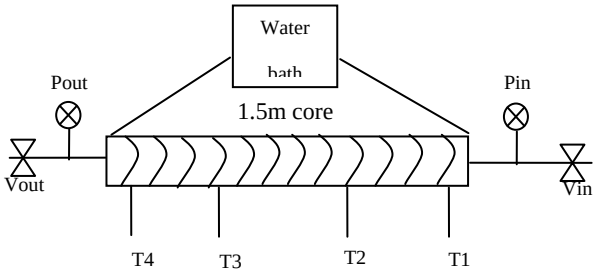

Figure 5.4 1.5m in length sand packed core rig

5.2.3.2 Temperature Control

Considering the highly compressible nature of the fluids inside the core, small temperature changes resulted in noticeable pressure fluctuations. Therefore, it is important to try and keep the temperature of the system as constant as possible.

To ensure this core can be scanned by CT and the temperature can be maintained, a heating and cooling water bath was used for this purpose. The core was wrapped by a long flexible plastic tube (as show in Figure 5.4), and both ends of the tube were connected to the inlet and outlet of water bath separately. The water bath temperature was set at 23℃ all the time and the core was isolated to prevent heat transfer to maintain a stable core temperature.

5.2.3.3 Data Acquisition

Each system required individual data acquisition. Programs were developed in Labview by Sam Wu to log and report all the related data to a computer display screen and save the data to a spreadsheet file for further study.

5.2.4 Calibration of Pressure Transducers

To get accurate data, all the pressure transducers used in this study were calibrated before connecting to the system using a Chandler Engineering Co. dead weight tester (Figure 5.5). A linear relationship between pressure and the voltage was attained and input into the software to automatically capture the pressure datum.

Figure 5.5 Photo of dead weight tester

5.3 Parameter Measurement before Experiment

After all the preparation works have been finished, the parameter measurement will be the last step before experiment. Core and fluid property measurements are included here.

5.3.1 Core Properties

5.3.1.1 Absolutely Permeability-Kg

- ✧ Connected core inlet to a Helium cylinder and outlet to a 50ml glass flow-meter (burette).
- ✧ Opened the core inlet and outlet valves.
- ✧ Slightly open Helium cylinder valve to make a tiny flow.
- ✧ The core inlet pressure should be monitored. If flow is detected and the pressure reading shown on the Low (0–69kPa) transducer read-out has stabilized, captured the time when a bubble went up and crossed certain volume in the glass flow-meter.
- ✧ Make four readings at this unique pressure and volume, recorded the time, volume, injection and atmosphere pressures.
- ✧ Make another tiny flow (about 13.8kPa more than the first one)to repeat the above procedures. At least four tiny flow should be tested to calculated the absolutely permeability by an excel spreadsheet.

5.3.1.2 Pore Volume and Porosity

The pore volume of the core and the dead volume of the lines were measured by gas expansion. First the lines to the core were pressured to around 66.9kPa using nitrogen; a digital gauge (+/- 0.005) was used to obtain an accurate pressure reading. The gas from the lines was expanded into a water filled vessel, and the produced water from this vessel was collected. Filled water to the top of water vessel to ensure water level was the same every time. Based on the mass of the produced water and the ambient room pressure, the volume of the lines was calculated.

The same procedure was used to determine the pore volume. Nitrogen gas pressured the 1.5m sand packed core, the core was then shut in and nitrogen cylinder was then disconnected. The pressure in the core was left to equilibrate for a time before expanding the gas into a large cylinder of water. The calculated volume based on the mass of produced water here minus the dead volume equals the core pore volume. The porosity is calculated as this core pore volume

divided by the bulk volume of the sand container. Several trails were performed to confirm the pore volume measurement. The pore volume for this 1.5m core was 152.77ml and its porosity was 37.24%.

5.3.1.3 Water Saturation and Water Permeability

5.3.1.3.1 Brine Saturation

As mentioned at above, the 1.5m core was leak free, evacuated, and ready to be used, air free brine solution was also ready for use in a piston cylinder. Joined this two together, the connection lines was linked to a vacuum pump, an ISCO pump was connected to the bottom of the brine piston cylinder.

- ✧ Refilled the pump, and then ran pump at 138kPa until stable.
- ✧ Vacuumed the connection lines for several minutes, closed the valve to vacuum pump, and stop vacuum.
- ✧ Opened the top valve of the piston cylinder to inject brine into the connection lines until stable. Recorded the pump volume V_1.
- ✧ Opened the core inlet valve to saturate brine in at 138kPa until stable, recorded the pump volume V_2.
- ✧ Calculated the volume of brine saturated, V_2-V_1=158.0234ml
- ✧ Calculated the water saturation, (V_2-V_1)/V=38.52%, V is core bulk volume.

CT scan was performed after brine saturation.

5.3.1.3.2 Water Permeability Measurement

Due to higher permeability, water head method was used to this measurement. Placed the 1.5m fully brine saturated sand packed core horizontally on the floor, recorded the height of core outlet to ground. The brine container was fastened at a certain height with scale unit. Opened the core outlet valve to flow brine in for at least 20min, began measurement. Recorded the time, heights of brine head, and water weights at begin and end. The calculated differential pressure and flow rate were used to calculate the water permeability of the core. This was repeated at different height of brine head. The slope of velocity-pressure gradient profile was used to calculate the water permeability using Darcy's Law. The Figure 5.6 was showed below.

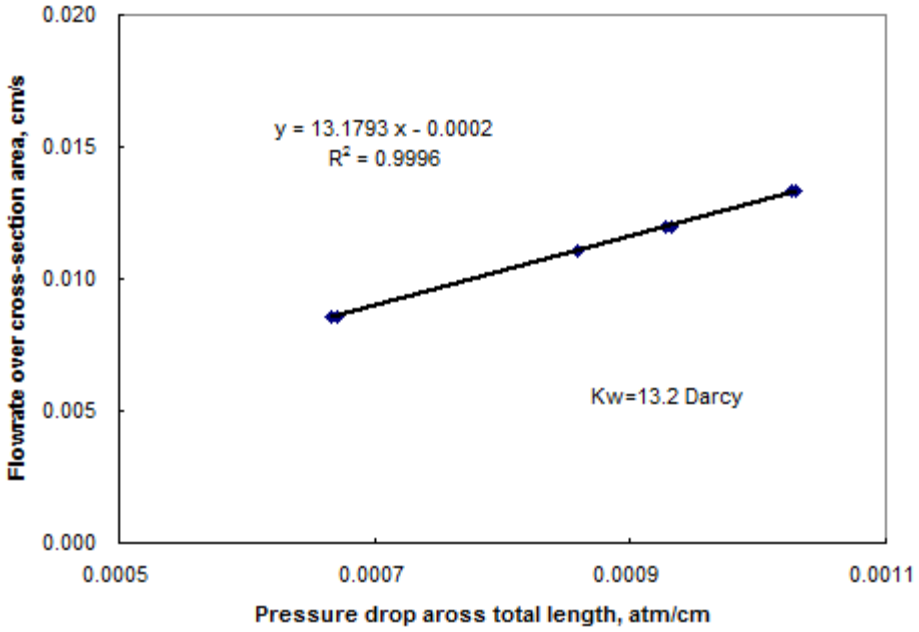

Figure 5.6 Brine permeability of 1.5m core

5.3.1.3.3 Connate Water Saturation S_{iw}

Once the brine permeability was measured, live oil was injected into the sand using an ISCO pump. The BPR at the production end was set to a pressure above the bubble point. The produced brine, oil and brine mixture were collected and measured. The total water produced was 138.9216g. The connate water saturation was calculated as the difference between the initial brine saturated pore volume of sand and the total produced volume of brine when the core was saturated with the live oil. It was 4.65%.

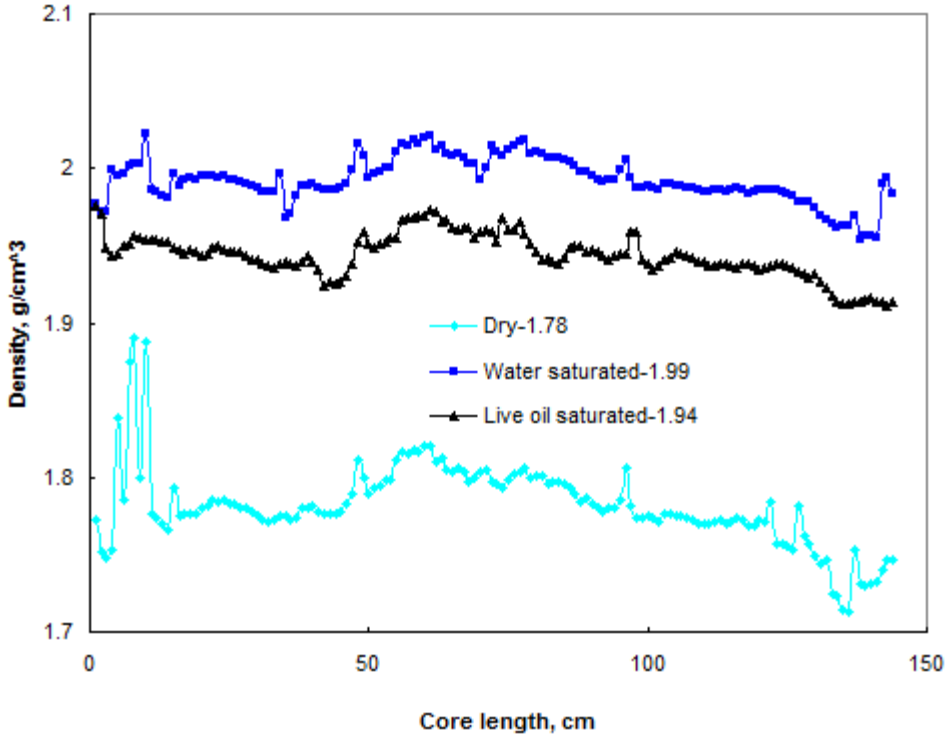

Figure 5.7 1.5m core density summary before experiment

CT scan was performed after live oil saturation. Figures 5.7 and 5.8 show the 1.5m core density summary after each core preparation process and images after live oil saturation. The average density of the dry core was 1.78g/cm^3, the lowest one. The core inlet and outlet ends were not packed uniformed, especially at the inlet end with a higher density due to locally tight pack. After brine was saturated, core density increased to 1.99g/cm^3, and both ends of the core became more uniform. The core density dropped down to1.78g/cm^3 after live oil saturation. After the live oil saturation, the CT images (Figure 5.8) showed that the higher density areas were near the core inlet end and in the middle of the core, the lower density area was at the core outlet. The pink areas of some CT images were dural aluminum tube because the core was not placed horizontally enough during scanning.

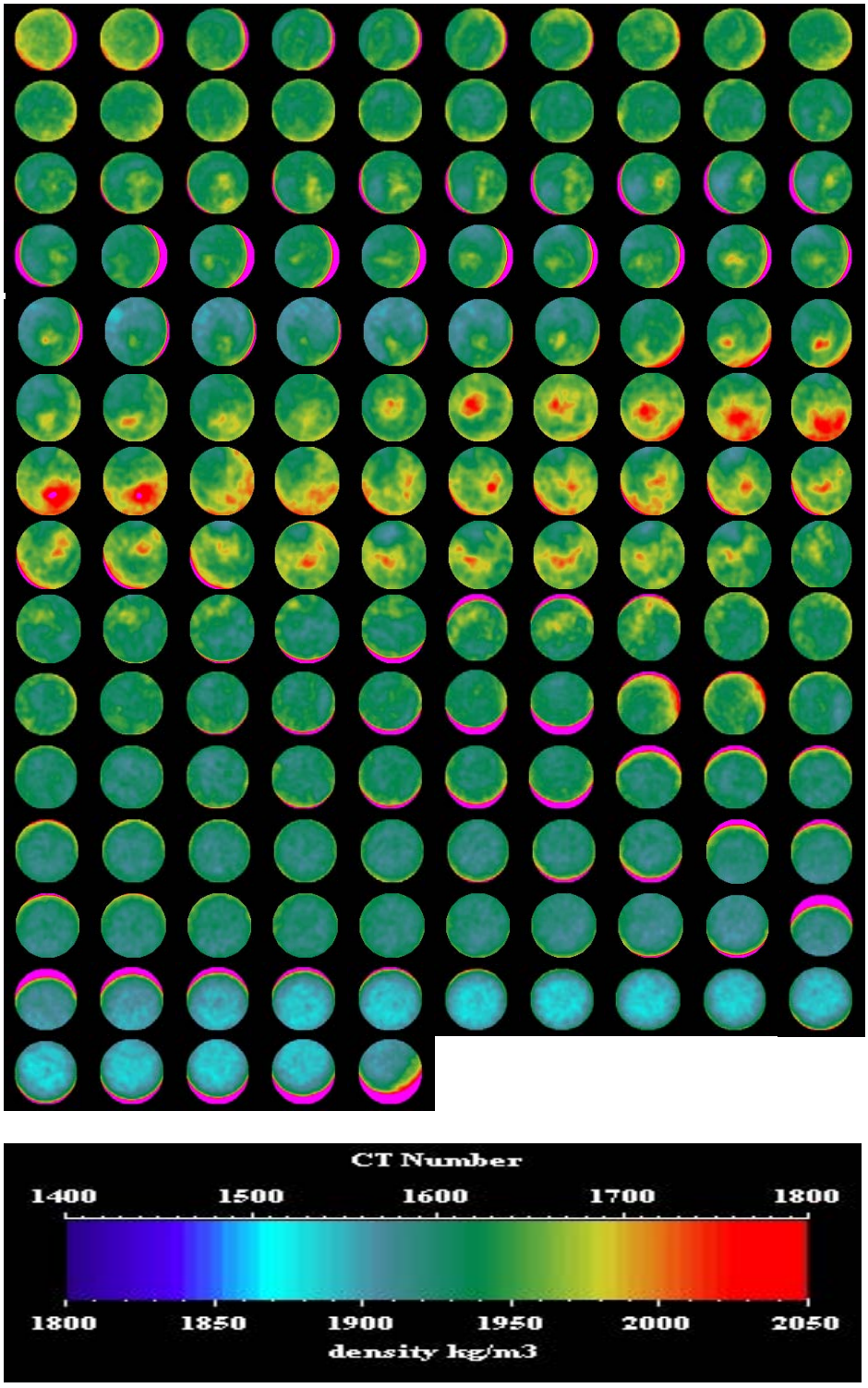

Figure 5.8 CT images of the core after live oil saturation

5.3.2 Fluid Properties

5.3.2.1 Dead Oil

5.3.2.1.1 Viscosity

A Wells-Brookfield cone and plate viscometer was used to measure the viscosity of the Luseland dead oil at different temperatures. A DV-II+ Pro Brookfield viscometer was used to measure all produced dead oil viscosity after various gas recharging processes (Figure 5.9).

The two viscometers were both connected to a temperature controlled water bath separately, allowing the viscosity to be measured as a function of temperature. The dead oil viscosities at different temperatures are shown in Figure 5.10. As expected, the dead oil viscosity decreases exponentially with increasing temperature. The dead oil viscosity at 23℃ was 11230mPa.s.

Figure 5.9 Brookfield viscometers

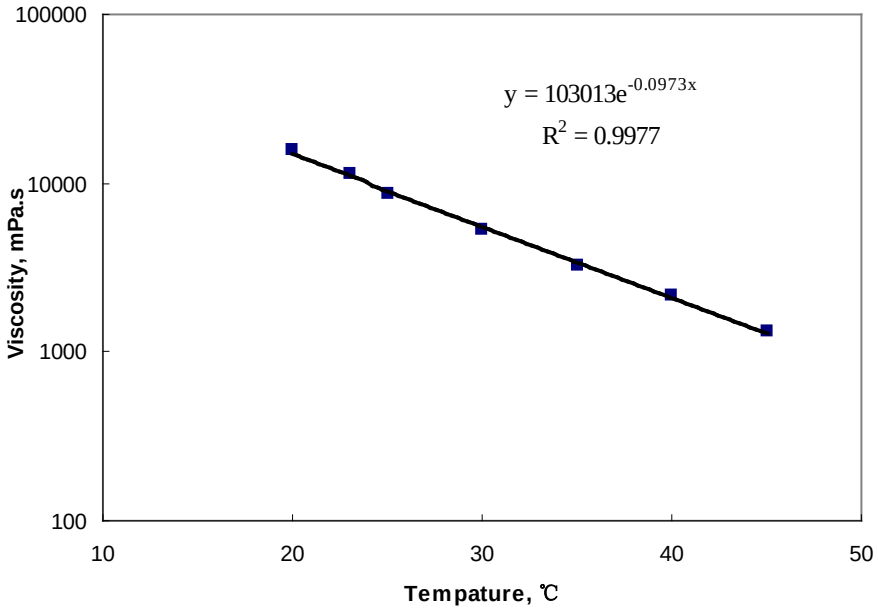

Figure 5.10 Viscosity of dead oil at different temperatures

5.3.2.1.2 Density

The density of the dead oil was measured using Anton Paar DMA 45 calculating digital density meter with a built in thermostat (Figure 5.11).

Figure 5.11 Anton Paar DMA 45 calculating digital density meter

The density meter was first calibrated using air and DI water at the operating temperature. Circulating water from a controlled bath allows for density measurements to be made at different temperatures. The sample density was measured between 20-40℃ and the results are shown in Figure 5.12. The dead oil density measured at 23℃ is 983.6 kg/m^3.

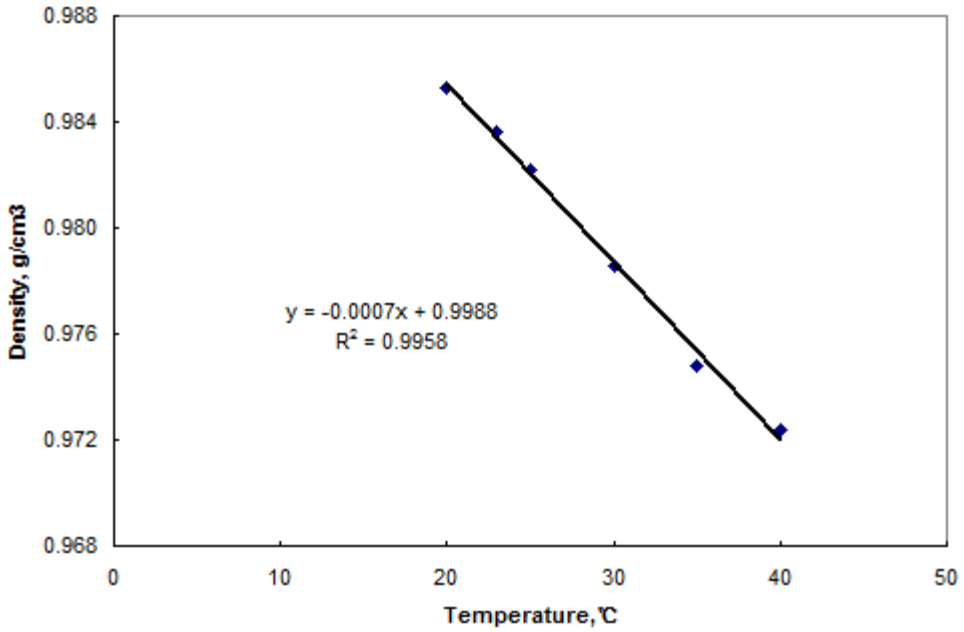

Figure 5.12 Density of dead oil at different temperatures

5.3.2.2 Live Oil

5.3.2.2.1 Viscosity

A spiral-shaped capillary viscometer was used to measure the live oil viscosity at room temperature 23℃. In this case, a 0.3175 cm (1/8 inch) OD tube of a known inner diameter and length was connected to a transfer vessel containing live oil at the inlet, and a BPR at the outlet. A Validyne differential pressure transducer measured the pressure across the stainless steel tube. An ISCO pump injected oil at a constant flow rate into the capillary tube. Once the differential pressure reading stabilized, the pump flow rate was increased and process was repeated several times. Viscosity was then calculated from the slope of the flow rate and differential pressure plot using the Hagen-Poiseuille equation $\triangle p = (8\mu LQ)/(\pi r^4)$. These plots are presented at Figure 5.13. The live oil viscosity measured at room temperature 23℃ is 5210mPa.s.

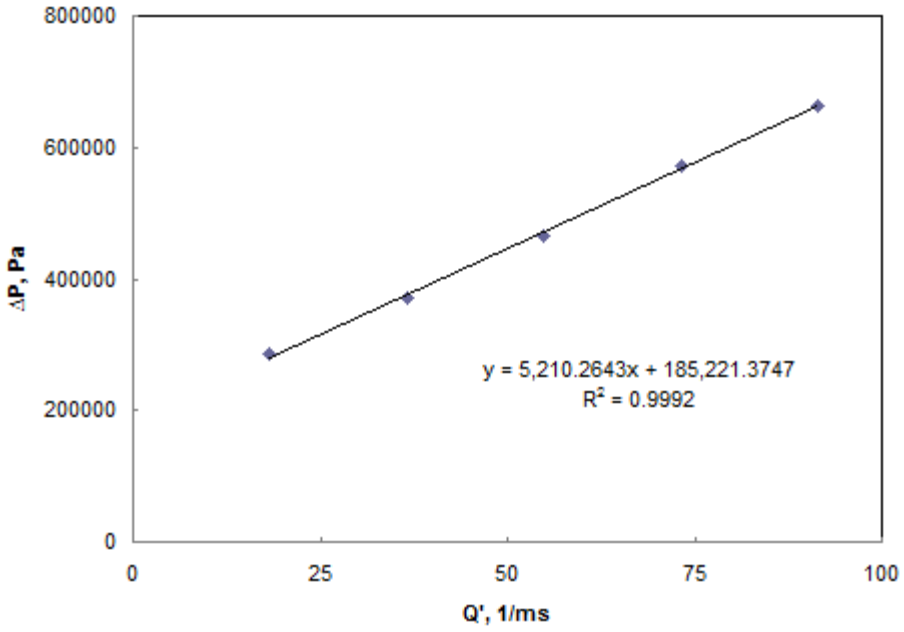

Figure 5.13 Viscosity of Luseland live oil at 23℃

5.3.2.2.2 Density

As Figure 5.14 shows, a small stainless steel piston cylinder with a tiny hole in the middle of the piston's right side was designed for live oil density measurement. This design was chosen for preventing live oil degassing during transfer process. The transfer pressure was set at 6895kPa far beyond the bubble point pressure and the measuring was at room temperature 23℃. Live oil density was calculated by measuring the mass difference of the cylinder, both empty and full of live oil. The live oil density is the mass of the live oil divided by the internal volume of the cylinder. Several trials were measured in order to ascertain that measurement were accurate. The live oil density measured at 23℃ is 969.2kg/m^3 in Table 5.2. A detailed procedure was shown below.

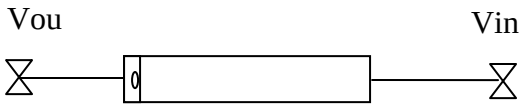

Figure 5.14 Live oil density measuring equipment

Table 5.2 Live oil density summary at 23℃

No.	Density, g/cm^3
1	0.9642
2	0.9661
3	0.9774
Average	0.9692

5.3.2.2.2.1 Dead Volume and Weight Measurements

1. Empty weight W_0

- ✧ Opened both inlet and outlet valves.
- ✧ Weighted the empty, dry and clean density measuring equipment to get empty weight W_0

2. Dead volume V_1 from V_{in} to the piston when it was to the left end of the cylinder and dead weight W_1 when DI water was filled in this dead volume at 6895kPa

- ✧ Used nitrogen pushing piston down to the right end of the cylinder.
- ✧ Evacuated from the inlet valve for 5 minutes and close this valve.
- ✧ Injected DI water from inlet valve by ISCO pump A at constant 6895kPa pressure until stable, recoded pump A volume 1.
- ✧ Opened the inlet valve slightly and kept 6895kPa injection until stable, recoded pump A volume 2.
- ✧ Closed the inlet valve and stopped pump.
- ✧ Took the density measuring equipment off and cleaned the water at the right end of inlet valve.
- ✧ Weighed the equipment again to get W_1.
- ✧ V_1 equals volume 1 minus volume 2.

3. Dead volume V_2 from V_{out} to piston when it was to the left end of the cylinder and dead weight W_2 when DI water was filled in this dead volume at 6895kPa.

- ✧ Vacuumed from the outlet valve for 5 minutes and close this valve.

- ✧ Injected DI water from outlet valve by ISCO pump B at constant 6895kPa pressure until stable, recoded pump A volume 3.
- ✧ Opened the outlet valve slightly and kept 6895kPa injection until stable, recoded pump B volume 3.
- ✧ Closed the outlet valve and stopped pump.
- ✧ Took the density measuring equipment off and cleaned the water at the left end of outlet valve.
- ✧ Weighed the equipment again to get $W_{full\text{-}left}$.
- ✧ V_2 equals volume 3 minus volume 4.
- ✧ W_2 equals $W_{full\text{-}left}$-W_1.

4. Dead volume V_3 and V_4 of the piston cylinder when piston at outlet end and at left end separately, dead volume V_5 from Vin to piston when it was at the inlet end of cylinder. Dead weight W_3 of the equipment when DI water was filled in at 6895kPa and piston was at the inlet end.

- ✧ Ran pump A and Pump B at 6895kPa from V_{in} and V_{out} together until stable, recorded Pump volume V_{A1} and V_{B1} separately.
- ✧ Opened both V_{in} and V_{out} valves slightly.
- ✧ Increased pump B injection pressure from 6895kPa to 8274kPa step by step until both pumps stable. Recorded pump A volume V_{A2}.
- ✧ Decreased pump B pressure back to 6895kPa step by step until both pumps stable. Recorded pump B volume V_{B2} and Pump A volume V_{A2}'.
- ✧ Closed both inlet and outlet valves and stopped both pumps.
- ✧ Took the density measuring equipment off and cleaned the water at the right end of inlet valve and left end of outlet valve.
- ✧ Weighed the equipment again to get $W_{full\text{-}right}$, which is W_3.
- ✧ V_4 equals V_{B1} minus V_{B2}.
- ✧ V_3 equals V_{A2}-V_{A1}.
- ✧ V_5 equals V_1-V_3.

5. Recorded room temperature and atmosphere pressure before and after each density measurement.

5.3.2.2.2.2 Live Oil Density Measurement

- ✧ The live oil density measurement was set up as Figure 5.15 shows. The whole system was gas free.
- ✧ The inlet and outlet valves were both closed with 6895kPa DI water sealed in the density measuring equipment while piston was at the inlet end of cylinder.
- ✧ The other valves were all opened and both pumps ran at 6895kPa until stable. Recorded pump volume V_{A3} and V_{B3}.
- ✧ Opened outlet valve slightly until pump B stable, recorded pump volume V_{B3}'.
- ✧ Opened inlet valve slightly and increased pump A injection pressure from 6895kPa to 11032kPa step by step until both pumps were stable.
- ✧ Decreased pump A injection pressure back to 6895kPa step by step until both pumps were stable. Recorded pump volume V_{A4} and V_{B4}.
- ✧ Close inlet and outlet valves and others valves, stopped both pumps.
- ✧ Took off density measuring equipment, cleaned right end of inlet valve and left end of outlet valve, then weighed it for W_4.
- ✧ Live oil volume $V_{live\ oil}$ was from inlet valve to piston while it was at the outlet end of cylinder. $V_{live\ oil}$ equals V_{A3} minus V_{A4} and is the same as V_1.
- ✧ The volume of DI water V_{water} was V_2 (from outlet valve to piston while it was at the outlet end of cylinder) plus V_5 (from inlet valve to piston while it was at the inlet end of piston). Water weight W_{water} could be calculated next.
- ✧ The weight of live oil $W_{live\ oil}$ equals W_4 minus W_0 minus W_{water}.
- ✧ Live oil density equals live oil weight $W_{live\ oil}$ divided by its volume $V_{live\ oil}$.

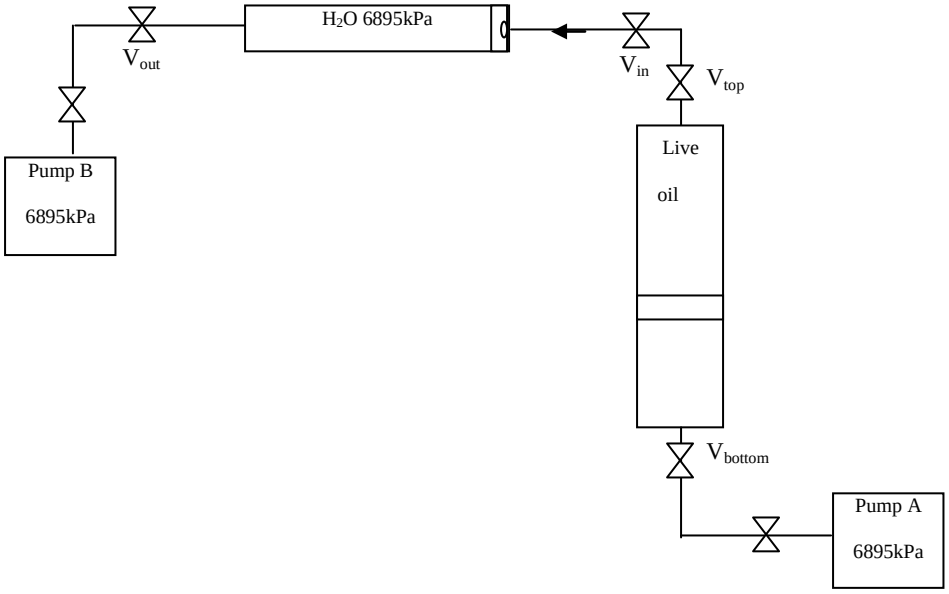

Figure 5.15 Live oil density measurement

5.3.2.2.3 GOR

After live oil density measurement, the density measuring equipment was used for gas oil ratio measurement at room temperature 23℃ (Figure 5.16). Its outlet valve (water end) was connected to an ISCO pump running at 6895kPa. Its inlet valve (oil end) was joined to screw piston sampler. The sampler was then connected to a gas-oil separator, which consists of a test tube that the live oil is injected into, and an inverted graduated cylinder submerged in water. A line from the top of the test tube routes the gas into the graduated cylinder. Initially, water was evacuated to a pre-recorded increment and as the gas expanded the water level drops; from this expansion the volume of gas was measured. The oil volume was measured from the weight of the test tube empty and with oil.

Opened the outlet valve slightly to release some live oil out to the test tube, then closed the outlet valve and waited until water level in the graduated cylinder was stable. Several trials were performed to get a accurate result. The first trial result is useless because there was DI water at the outlet end of the piston cylinder after live oil density measurement. The gas-oil ratio at 23℃ was 14.48 (Table 5.3).

Figure 5.16 Gas oil ratio measuring equipment

Table 5.3 Live oil gas oil ratio at 23℃

No.	Tube weight g	Tube and oil weight g	Oil weight g	Oil volume ml	Gas volume ml	GOR
2	11.8343	14.6163	2.782	2.8284	41	14.50
3	20.4336	23.0227	2.5891	2.6323	38.1	14.47
4	9.8771	12.7847	2.9076	2.9561	42.8	14.48
Remark	Dead oil density at 23℃ is 0.9836 g/cm^3. Average GOR is 14.48.					

Table 5.4 Properties of one 1.5m and two 18m core systems

Type	Properties			
Core	Name	Sand	Glass beads	Sand
	Length	18.55m	18.2m	1.5m
	Cross-sectional area	2.85cm^2	2.85cm^2	2.73cm^2
	Absolute water permeability	1.92darcy	11.81darcy	13.2darcy
	Pore volume	2607ml	2099ml	152.77ml
	Porosity	36.4%	37.8%	37.24%
	Connate water saturation	9.21%	7.6%	4.65%
Fluid	Dead oil viscosity at 23℃	10695mPa.s	10711mPa.s	11230mPa.s
	Dead oil density at 23 ℃	982 kg/m^3	982 kg/m^3	983.6 kg/m^3
	GOR at 23℃	14 m^3/m^3	14 m^3/m^3	14.48 m^3/m^3
	Live oil viscosity at 23℃	4837mPa.s	5688mPa.s	5210mPa.s
	Live oil density at 23 ℃	975kg/m^3	971 kg/m^3	969.2kg/m^3

The properties of 1.5m in length sand packed core system were summarized in Table 5.4. Compared with 18m in length glass beads packed core system, their fluid and core properties were much similar except the core length difference.

5.4 Experiment Processes

As we mentioned before, 3 gas recharging processes will be tested at this 1.5m in length core. But before that, primary depletion process should be applied first.

5.4.1 Primary Depletion

5.4.1.1 Demonstration and Methodology

Figure 5.17 shows the photo of wrapped 1.5m core. Figure 5.18 is the primary depletion rig set up which includes two parts. Part A is the 1.5m core system. Part B is the production system. An oil and gas collection system is designed for produced fluid collection, a mass flow controller (MFC) is used to control the BPR pressure depletion rate close to 2.34kPa/min, which is the same as what did at two long cores before.

Figure 5.17 Photo of the wrapped 1.5m in length sand packed core

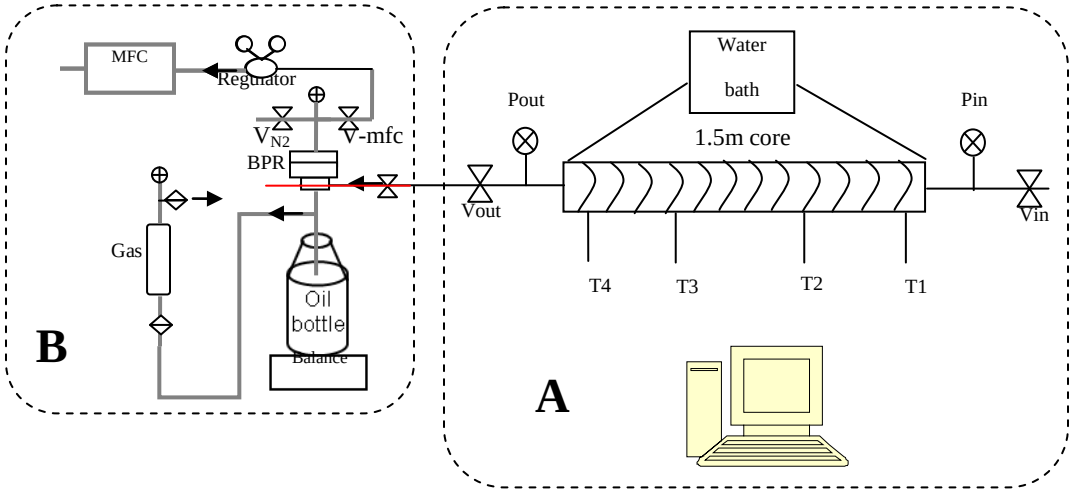

Figure 5.18 Primary depletion rig set up

5.4.1.2 Experiment Results

A dead volume measurement should be introduced before primary depletion. As Figure 5.18 shows, the red line is the dead volume, which had been tested for several trials before live oil saturation by DI water injection. After live oil saturation, live oil filled up there was 4.985ml.

Figure 5.19 is the primary depletion process for 1.5m in length sand packed core. Core outlet pressure followed the BPR depletion tendency closely. The core differential pressure changed dramatically during this process. At 20.34 days, core inlet pressure increased, this indicated the solution gas evolved from the oil, trapped and swelled the oil, thus increased the pressure to displace oil out. Foamy oil flow could happen here. Due to primary production, the oil and gas production started at the same time around 20.34 days too. After gas production finished, oil production slowed down but continued, this inferred: First, the evolved gas near outlet was produced out and left an oil bank there. Second, it was driven out partially by the energy behind it later, but the gas path was still blocked. Third, the oil produced here was foamy oil, gas was still trapped within the oil for a period of time. Separated oil samples should have been taken here to verify these guesses. Based on balance reading and NMR results, the oil produced out totally was 41.27g with the dead volume and water deducted. The oil recovery was 30.2% OOIP.

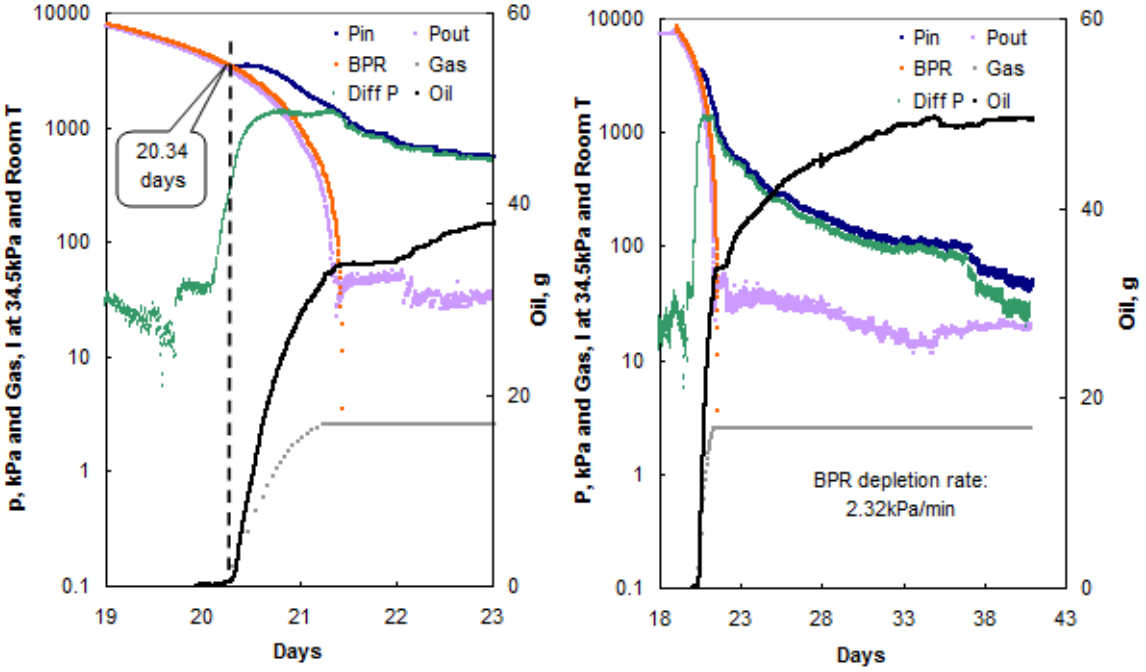

Figure 5.19 Primary depletion process-1.5m core

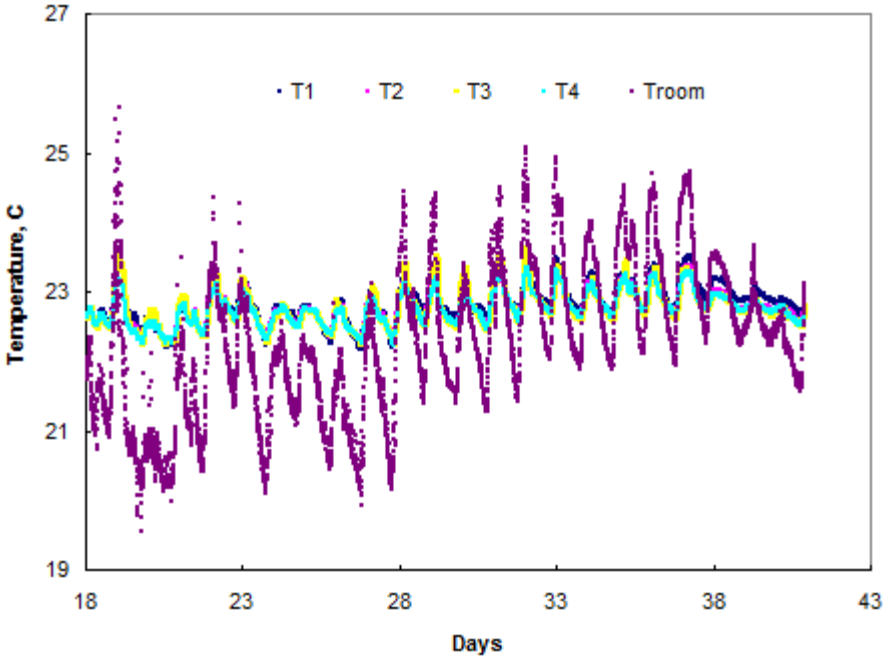

Figure 5.20 Temperature curves of primary depletion process-1.5m core

Figure 5.20 was the temperature variation during 1.5m core primary depletion process. The core temperatures were relatively stable around 23℃, but room temperature varied between 20℃ to 25℃.

CT scan was performed after primary depletion. Figure 5.21 indicates core average density dropped from 1.94 to 1.89 g/cm^3. After stripping out energy, density decreased evenly except some oil left at core outlet. Figure 5.22 clearly showed a higher density at core outlet. Compared to the CT images (Figure 5.8) after live oil saturation, the higher density area, in the middle of the core, moved towards core outlet. The density near the core inlet area decreased more. The density near core outlet area decreased less. All these demonstrated the oil migration graph from core inlet to outlet. Again, the pink areas of some CT images were dural aluminum tube because the core was not placed horizontally enough during scanning.

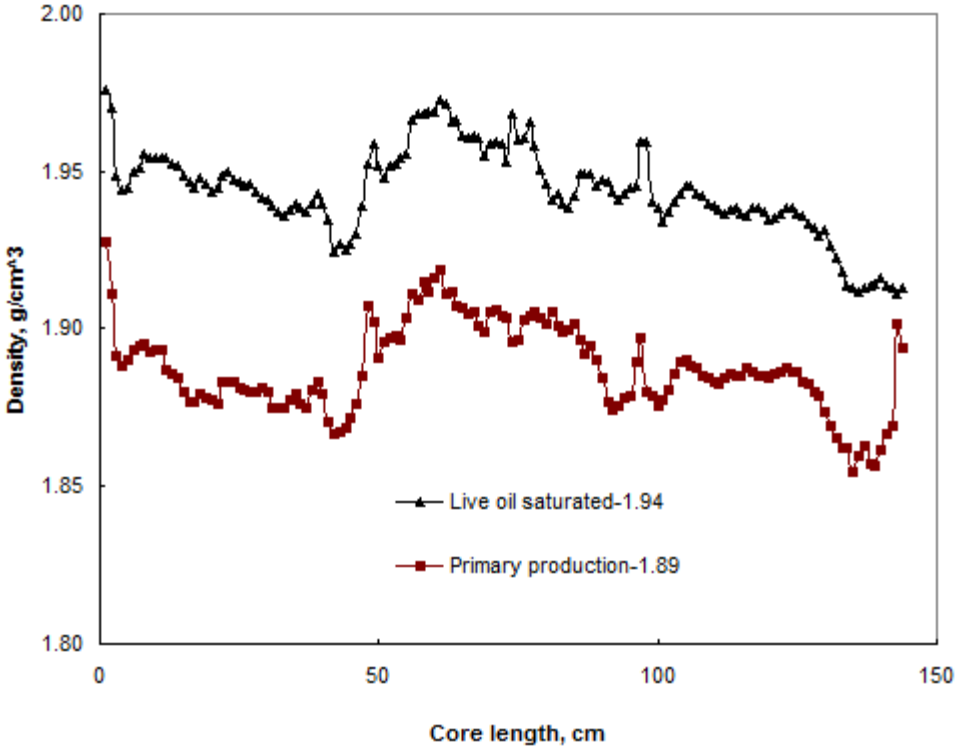

Figure 5.21 Density comparison-live oil saturated and primary depletion

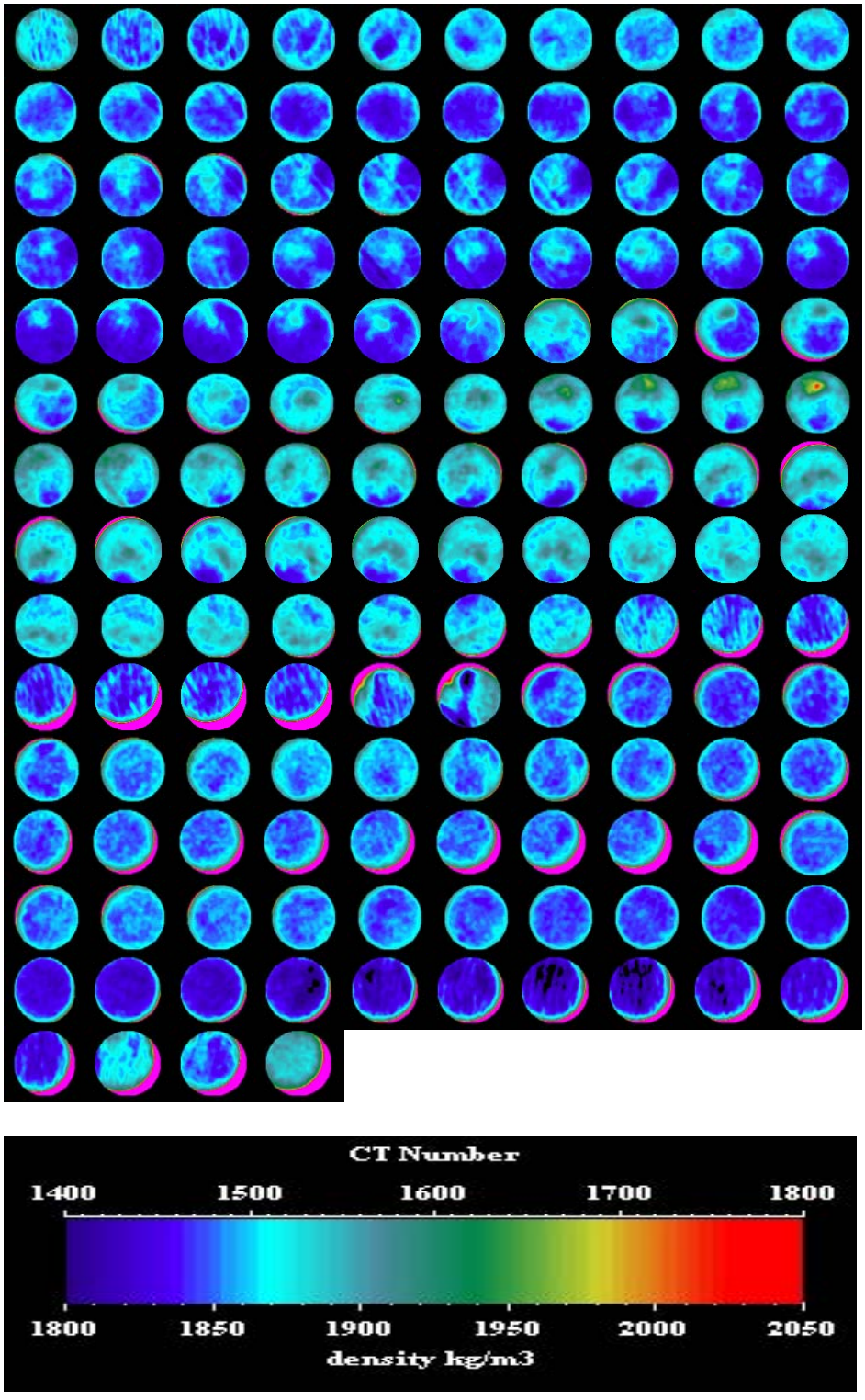

Figure 5.22 CT images of the core after primary depletion

5.4.2 Methane Recharging and Depletion Process

After primary depletion, there is still 70.26% OOIP left in the core, methane recharging and depletion process will be applied next.

5.4.2.1 Demonstration and Methodology

The demonstration and methodology of production process were the same as the two 18m in length cores except by using one gas collection bottle instead of two bottles. But the injection process, which is demonstrated below, was a little bit different from the two long cores. Instead of injection methane by methane tank, methane was transferred to a piston cylinder until 6895kPa, and then injected by an ISCO pump at constant pressure 6895kPa.

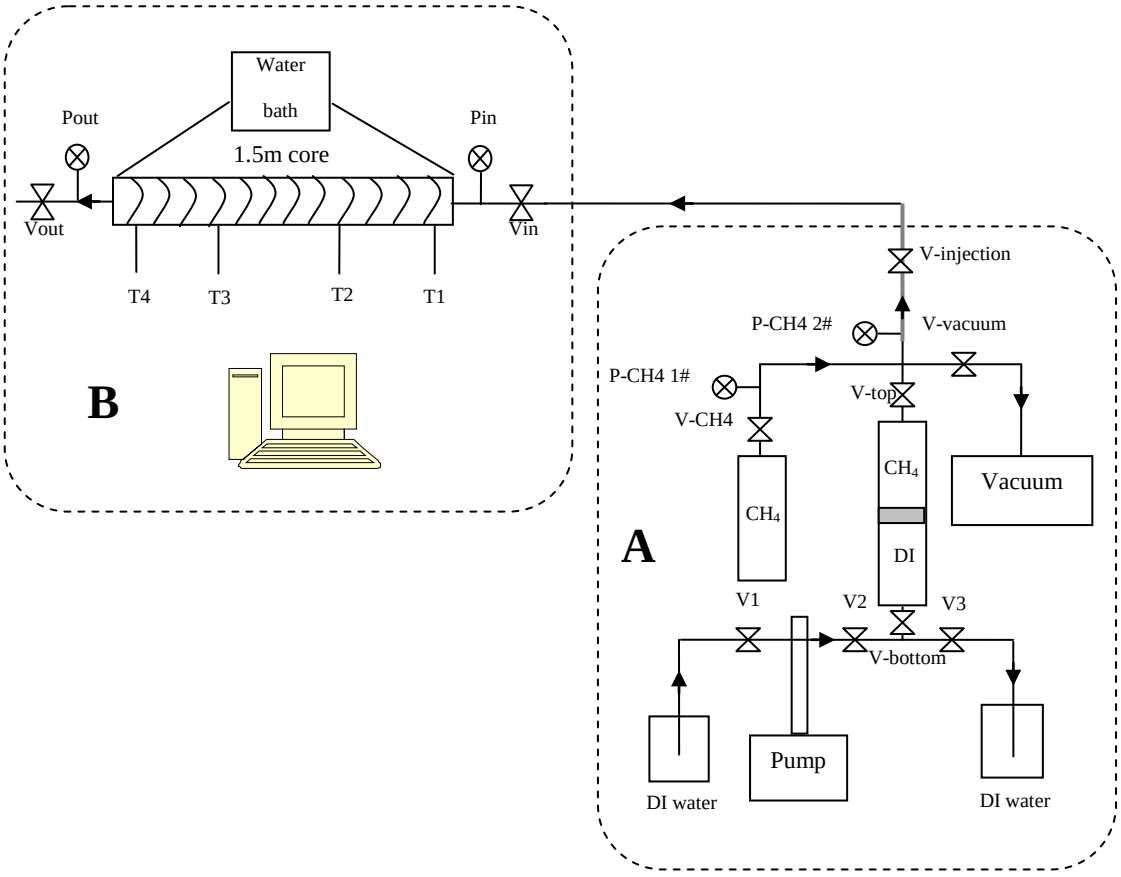

Figure 5.23 Methane recharging rig set up

5.4.2.2 Experiment Results

5.4.2.2.1 Injection and Soaking

Figure 5.24 shows that methane recharging finished very quickly due to the high permeability and short length of the core. The differential pressures did not make an obvious change and were affected by temperature. This infers that there must be a gas channel throughout the core. After injection, the core was shut in for 12 days for soaking to take place. The pressure drop was not clearly observed here but it was affected by temperature change obviously. Probably the soaking period was not long enough. CT scan was performed after that. The core temperatures were affected by room temperature at the later stage of soaking period due to the power off of the water bath.

Figure 5.25 shows the CT images of the core after methane injection. No clear changes can be seen compared CT images after primary production (Figure 5.22). Again, the pink areas of some CT images were dural aluminum tube because the core was not placed horizontally enough during scanning.

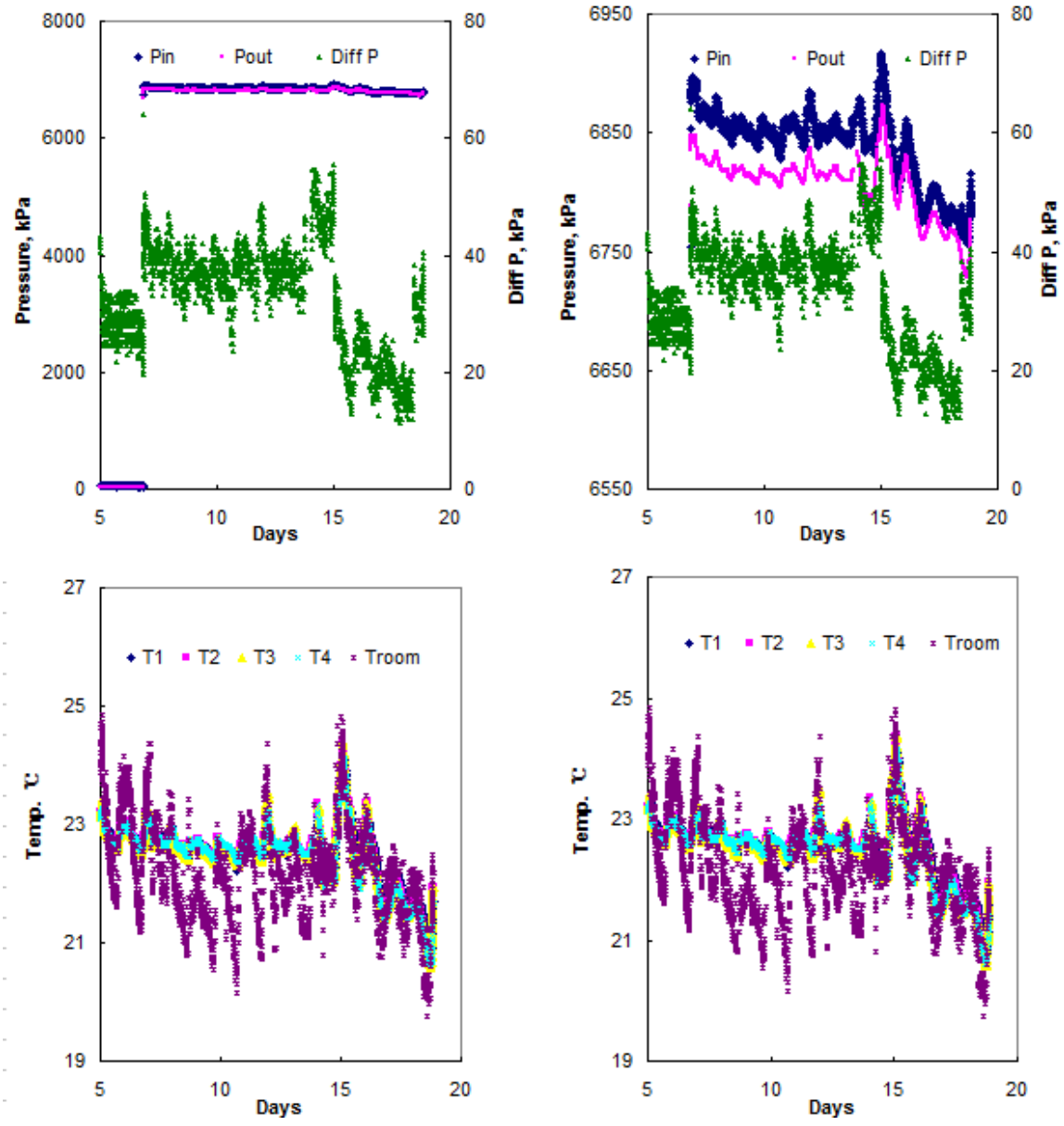

Figure 5.24 Methane recharging and soaking processes-1.5m core

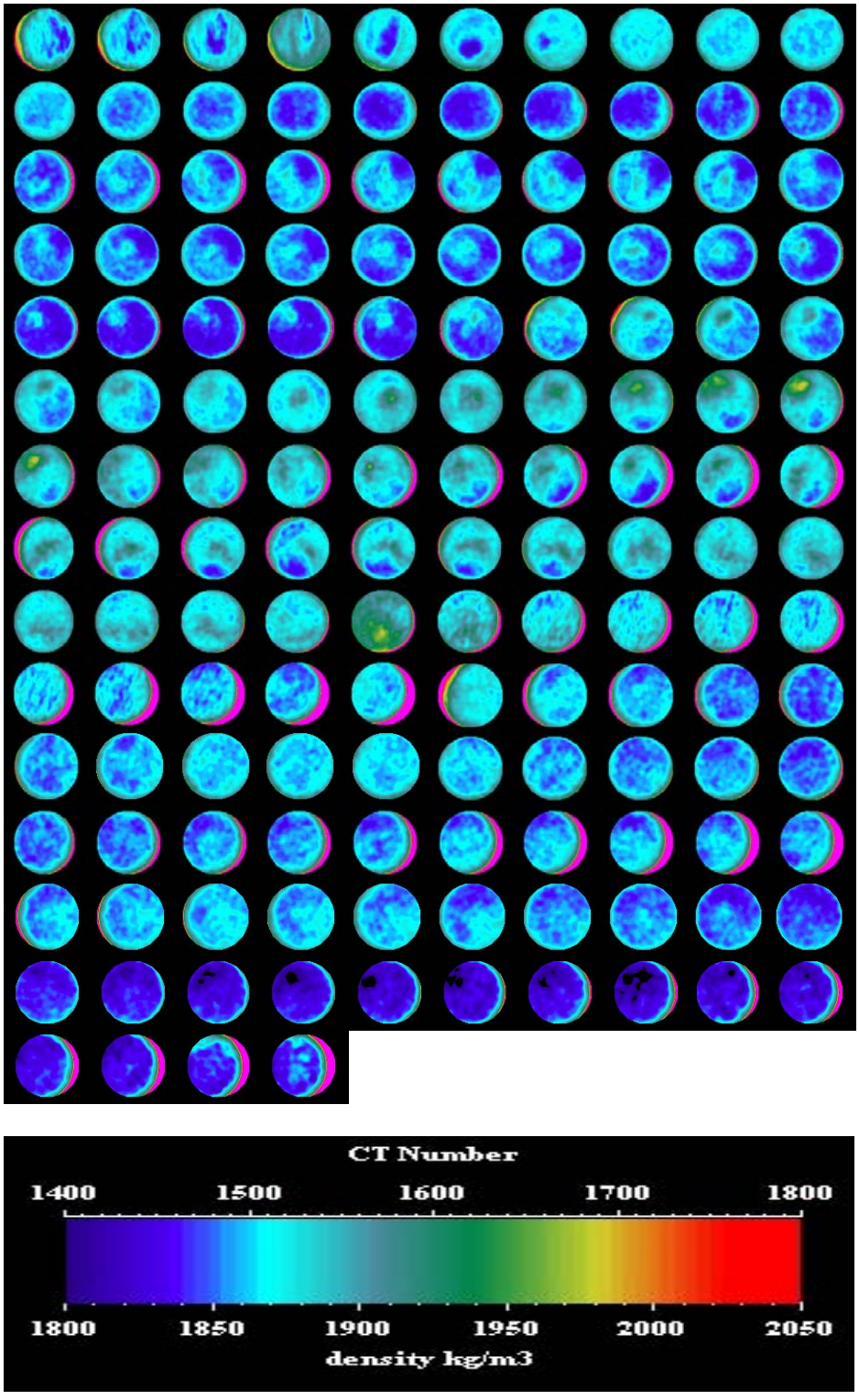

Figure 5.25 CT images of the core after CH_4 injection

5.4.2.2.2 Production

Figure 5.26 shows that core inlet and outlet pressures both decreased closely following the BPR depletion rate. This indicated there must be gas channel throughout the core, which made the oil production become more difficult. No oil was produced. Gas production started just when BPR pressure depleted to core outlet pressure equally. Differential pressure was lower throughout this process. Solution gas drive was hard to be observed here.

Temperature graph shows the water bath was turned on a little bit earlier before depletion process. At the first day production period, core temperatures were not stable, after that they got better.

CT scan was performed after methane depletion process. No clear changes can be seen in Figure 5.27 compared to the CT images after methane injection process (Figure 5.25). Figure 5.28 indicates the core average density rose a little bit from 1.89g/cm^3 to 1.9g/cm^3 after methane injection, and decreased down a little bit to 1.895g/cm^3 after depletion process. There was almost no obvious change throughout the core. Overall, methane recharging and depletion processes did not make meaningful change to the core. Again, the pink areas of some CT images were dural aluminum tube because the core was not placed horizontally enough during scanning.

The higher oil recovery during primary production is probably the main factor to effect methane recharging and depletion process. The gas channel was built up throughout the core after primary production, which prevented the pressure difference to build up later. The BPR depletion rate was relative high due to short core length, which helped the conventional solution gas drive to occur. The shorter soaking period was also a potential factor. All these make the methane recharging and depletion process ineffective on the 1.5m core.

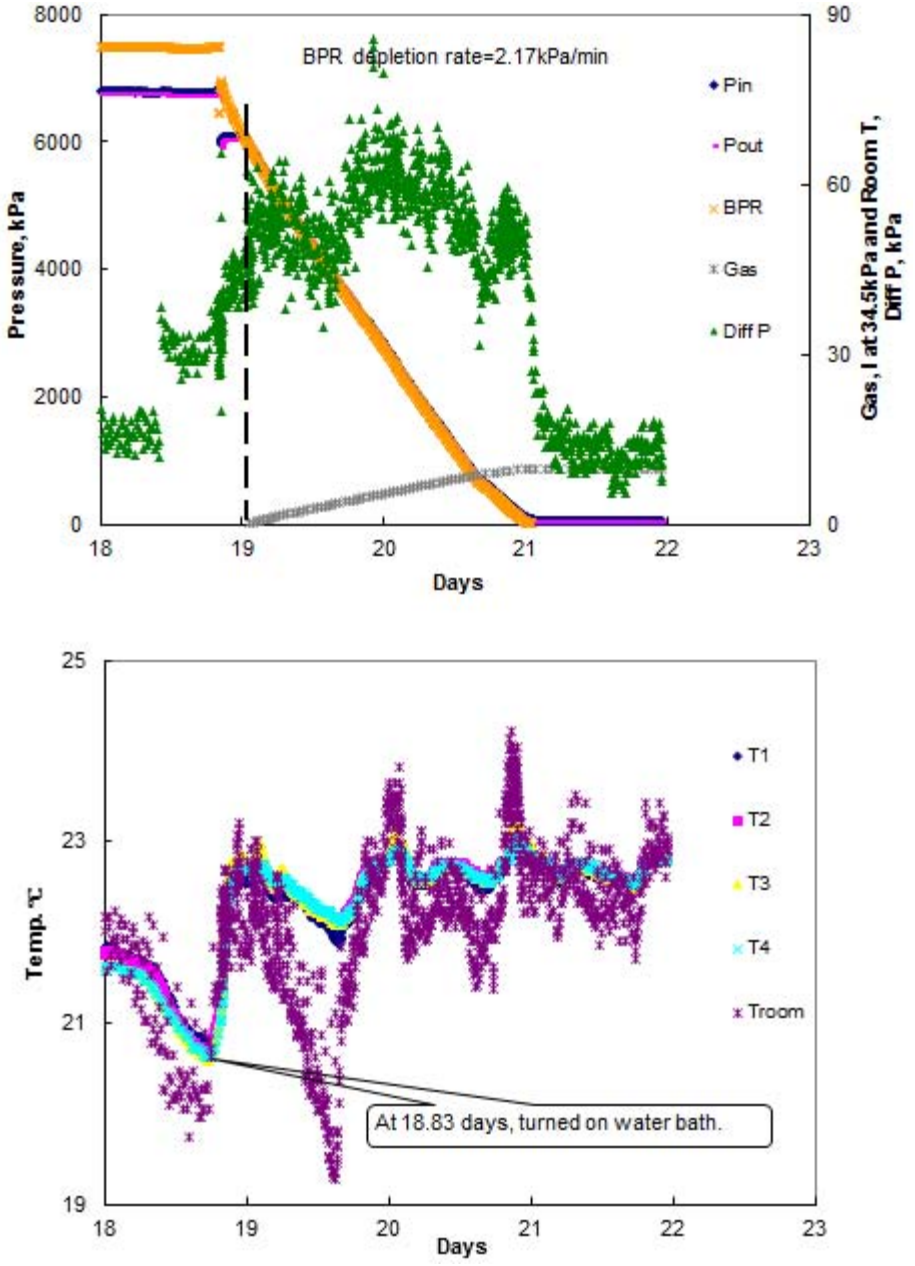

Figure 5.26 Methane depletion process-1.5m core

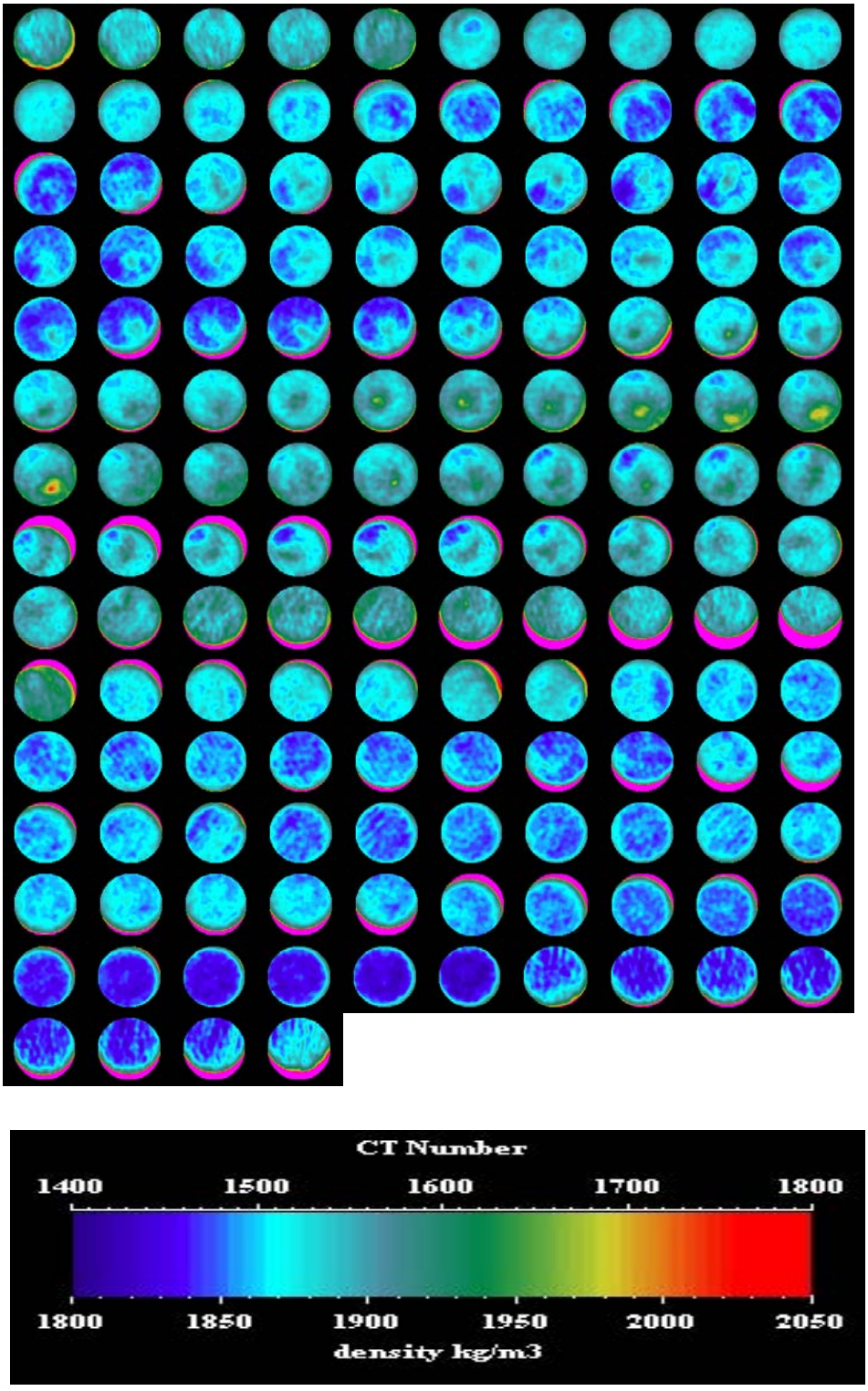

Figure 5.27 CT images of the core after CH_4 depletion

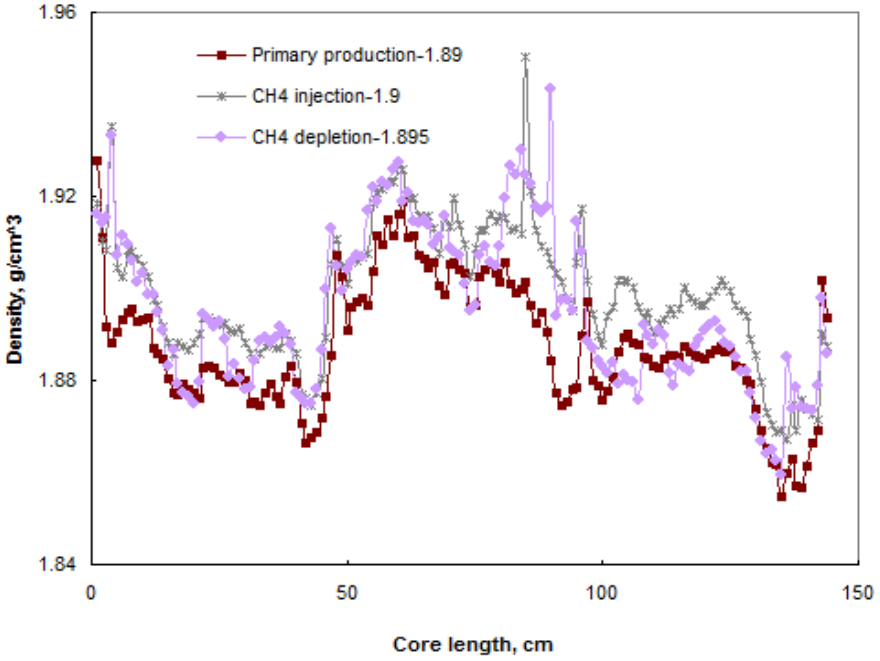

Figure 5.28 Density comparison-primary depletion and CH_4 injection and depletion

5.4.3 Propane and Carbon Dioxide Huff-Puff

After methane depletion, carbon dioxide recharging and depletion process was by passed. Propane and carbon dioxide huff-puff followed.

5.4.3.1 Demonstration and Methodology

Methodology and demonstration of this process are all the same as the two 18m in length cores.

5.4.3.2 Experiment Results

5.4.3.2.1 Injection and Soaking

The sharp light blue peak in Figure 5.29 indicates a gas zone throughout the core. The slow-down of pressure increase and the speed-up of differential pressure both caused by phase behavior variation from gas to liquid and together with the process of injection fluid dissolving into the oil. When injection was finished, the core was left alone for soaking. It could be clearly seen that the core pressures decreased during soaking period. The final balanced pressure was above 4826kPa to ensure the inner fluid was in liquid phase.

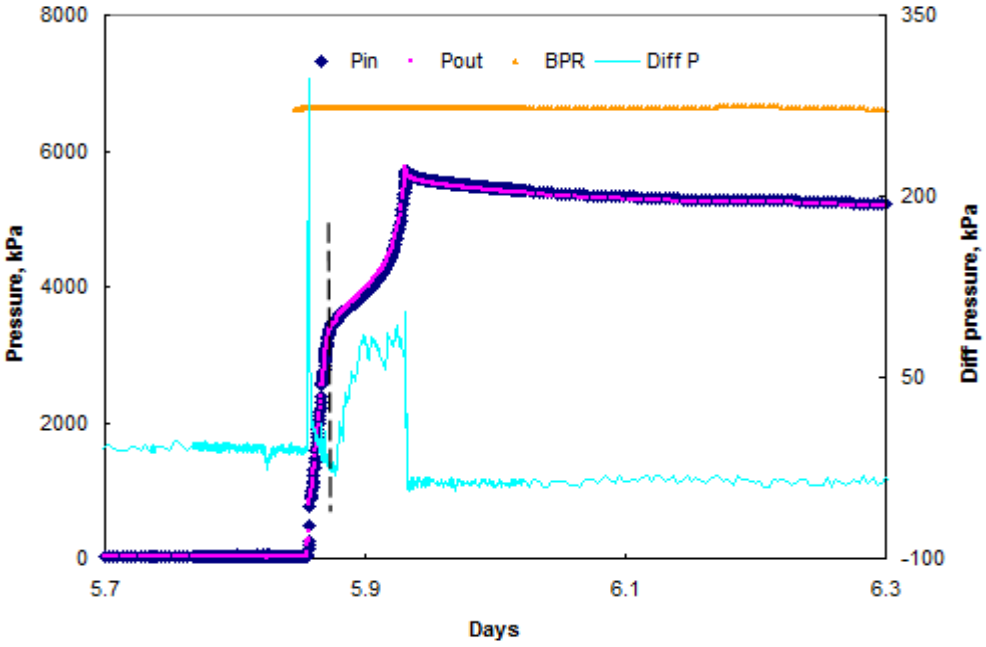

Figure 5.29 Huff-puff injection process-1.5m core

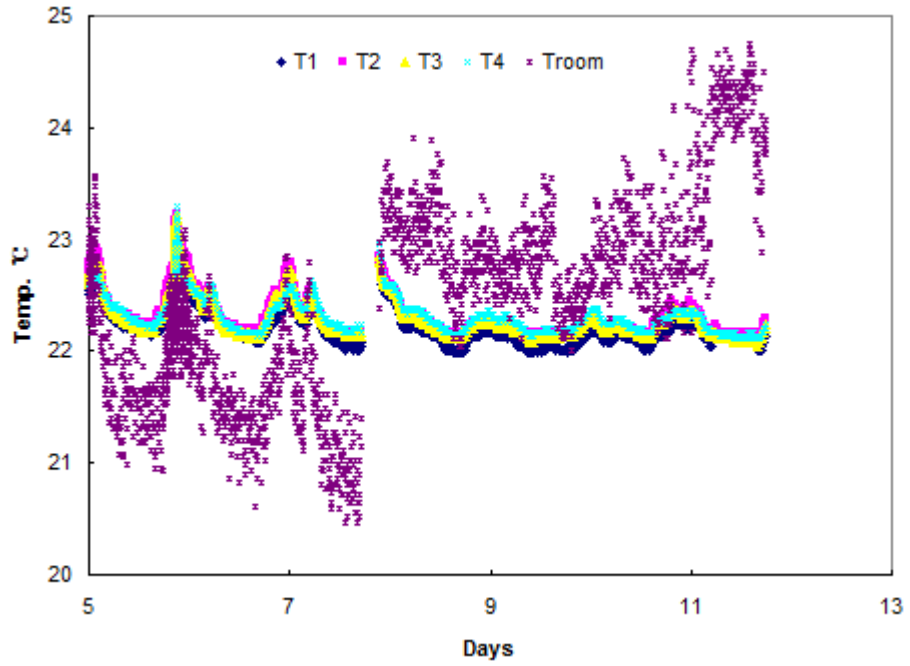

Figure 5.30 Temperature variation of huff-puff injection process-1.5m core

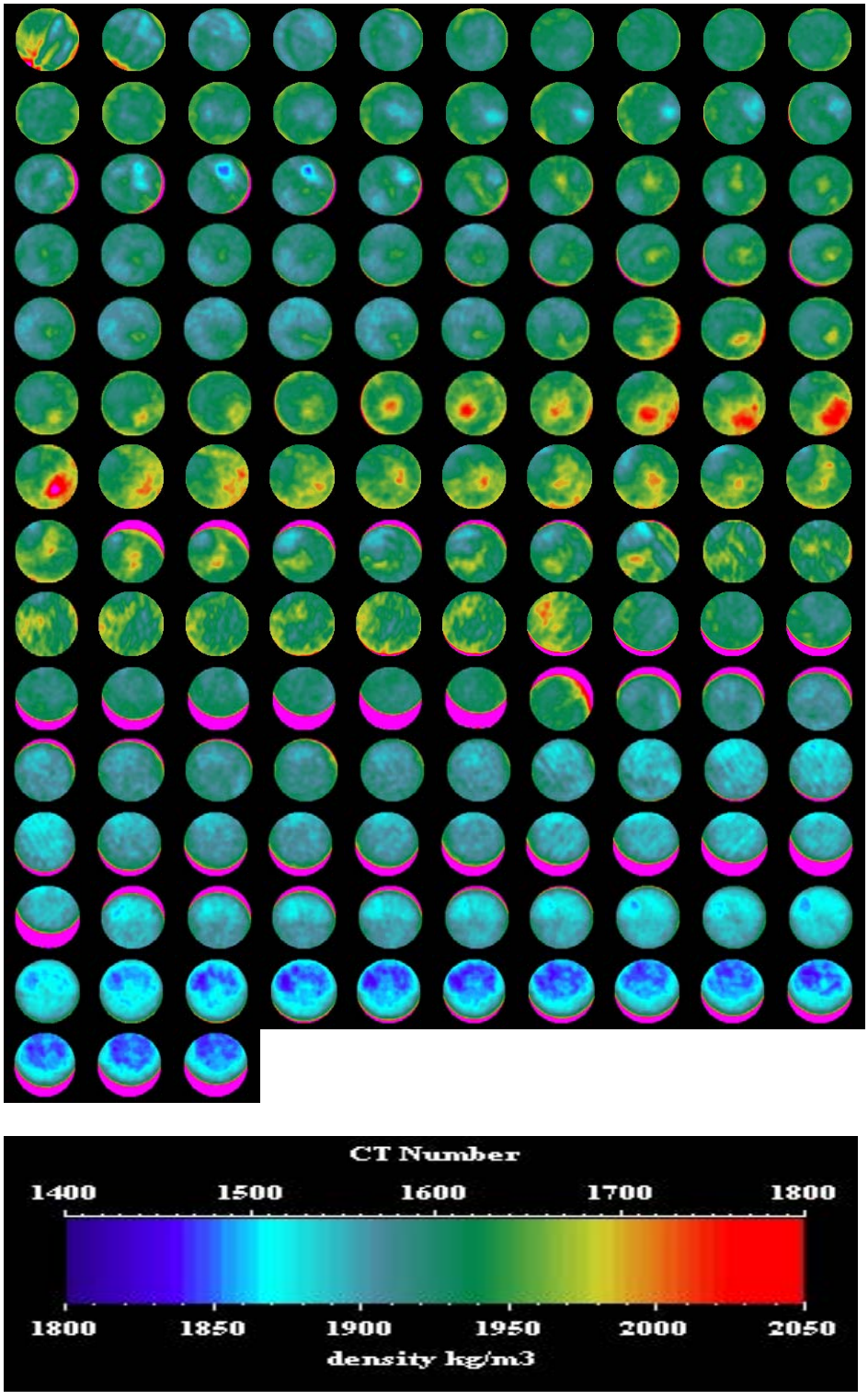

Figure 5.31 CT images of the core after huff-puff injection

Figure 5.30 indicates the core temperatures were relatively stable during the huff-puff injection process although still was affected by room temperature a little bit.

Figure 5.31 shows the CT images of the core after huff process. All the densities went up than the period after methane depletion. These CT images were much similar to the CT images of the core after live oil saturated except the densities near core outlet area were lower which infers some oil there was pushed back towards inlet during the huff process. Again, the pink areas of some CT images were dural aluminum tube because the core was not placed horizontally enough during scanning.

5.4.3.2.2 Production

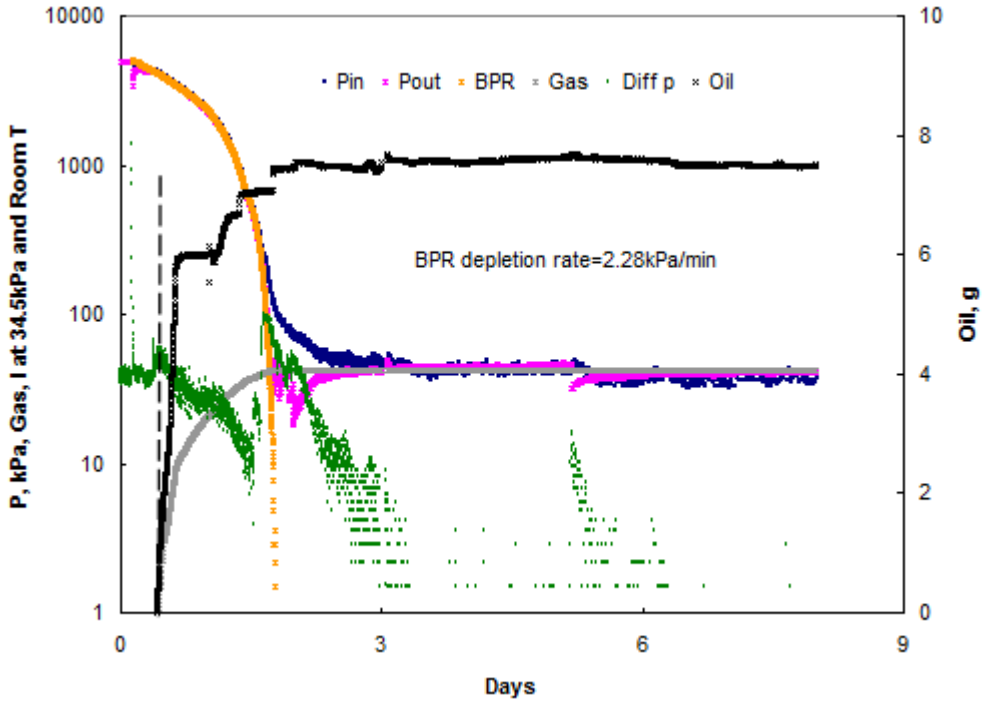

Figure 5.32 Huff-puff production process-1.5m core

Figure 5.32 indicates that core pressures decreased followed BPR depletion tendency until solution gas evolved and swelled the oil, increased the differential pressure. Core outlet pressure increased and inlet pressure decreased slower than before. Foamy oil flow probably happened here. Oil and gas production happened at almost the same time but only lasted a short period of time due to higher permeability and short length of the core. The oil production in Figure 5.32

was the weight of produced fluid (contained water). Based on the difference of balance reading of the produced fluid and water weight from NMR results, the real oil production was 5.86g, oil recovery was 4.29% totally here.

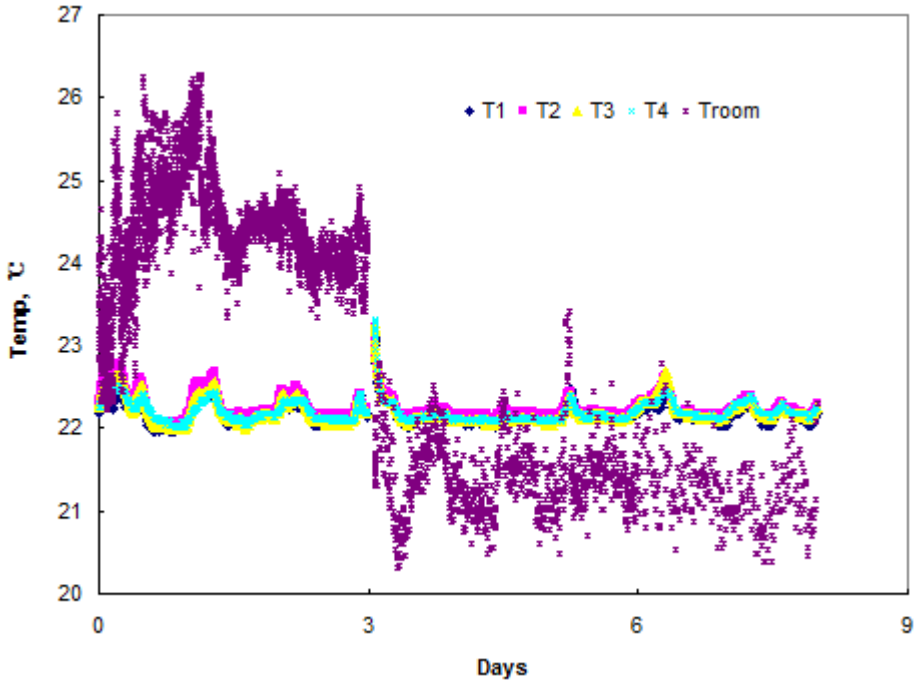

Figure 5.33 Temperature variation of huff-puff production process-1.5m core

Figure 5.33 indicates the core temperatures were relatively stable during the huff-puff production process except the room temperature.

Figure 5.34 indicates the core density decreased after puff process. Inlet, middle and not far from outlet of the core had relatively higher density areas. This infers that there must be oil-rich regions or oil banks left there due to the shortage of drive force. At outlet, density dropped a lot. This means not only injection fluid but also oil left there were produced. Again, the pink areas of some CT images were dural aluminum tube because the core was not placed horizontally enough during scanning.

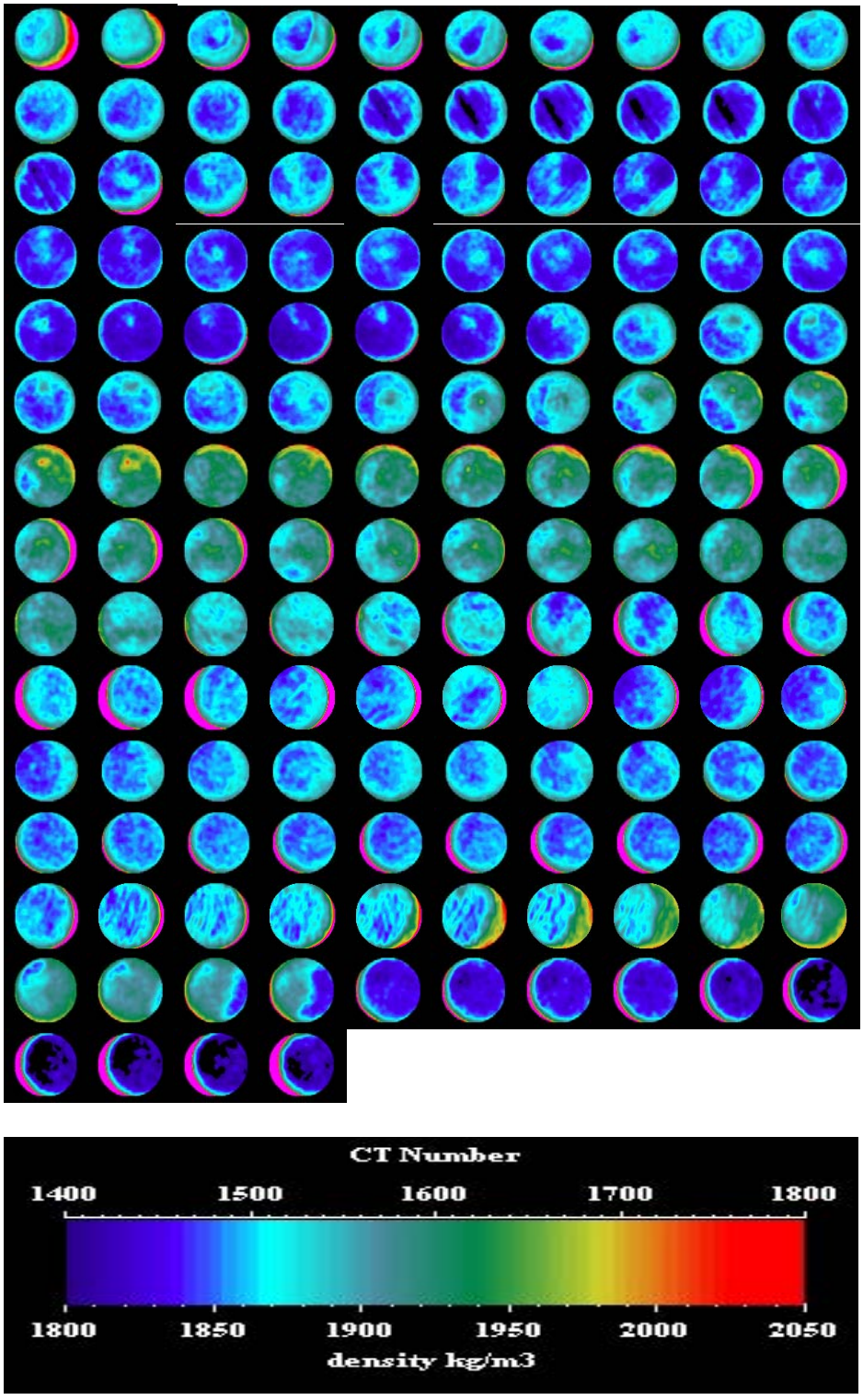

Figure 5.34 CT images of the core after huff-puff production

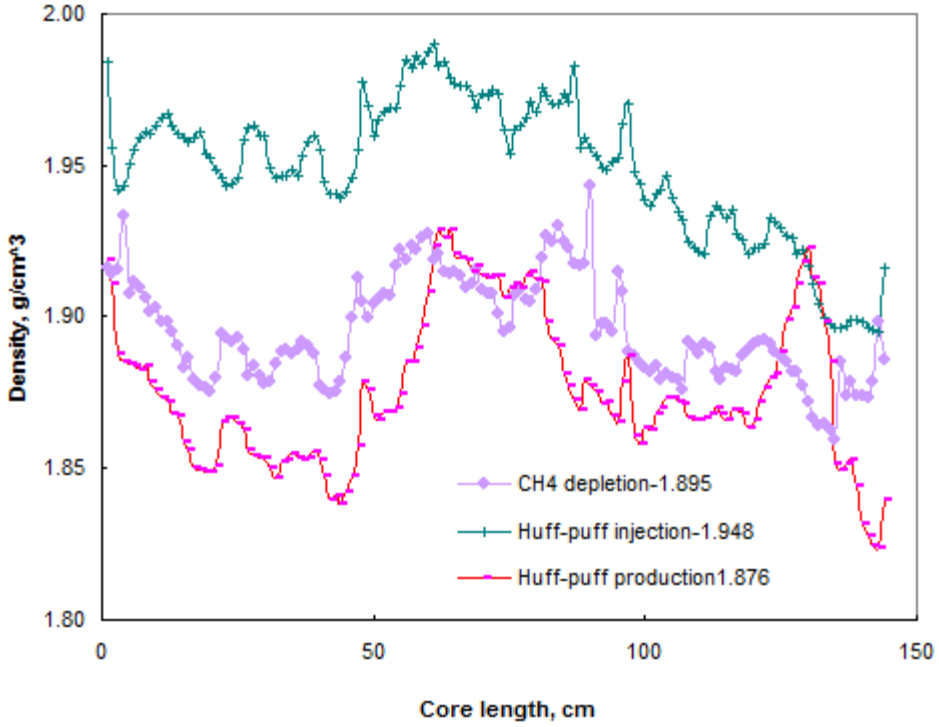

Figure 5.35 Density comparison- CH_4 depletion and huff-puff processes

Figure 5.35 is the core density comparison before and after huff-puff process. After huff injection process, the core average density increased from 1.895g/cm^3 to 1.948g/cm^3 (similar to the core average density after live oil saturated 1.94g/cm^3). Overall, the lower the density after methane depletion is, the more the increase amount after huff-puff injection is. The density near core outlet area was obvious lower than other place; it is possible to infer that some of oil at this area was pushed back towards the core inlet during huff-puff injection process.

After production, it dropped to 1.876g/cm^3, which is lower than the density (1.89g/cm^3) after methane depletion; this indicates oil was produced out during this process. Comparing the density curve from outlet to inlet, the core density dropped a lot at outlet area and was obviously lower than the density after methane depletion. This indicated not only injection fluid but also oil left at that area were moved out of there. Behind that area, a big pink peak followed up, its peak density was ever higher than the density after huff process. This reveals that there must be an oil enrichment region there. These amounts of oil probably came from the lower density area just following the pink peak. In the middle of the core, the second big red peak showed up, its density

was higher than the density after methane depletion process. This indicates that there must be the second oil enrichment region coming from the lower density area just behind it. Near the core inlet end, there was still a big pink density peak there. At the end of core inlet, the core density was even higher than the density after methane depletion. This amount of oil was left there because of the drive force shortage. The closer the position is to the core inlet, the serious the shortage of drive energy is, and the more the oil is left. The BPR depletion rate also need to be further studied to get higher oil recovery.

5.4.4 Propane Flooding

5.4.4.1 Demonstration and Methodology

Demonstration and methodology of this process are all the same as the two 18m in length cores.

5.4.4.2 Experiment Results

Figure 5.36-A is the early stage curves of propane flooding process. Before injection, BPR was set at a higher level and propane piston cylinder was filled up first time. When injection began, the pump was set at constant pressure (724kPa) injection mode, the core inlet pressure increased quickly until core pressure difference reached a small value. After that, the pump injection was set at constant rate injection mode throughout the whole flooding process, but the flow rate was adjusted occasionally. Both core inlet and outlet pressures went up gradually to around 689kPa. Core outlet pressure followed the injection propane pressure closely. The minor pressure difference indicated the core permeability was high and there was a gas path throughout the core. The flat area of the pressure curves was caused by decreasing the pump flow rate to 0.2ml/min overnight. Core outlet valve was opened at 0.26 day.

To start propane flooding, the BPR pressure was decreased to 689kPa at 0.29 day while the injection continued. Once the core outlet pressure went up beyond the BPR pressure, propane flooding occurred, core pressures dropped from outlet to inlet a little bit then stayed stable. The gas and oil productions followed afterwards. A huge amount of oil and seldom gas were produced. Figure 5.35 could help to explain this phenomenon. As we discussed above, after huff-puff process, there was a big pink sharp density peek near the core outlet area. That was an oil enrichment region (gas-oil dispersion) where gas produced with oil together during this period.

Figure 5.36-B is the whole process of propane flooding. The light blue curve shows there were totally 3 refills for the propane piston cylinder. The first flat line of oil production curve was caused by decreased the pump injection rate from 10ml/min to 0.2ml/min overnight. The oil production increased when the pump injection rate rose up to 1ml/min. The BPR pressure was released from 689kPa to 552kPa when the oil production slowed down, then the second sudden increase of oil production occurred. This was caused by the pressure difference. The foamy oil formed at huff-puff process was driven out. The gas channel formed. The follow up BPR pressure drops did not contribute to oil production. After the BPR pressure reached atmosphere pressure, a blowout process was performed; a little more oil was recovered there. The oil production in this process was mostly benefited from huff-puff process. The jumps of gas production and differential pressure related to the pressure drops of propane piston cylinder and BPR closely.

After the water was deducted based on NMR results, there was 22.8g oil produced out totally, additional 15.97% oil was recovered from propane flooding process.

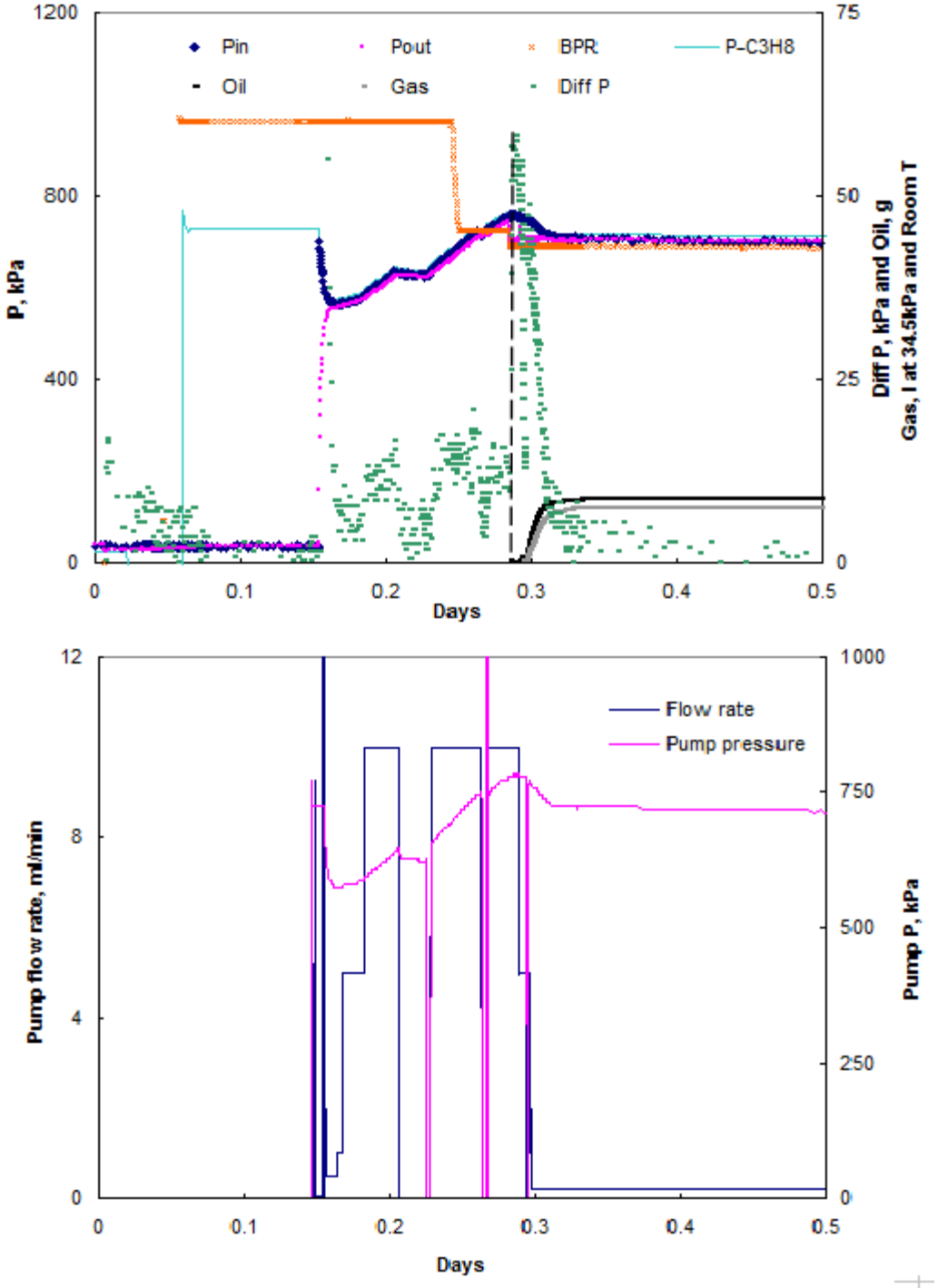

Figure 5.36-A Propane flooding process at early stage-1.5m core

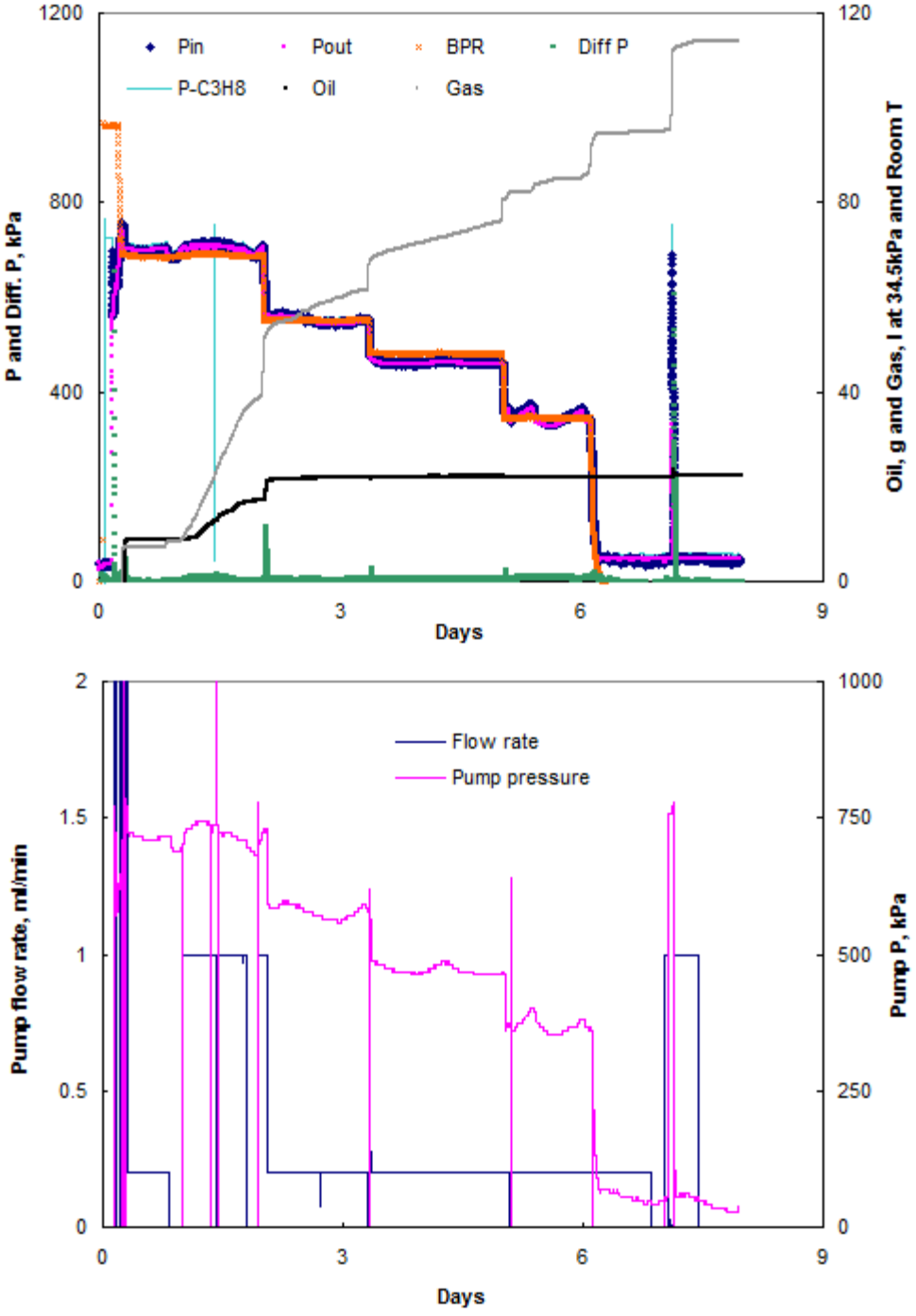

Figure 5.36-B Propane flooding process-1.5m core

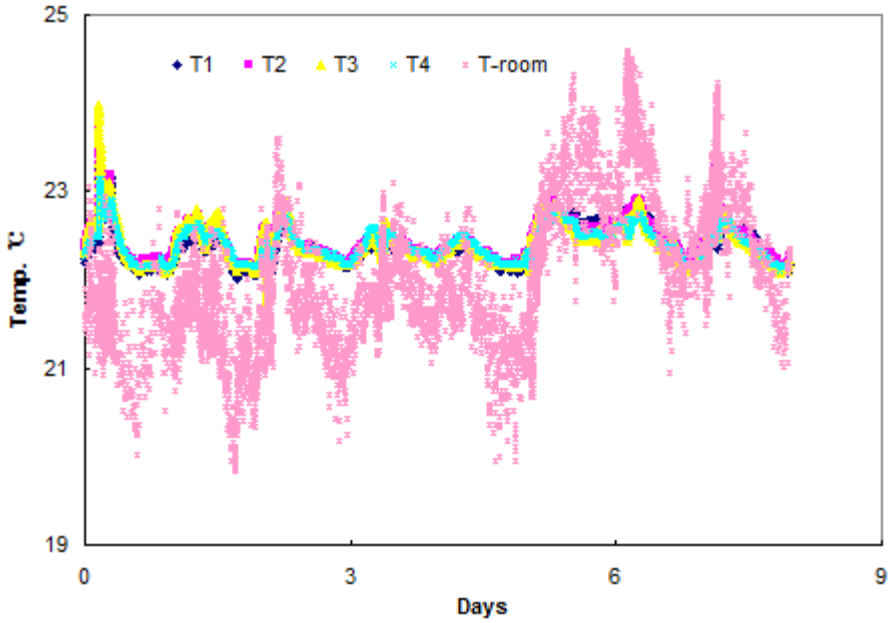

Figure 5.37 Temperature variation of propane flooding process-1.5m core

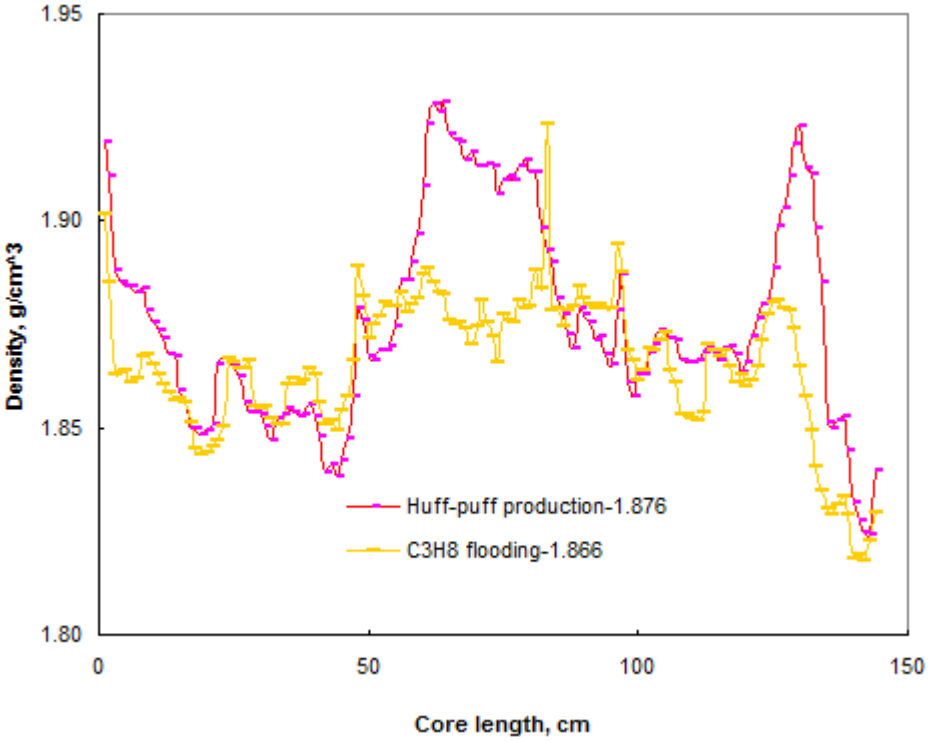

Figure 5.38 Density comparison-puff and C_3H_8 flooding

Figure 5.37 indicates the core temperatures were relatively stable during the propane flooding process.

At the core outlet, middle, and inlet areas (Figure 5.38), core densities dropped lower than densities after huff-puff process and the three big pink peaks were disappeared or significantly decreased. These indicated the oil in that area was moved towards the core outlet and produced out during propane flooding process. The core average density dropped to 1.866g/cm^3.

Figure 5.39 verified the above discussion; the densities across the core were decreased clearly. Again, the pink areas of some CT images were dural aluminum tube because the core was not placed horizontally enough during scanning.

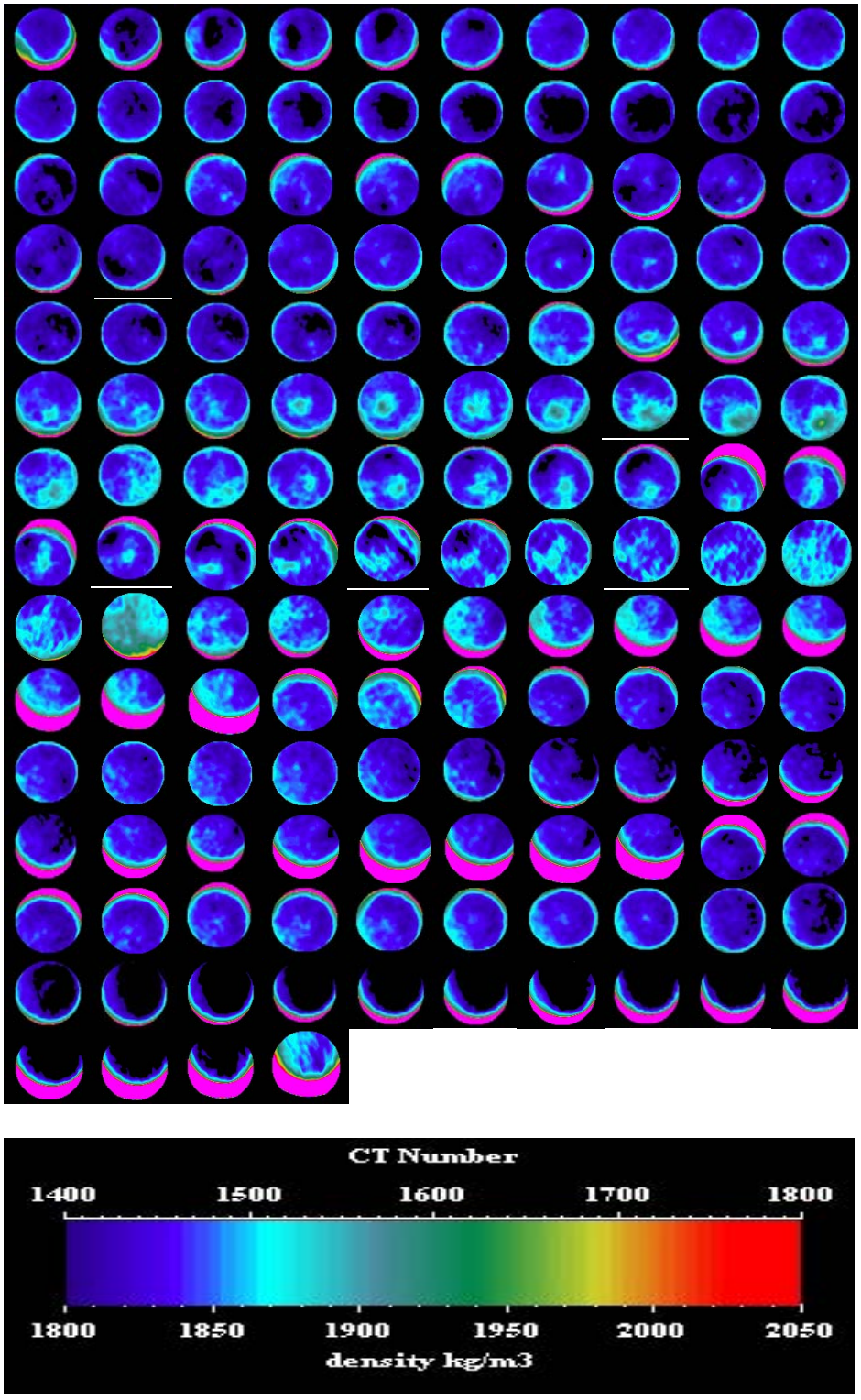

Figure 5.39 CT images of the core after C_3H_8 flooding

Chapter Six: Experimental Comparison and Discussion

6.1 Viscosity Comparison of Produced Oil

Table 6.1 Viscosity summary of produced oil at 22.5℃

Process	Viscosity of produced oil, mPa.s		
	Sand pack-18m	Glass beads-18m	Sand pack-1.5m
Dead oil at 23℃	10695	10711	11230
Primary depletion	No data -by N.N. Goodarzi	No data -by N.N. Goodarzi	15112[a]
CH_4 depletion	14280*	12981**	No oil production
CO_2 depletion	No data -by R.P. Shi	No data -by R.P. Shi	/
CO_2 and C_3H_8 huff-puff	No oil production	No oil production	1444[b]
C_3H_8 flooding	No oil production	60440[1], 10396[2], 13313[3]	9365[c]
Remark	The date of oil produced: *-2008/01/02, **-2007/03/27 1-2010/06/14-9.64g, 2-2010/06/22-77.37g, 3-2010/07/15-13.22g a-2010/03/08, b-2010/09/22, c-2010/09/30 The date of viscosity measurement: 2010/10/07		

Table 6.1 summarized all the viscosities of produced oil from each process at three different cores. All samples were collected into plastic bottles and sealed with lids at different time, but they were measured at the same day.

18m in length sand packed core only have one methane depletion data available, which was higher than the dead oil viscosity.

Figure 6.1 shows the viscosity summary for 18m in length glass beads packed core. Only one bottle of oil was collected during the whole methane depletion process, its viscosity was 12981mPa.s at 22.5℃, which is a little bit higher than its dead oil viscosity (10711mPa.s at 23℃). Totally 3 bottles of oil were collected during propane flooding process. Their produced fluid weights were 1#-9.46g, 2#-77.37g, 3#-13.22g. The first small sample's viscosity was abnormal high; the viscosities of the second big sample and the third small sample were a little lower and a

bit higher than its dead oil viscosity respectively. The possible reasons for these will be discussed as follows:

First, the light and intermediate components of residual oil after CO_2 depletion process was pushed towards inlet by huff process and left the heavy components behind. Oil was redistributed and several oil banks formed at puff process. Due to the longer core length, shortage of drive force, lots of injected fluids were still trapped in the oil to lower its viscosity. At propane flooding process, oil banks could block the gas path way to some extent and were driven by propane flooding towards outlet, which could modify mobility ratio. The heavy component near outlet was driven out first by oil bank which was closer to outlet.

Second, the yellow sample should contain large amount of oil produced from oil banks. Therefore, viscosity is lower than dead oil.

Third, The blue sample was produced the last, its viscosity is a little bit higher than dead oil which probably contains less oil from oil banks.

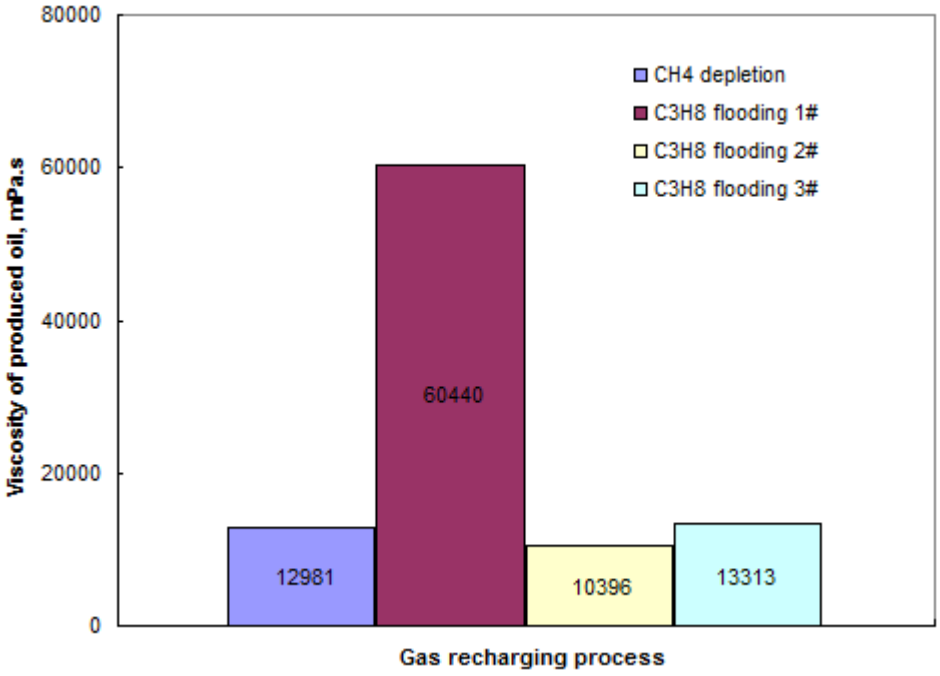

Figure 6.1 Produced oil viscosity summary-glass beads

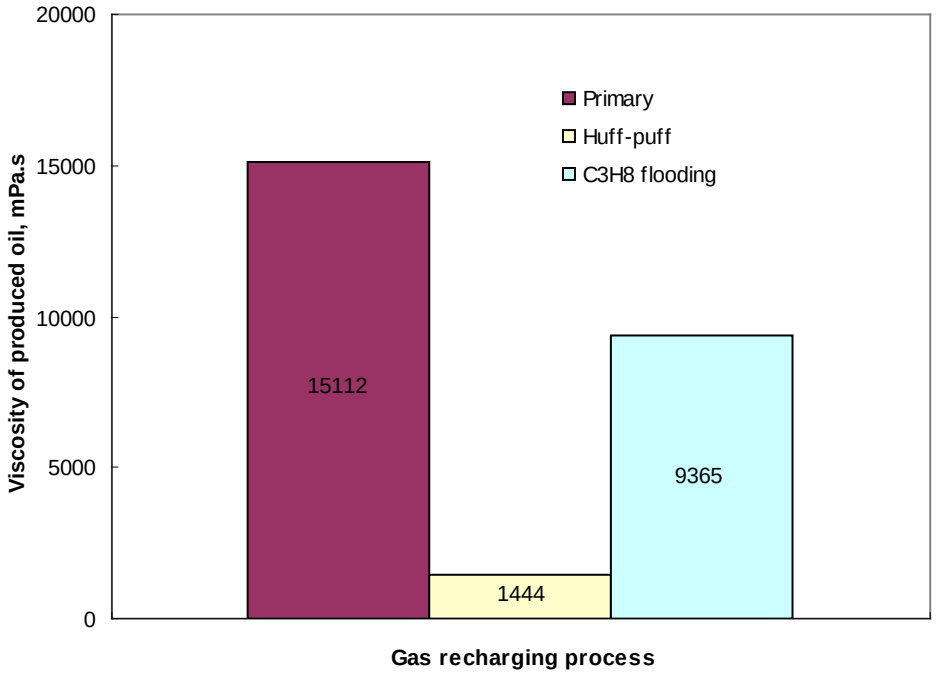

Figure 6.2 Produced oil viscosity summary-1.5m core at 22.5℃

Butler and Mokrys[50], Luo et al.[53] have reported produced oil viscosity can be dramatically reduced by C_3H_8 injection due to asphaltene precipitation. Pressure increase is helpful for this process. Yarranton et al.[55] observed that the mixed CO_2 and C_3H_8 is less likely to precipitate asphaltenes than pure C_3H_8. That means the mixture can also reduce viscosity of produced oil. Figure 6.2 shows the viscosity summary for 1.5m sand packed core.

First, it can be seen that the produced oil viscosity is abnormally low after puff process (1444mPa.s). Based on other person's theory, pressure after huff process was high; therefore, propane there can sharply decrease the viscosity of produced oil during puff process. Based on this study, a foamy oil flow happened there. The injected fluids were still trapped within the produced oil to lower its viscosity dramatically.

Second, after propane flooding, produced oil viscosity is lower than dead oil but higher than the one after puff process. Based on other person's theory, the pressure at propane flooding process was lower than the one at huff process; therefore, the oil viscosity was decreased less at flooding process. Based on Figure 5.38-Density comparison-huff-puff production and C_3H_8 flooding, most

oil produced during propane flooding was formed during huff-puff process-three oil banks. The produced oil here should contain the oil from oil banks to decrease its viscosity.

Third, the highest viscosity of produced oil is got after primary depletion. This infers methane is less easily trapped within the oil than propane.

6.2 GC Results Comparison-Two Long Cores

During puff process, GC samples were taken and measured for both two long cores. The relationship of GC results and production curves has been discussed at section of 4.3.3.2 for each core separately. But only the produced gases with large quantity (CO_2, C_3H_8, and H_2) were involved. The produced gases with less quantity will be compared below:

Figure 6.3 and 6.4 are the GC results of puff process on glass beads and sand packed long core separately. The bottom graph of each figure only contains tiny gases and uses a small but same range for y axis to compare their productions.

At Figure 6.3, iC_4 follows the propane (C_3H_8) production rule closely. This probably is caused by Similarity Principle. Methane (CH_4) also increases except two drops (probably error points) and its rate speeds up at later stage. It might come from the one left after methane depletion process and pushed towards inlet by huff process. C_6^+ group has a little rise-up at early stage and maintains the same production level to the end. Productions of other components are very low during the whole period.

At Figure 6.4, iC_4 curve also shapes itself the similar way as propane curve. Its production decreases when H_2 begins to produce. Comparing to the glass beads packed core, its production is much higher in sand packed one. Methane's production mode is similar as the one at glass beads packed core, but it is unusually higher and without two drops. The big production increase of iC_5, small increases of C_6^+ group, n-C_4 and n-C_5 and tiny increases of C_2 and n-C_6 at sand packed core should also be noticed. H_2S production does not make visible change at both cores. All these changes most probably come from the chemical reaction (thermal cracking) happened at abnormal heating area during the interval of CO_2 depletion and huff process.

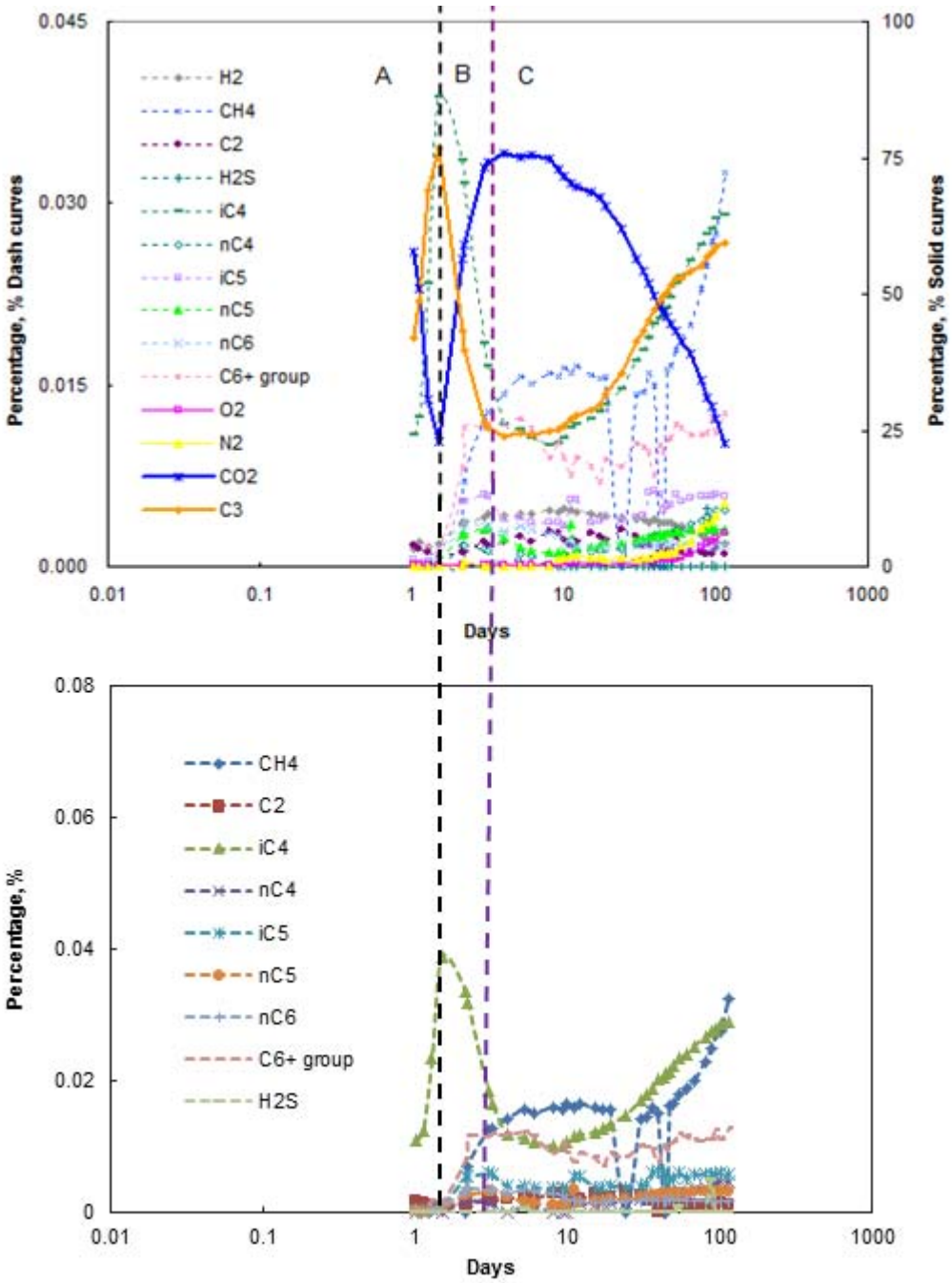

Figure 6.3 GC results of puff process - glass beads

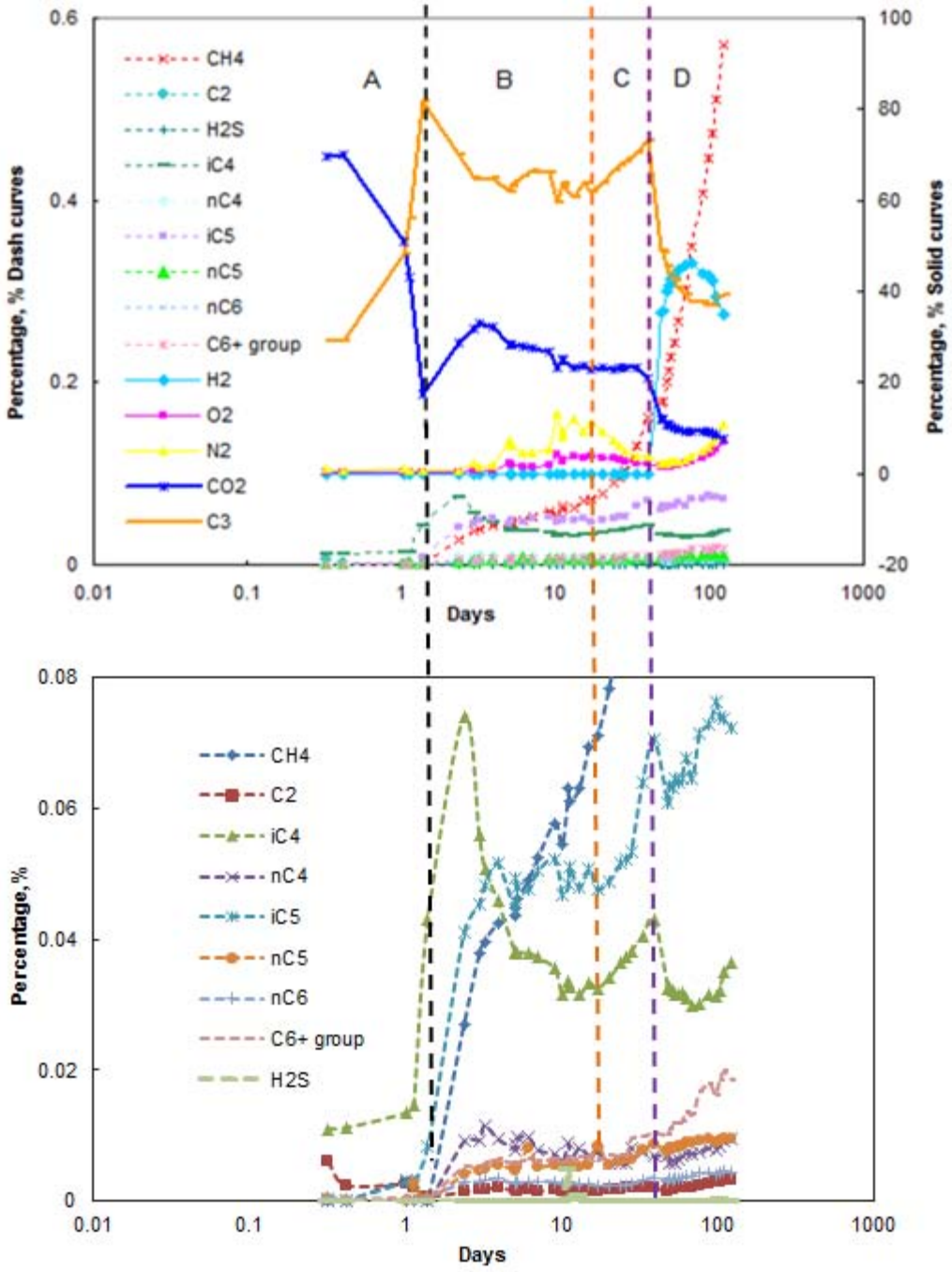

Figure 6.4 GC results of puff process-sand packed

6.3 Core Density Comparison after Each Process-1.5m Core

The density variations after each process were better measured by CT scan technique at 1.5m sand packed core. Figures 6.5, 6.6 and 6.7 show the average density, CT images and density summary after each process. Huff-puff process makes the biggest change of core density. The liquid mixture fluid (CO_2 and C_3H_8) more easily to dissolve into the residual oil and redistributed the oil by injection and production process. The three big peaks of the pink curve showed up in Figure 6.7 further verified this explanation. Therefore, the huff-puff process is more powerful for the follow-up process to recover more oil.

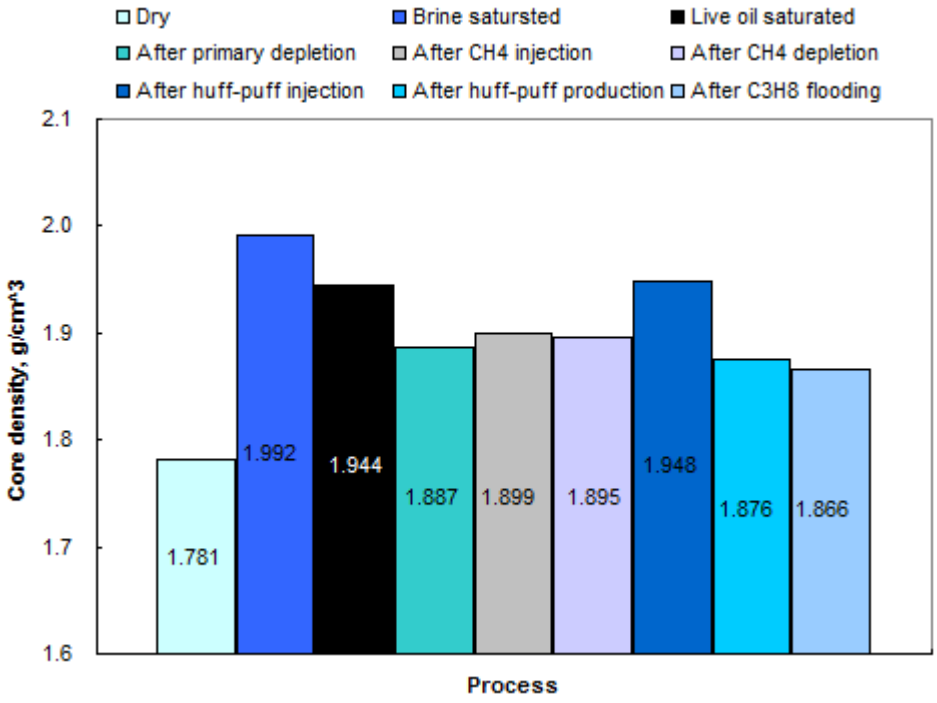

Figure 6.5 Average density of each process-1.5m core

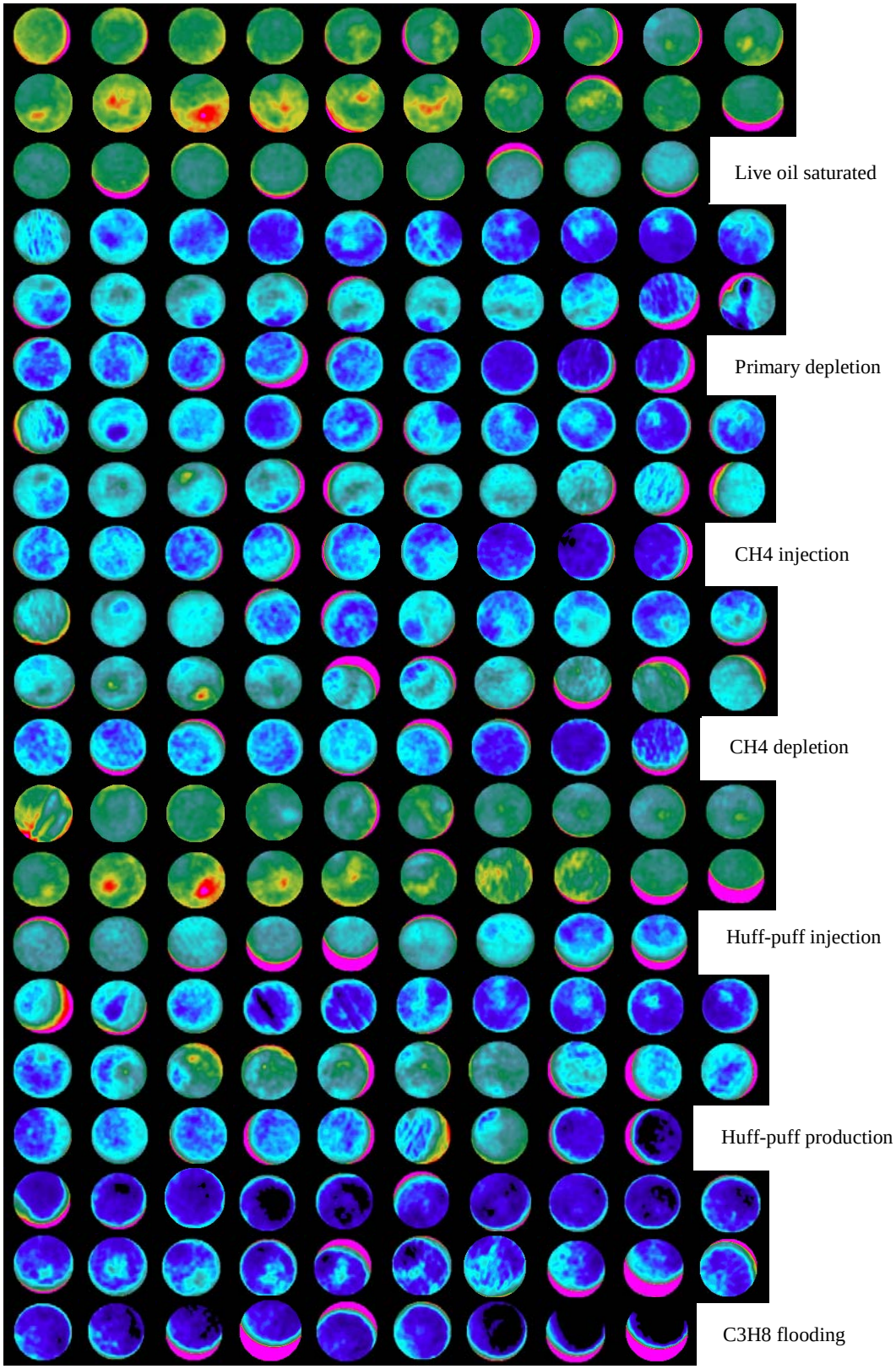
Live oil saturated
Primary depletion
CH4 injection
CH4 depletion
Huff-puff injection
Huff-puff production
C3H8 flooding

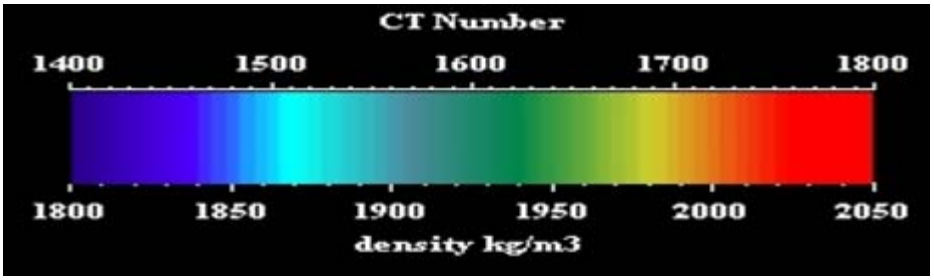

Figure 6.6 CT image summary of each process-1.5m core

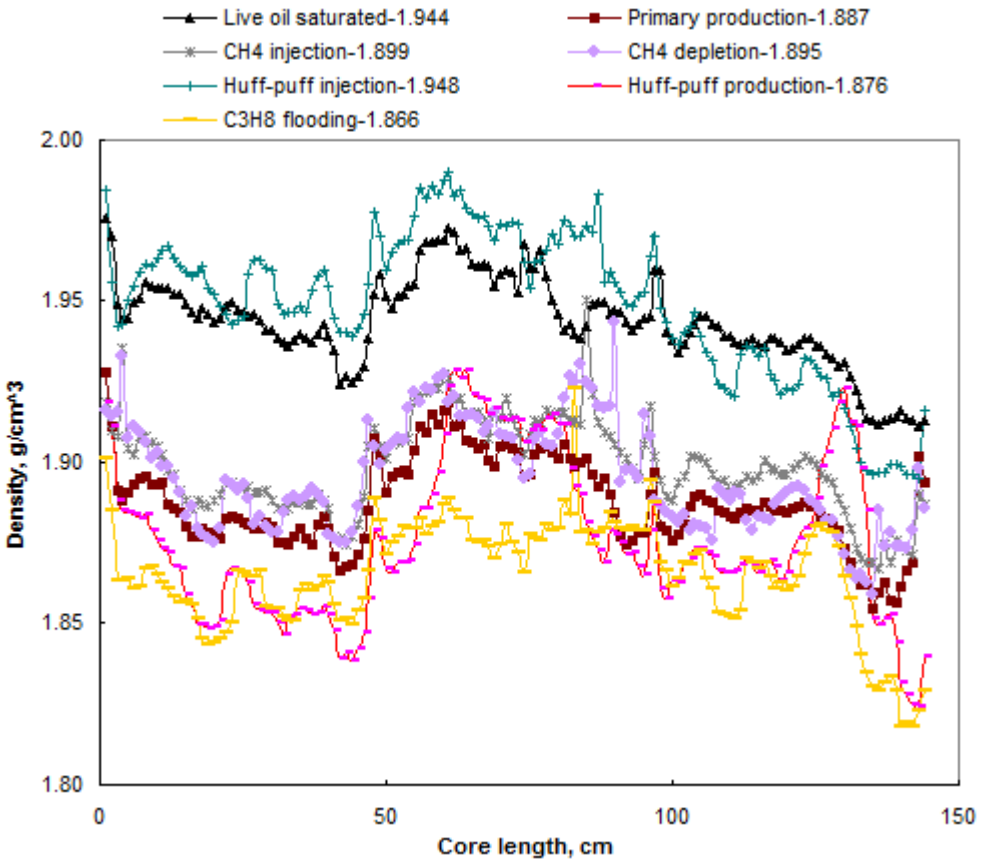

Figure 6.7 Density summaries after each process-1.5m core

Figure 6.8 shows the density difference of every adjacent process at 1.5m sand packed core. The far away from the zero density the curve is, the more difference the process makes. Primary depletion and huff-puff processes made bigger changes to the core, methane recharging and depletion processes made little changes throughout the core. Propane flooding process helped the oil enriched area during huff-puff process to be produced out.

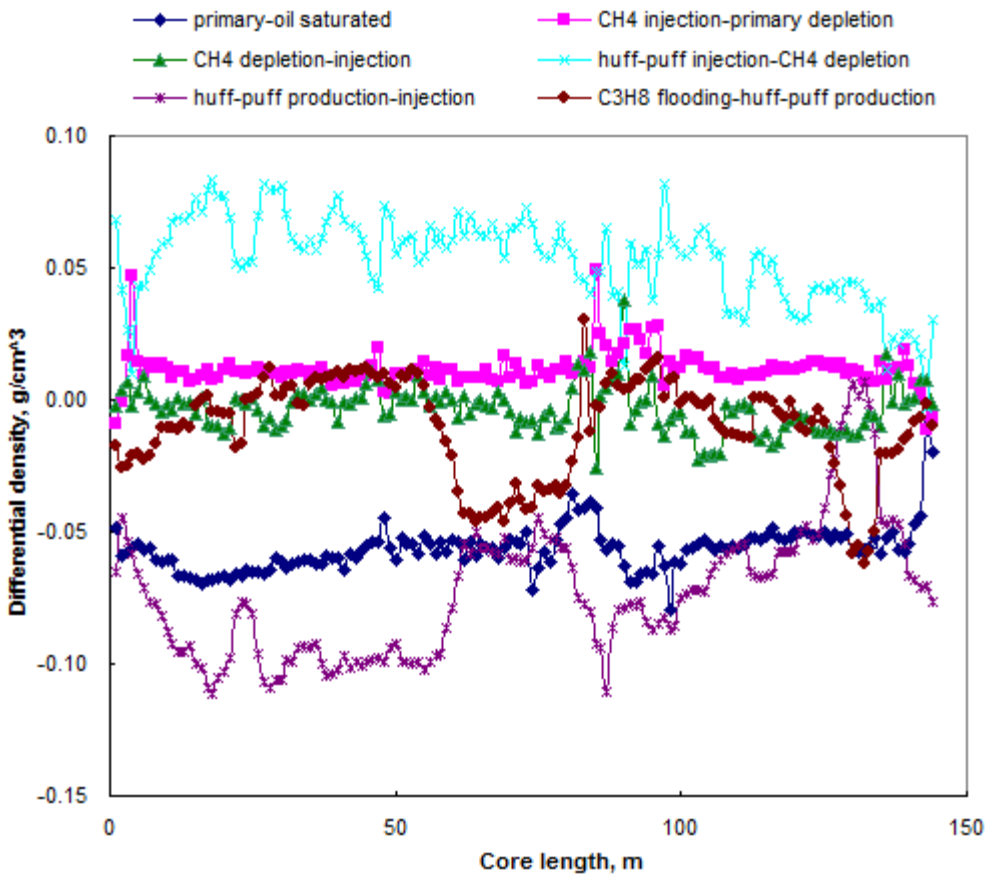

Figure 6.8 Density difference of every two adjacent processes-1.5m core

The 18m in length core behaviours probably could be explained by the density profiles of 1.5m sand packed core. As we discussed above, liquid phase CO_2 and C_3H_8 huff-puff process could change the oil distribution and helped to build up oil enrichment areas in the core. The propane flooding process could not be performed to the end at 18m in length sand packed core was most likely caused by these. If the propane injection rate would be increased greatly to liquid propane flooding, more oil should have been recovered through propane flooding process.

6.4 Water Cut after Each Process-1.5m Core

Figure 6.9 shows that water cut in huff-puff process was obviously higher than it in primary depletion and propane flooding processes. This indicates that the sweep efficiency is high in this process.

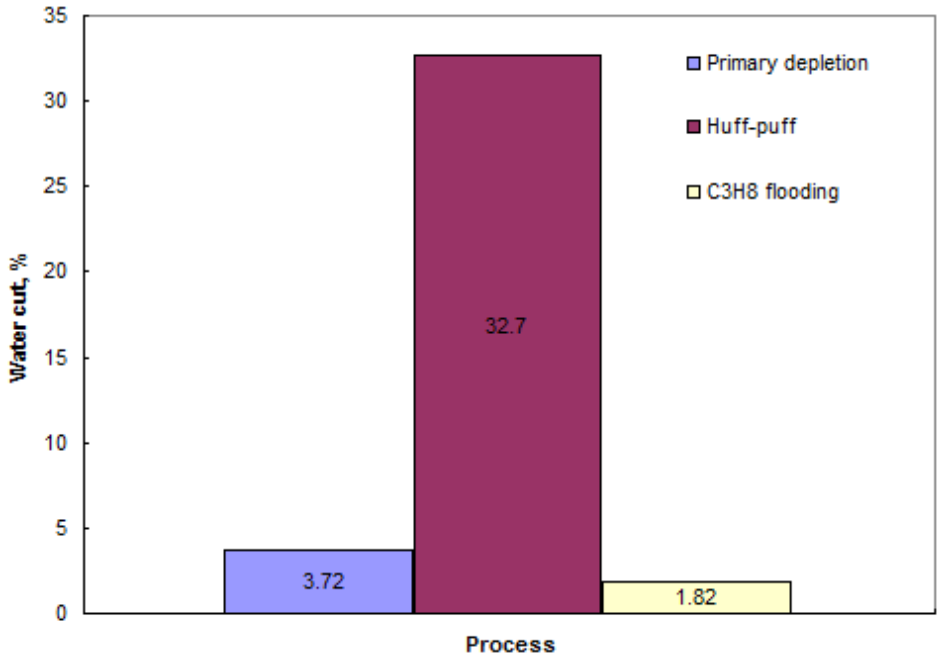

Figure 6.9 Water cut at different processes-1.5m core

6.5 Oil Recovery Comparison-Effects of Core Length and Permeability

Table 6.2 summaries the core and fluid properties. The fluid properties were all similar to the three cores, but the core properties varied among them. Core length effect can be compared between 18m in length glass beads packed core and 1.5m sand packed core because both of the cores had similar permeability. Permeability effect can be compared between two 18m in length cores.

Figure 6.10 summarizes the oil recoveries of each process at the three cores. It could be seen clearly that core length not only affects oil recovery at each process but also affect at which process the oil can be recovered. That means that the selection of gas recharging methods is closely related to core length. The shorter core recovers more oil than the longer core at comparable processes. The core permeability also affects oil recovery; the higher one recovers more oil based on this study. Detailed research should be performed later.

Table 6.2 Core and fluid property summary

Type	Properties			
Core	Name	Sand -N.N. Goodarzi	Glass beads -N.N. Goodarzi	Sand
	Length (m)	18.55	18.19	1.5
	Cross-sectional area (cm^2)	2.85	2.85	2.73
	Absolute water permeability (Darcy)	1.92	11.81	13.2
	Pore volume (ml)	2607	2099	152.77
	Porosity (%)	36.4	37.8	32.78
	Connate water saturation (%)	9.21	7.6	4.65
Fluid	Dead oil viscosity at 23℃ (mPa.s)	10695	10711	11230
	Dead oil density at 23 ℃ (kg/m^3)	982	982	983.6
	GOR at 23℃ (m^3/m^3)	14	14	14.48
	Live oil viscosity at 23℃ (mPa.s)	4837	5688	5210
	Live oil density at 23 ℃ (kg/m^3)	975	971	969.2

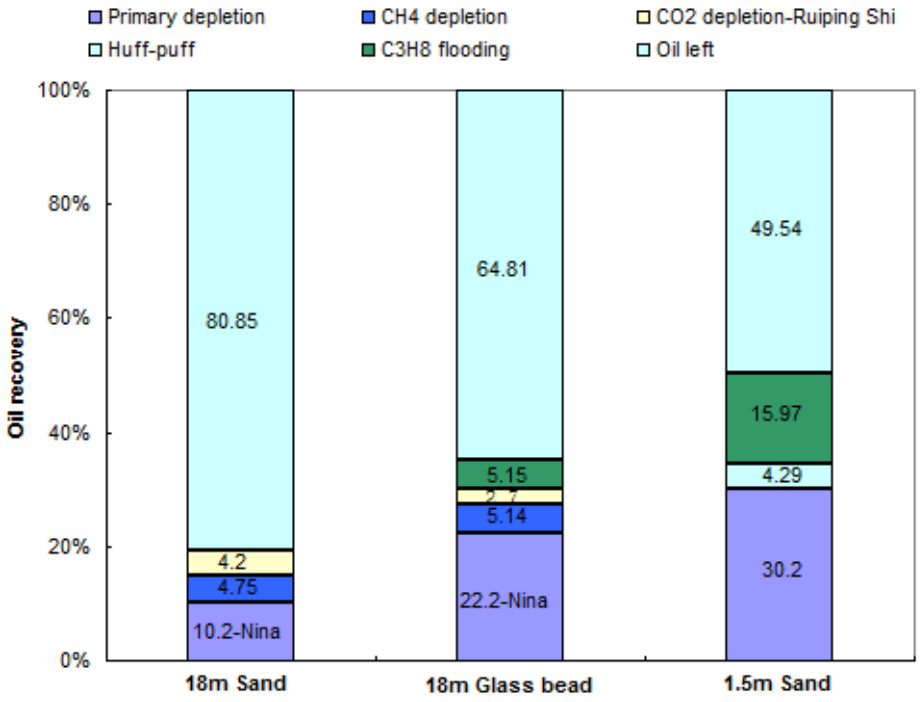

Figure 6.10 Oil recovery summaries

Chapter Seven: Conclusions and Recommendations

7.1 Conclusions

To further study the heavy oil solution gas drive mechanisms, methane recharging and depletion, carbon dioxide and propane huff-puff and propane flooding processes were performed at three cores with different permeabilities and lengths. CT scanning, NMR and GC tools were applied to understand what happened at each process. The following summarizes the results of this study:

1. Gas recharging processes did help to produce more oil.
2. For a certain heavy oil reservoir, the selection of gas recharging techniques should carefully combine multiple factors together. For example the gas type, recharging methods, depletion rate, reservoir condition, fluids properties, etc.
3. Foamy oil flow was clearly observed at long core methane depletion processes, lower core permeability is helpful for foamy oil flow.
4. Foamy oil flow was also inferred at long core puff process.
5. GC tool was effectively used to analysis production curves at long core huff-puff process. GC results comparison for tiny gases verified a chemical reaction (thermal cracking) had happened at the abnormal heating area before huff process on sand packed long core.
6. CT scanning and NMR techniques were successfully used at each short core process. It was better applied to explain long core phenomenon later.
7. The comparisons of viscosity and water cut of produced oil from short core indicate that huff-puff process not only can enlarge swept efficiency, but also can dilute oil viscosity a lot.
8. By the comparisons of CT images and density variations of short core , huff-puff process helps to redistribute the residual oil and form oil banks.
9. According to the comparison of oil recovery at each process from three cores, the shorter length and higher permeability of the core are helpful for oil recovery.

7.2 Recommendations

This research provides only a small contribution to the vast complexities of heavy oil solution gas drive. Based on the results and experiences, suggestions for future work are proposed:

1. To help further understanding the mechanisms of gas recharging processes, a continuous produced fluid sample should be taken and more analysis techniques should be applied. For example, at each process, taking produced oil samples at more containers one by one for viscosity, water cut analysis and composition analysis as well.
2. CT scan technique should be applied not only before and after but also during each process to visually observe the foamy oil flow in heavy oil.
3. To complement this work, the effect of core length should be further studied. Ideally, experiments with series of lengths (15m, 12m, 9m, 6m and 3m) will provide results to effectively compare with the results of this study.
4. Permeability effect should be deeply investigated to provide a clear understanding of the role it plays in the heavy oil solution gas drive.
5. Gas recharging experiments at different depletion rates and modes should be tested as well to maximize the oil recovery.
6. Energy supplement methods during puff process should be further studied at two long cores to help produce oil. For example: gas flooding or water flooding with puff process together.
7. This study is just a point, there is still much left to be further addressed: the injection pressure, the length of soaking period, the relationship of core length and permeability, the thickness of the oil layer, gas top, bottom water, and so on.

References

1. M.B. Dusseault, "Comparing Venezuelan and Canadian Heavy Oil and Tar Sands", Paper 2011-061 presented at the Petroleum Society's Canadian International Petroleum Conference 2001, Calgary, Alberta, Canada, June 12-14, 2001.
2. M. Metwally, "Enriched Gas Pressure Cycling Process for Depleted Heavy Oil Reservoirs", The Journal of Canadian Petroleum Technology, December 1998, Volume 37, No. 12, page 56-60.
3. F.M. Garcia, "A Successful Gas-Injection Project in A Heavy Oil Reservoir", SPE 11988 presented at the 58th Annual Technical Conference and Exhibition held in San Francisco, CA, October 5-8, 1983.
4. A. Aladasani and B. Bai, "Recent Developments and Updated Screening Criteria of Enhanced Oil Recovery Techniques", SPE 130726 presented at the CPS/SPE International Oil and Gas Conference and Exhibition held in Beijing, China, 8-10 June 2010.
5. S. Chen, H. Li, D. Yang and P. Tontiwachwuthikul, "Optimal Parametric Design for Water-Alternating-Gas (WAG) Process in a CO_2-Miscible Flooding Reservoir", October 2010, Volume 49, No. 10.
6. K.P. Ramachandran, O.N. Gyani and S. Sur, "Immiscible Hydrocarbon WAG: Laboratory to Field", SPE 128848 presented at the SPE Oil and Gas India Conference and Exhibition held in Mumbai, India, 20-22 January 2010.
7. J.R. Christensen, E.H. Stenby and A. Skauge, "Review of WAG Field Experience", SPE 71203 presented at the 1998 SPE International Petroleum Conference and Exhibition of Mexico, Villahermosa, Mexico, 3-5 March, 1998.
8. S.H. Behzadi and B.F. Towler, "A New EOR Method", SPE 123866 presented at the 2009 SPE Annual Technical Conference and Exhibition held in New Orleans, Louisiana, USA, 4-7 October 2009.

9. Y.P. Zhang, P. Luo and S. Huang, "Improved Heavy Oil Recovery by CO_2 Injection Augmented with Chemicals", SPE 131368 presented at the CPS/SPE International Oil and Gas Conference and Exhibition held in Beijing, China, 8-10 June 2010.

10. A. Emadi, M. Sohrabi, M. Jamiolahmady, S. Ireland and G. Robertson, "Mechanistic Study of Improved Heavy Oil Recovery by CO_2-Foam Injection", SPE 143013 presented at the SPE Enhanced Oil Recovery Conference held in Kuala Lumpur, Malaysia, 19-21 July 2011.

11. S.I. Chou, D.L. Pisio, D.E. Jasek and J.A. Goodgame, "CO_2 Foam Field Trial at North Ward-Estes", SPE 24643 presented at the 67th Annual Technical Conference and Exhibition of the Society of Petroleum Engineers held in Washington, DC, October 4-7, 1992.

12. Y. Sun, L. Zhao, T. Lin, L. Zhong, D. Yu and H. Lin, "Enhance Offshore Heavy Oil Recovery by Cyclic Steam-Gas-Chemical Co-Stimulation", SPE 149831 presented at the SPE Heavy Oil Conference and Exhibition held in Kuwait City, Kuwait, 12-14 December 2011.

13. D. Wang, T. Zhu, D. Chen, F. Bao and D. Olsen, "Gas-Steam Slug Flooding to Enhance Recovery from a Medium Heavy Oil Reservoir", SPE 59332 presented at the 2000SPE/DOE Improved Oil Recovery Symposium held in Tulsa, Oklahoma, 3-5 April 2000.

14. L. Zhao, D. Law and J-Y. Yuan, "Numerical Investigation of Steam and Gas Mixing in Heavy Oil Production", Paper 99-45 presented at the 1999 CSPG and Petroleum Society Joint Convention, Digging Deeper, Finding a Better Bottom Line in Calgary, Alberta, Canada, June14-18, 1999.

15. C. Egboka and D. Yang, "Performance of a SAGD Process with Addition of CO_2, C_3H_8, and C_4H_{10} in a Heavy Oil Reservoir", SPE 150170 presented at the SPE Heavy Oil Conference and Exhibition held in Kuwait City, Kuwait, 12-14 December 2011.

16. B.S. Busahmin and B.B. Maini, "Effect of Solution-Gas-Oil-Ratio on Performance of Solution Gas Drive in Foamy Heavy Oil Systems", CSUG/SPE 137866 presented at the Canadian Unconventional Resources and International Petroleum Conference, Calgary, Alberta, Canada, 19-21 October 2010.

17. N.N. Goodarzi and A. Kantzas, "Observations of Heavy Oil Primary Production Mechanisms from Long Core Depletion Experiments", The Journal of Canadian Petroleum Technology, April 2008, Volume 47, No. 4, page 46-54.

18. R. Shi and A. Kantzas, "Enhanced Heavy Oil Recovery on Depleted Long Core System by CH_4 and CO_2", SPE/PC//CHOA 117610 PS2008-334 presented at 2008 SPE International Thermal Operations and Heavy Oil Symposium, Calgary, Alberta, Canada, 20-23 October 2008.

19. N.N. Goodarzi and A. Kantzas, "Observations of Heavy Oil Primary Production Mechanisms from Long Core Depletion Experiments", Paper 2008-086 presented at the Petroleum Society's 7th Canadian National Petroleum Conference, Calgary, Alberta, Canada, Jun.13-15, 2006.

20. Y.M. Bayon, R.M. Coats, D.A. Lillico, P.R. Cordelier and R.P. Sawatzky, "Application and Comparison of Two Models of Foamy Oil Behaviour of Long Core Depletion Experiments", SPE/ Petroleum Society of CIM/CHOA 78961 presented at the 2002 SPE International Thermal Operations and Heavy Oil Symposium and International Horizontal Well Technology Conference, Calgary, Alberta, Canada, 4-7 November 2002.

21. Y.M. Bayon and P.R. Cordelier, "A New Methodology to Match Heavy -Oil-Long-Core Primary Depletion Experiments", SPE 75133 presented at SPE/DOE Improved Oil Recovery Symposium, Tulsa, Oklahoma, U.S.A., 13-17 April 2002.

22. Soroush H. and Saidi A.M., "Vertical Gas-Oil Displacements in Low Permeability Long Core at Different Rates and Pressure Below MMP", SPE 53221 presented at the 1999 SPE Middle East Show, Bahrain, 20-23 February 1999.

23. J.D. Fambrough and D.P. Newhouse, "A Comparison of Short-Core and Long-Core Acid Flow Testing for Matrix Acidizing Design", SPE 26186 presented at the SPE Gas Technology Symposium, Calgary, Alberta, Canada, 28-30 June 1993.

24. S.K. Cheung and H.V. Arsdale "Matrix Acid Simulation Studies Yield New Results with a Multitap Long-Core Permeameter", January 1992, JPT. Volume 44, No. 1. Page 98-102.

25. A. Graue, K. Kolltveit, J.R. Lien and A. Skauge, "Image Fluid Saturation Development in Long-Core Flood Displacements", 17438PA, SPE Formation Evaluation, December 1990, Volume 5, No. 4.

26. B.H. Caudle and I.H. Siberberg, "Oil Recovery by System Injection in a Long Core System", not published, in e-Library with the permission of and transfer of copyright from the author, 1964. Society of Petroleum Engineers.

27. C.R. Holmgren, "Some Results of Gas and Water Drives on a Long Core", Petroleum Transactions, AIME, Volume 179, 1949, Pages 103-118.

28. J.N. Breston and R.V. Hughes, "Relation between Pressure and Recovery in Long Core Water Floods", Petroleum Transactions, AIME, Volume 186, 1949, Pages 100-110.

29. N.N. Goodarzi, "Investigating Heavy Oil Solution Gas Drive Fluid Properties and the Effect of Scale on Depletion Experiments", M.Sc. Thesis, University of Calgary, 2006.

30. R. Bora, B.B. Maini and A. Chakma, "Flow Visualization Studies of Solution Gas Drive Process in Heavy Oil Reservoirs with a Glass Micromodel", SPE 64226, SPE Reservoir Eval. & Eng. 3 (3), June 2000.

31. A. Sahni, F. Gadelle, M. Kumar, L. Tomutsa and A.R. Kovscek, "Experiments and Analysis of Heavy-Oil Solution-Gas Drive", SPE Reservoir Evaluation and Engineering, June 2004.

32. G.E. Smith, "Fluid flow and Sand Production in Heavy-Oil Reservoirs under Solution-Gas - Drive", SPE Production Engineering, 1988, page 169-180.

33. R.T. Johns, "Oil Recovery", Encyclopedia of Energy, Volume 4. 2004. Elsevier Inc.

34. D.D. Joseph, "Foamy Oil", Dec. 8, 1998, www.aem.umn.edu/people/faculty/joseph/.../decmemomarlene.pdf

35. L. Andarcia, C. Heny and A. Rico, "Experimental Study on Production Performance of Two Different Heavy Oils in Venezuela", Paper 2000-43 presented at Petroleum Society's Canadian International Petroleum Conference 2000, Calgary, Alberta, Canada, June 4-8, 2000.

36. B.B. Maini, "Foamy-Oil Flow", SPE 68885, Distinguished Author Series, Oct, 2001.

37. C. Hu, X. Liu, J. Wang, Z. Song, Z. Fan and F. Yang, "Cold Production of Thin-bedded Heavy Oil Reservoir in Henan Oilfield", SPE 50885 presented at the 1998 SPE International Conference and Exhibition in Beijing, China, 2-6 November 1998.

38. S. Akin and A.R. Kovscek, "Heavy-Oil Solution Gas Drive: A Laboratory Study", Journal of Petroleum Science and Engineering 35 (2002) 33-48.

39. J. Wang, Y. Yuan, L. Zhang and R. Wang, "The Influence of Viscosity on Stability of Foamy Oil in the Process of Heavy Oil Solution Gas Drive", Journal of Petroleum Science and Engineering 66 (2009) 69-74.

40. D.S. George, O. Hayat and A.R. Kovscek, "A Micro-visual Study of Solution-Gas-Drive Mechanisms in Viscous Oils", Journal of Petroleum Science and Engineering 46 (2005) 101-119.

41. J. Peng, G.Q. Tang and A.R. Kovscek, "Oil Chemistry and Its Impact on Heavy Oil Solution Gas Drive", Journal of Petroleum Science and Engineering 66 (2009) 47-59.

42. H. Sarma and B. Maini, "Role of Solution Gas in Primary Production of Heavy Oils", SPE 23631 presented at the Second Latin American Petroleum Engineering Conference, II LAPEC, Caracas, Venezuela, March 8-11, 1992.

43. B.B. Maini, H.K. Sarma and A.E. George, "Significance of Foamy-Oil Behaviour in Primary Production of Heavy Oils", The Journal of Canadian Petroleum Technology, November 1993, Volume 32 No. 9, page 50-54.

44. B.B. Maini, "Foamy Oil Flow in Primary Production of Heavy Oil under Solution Gas Drive", SPE 56541, presented at the 1999 SPE Annual Technical Conference and Exhibition held in Houston, Texas, 3–6 October 1999.

45. R. Kumar, M. Pooladi-Darvish and T. Okazawa, "Effect of Depletion Rate on Gas Mobility and Solution Gas Drive in Heavy Oil", SPE 78438 was revised for publication from paper SPE59336, first presented at the 2000 SPE/DOE Improved Oil Recovery Symposium, Tulsa, 3-5 April. 2000.

46. H. Sheikha and M. Pooladi-Darvish, "The Effect of Pressure Decline Rate and Pressure Gradient on the Behaviour of Solution Gas Drive in Heavy Oil", SPE 109643 presented at

2008 SPE Western Regional and Pacific Section AAPG Joint Meeting, Bakersfield, California, U.S.A., 31 March-2 April, 2008.

47. G. Meszaros, A. Chakma, K.N. Jha and M.R. Islam, "Scaled Model Studies and Numerical Simulation of Inert Gas Injection with Horizontal Wells", SPE 20529 presented at the 65th Annual Technical Conference and Exhibition of the Society of Petroleum Engineers held in New Orleans, LA, September 23-26, 1990.

48. A. Kantzas, B. Nikakhtar, P. de Wit, M. Pow and K.M. Jha, "Design of a Gravity Assisted immiscible Gas Injection Program for Application in a Vuggy Fractured Reef'", Journal of Canadian Petroleum Technology, December 1993, Volume 32, No. 10.

49. M.R. Islam, A. Chakma and K.N. Jha, "Heavy Oil Recovery by Inert Gas Injection with Horizontal Wells", Journal of Petroleum Science and Engineering 11 (1994) 213-226.

50. R.M. Butler and I.J. Mokrys, "Recovery oil Heavy Oils Using Vaporized Hydrocarbon Solvents: Further Development of the VEPAX Process", Paper No. 7 presented at the 4th Petroleum Conference of the South Saskatchewan Section, Regina, 7-9 October 1991.

51. M. D. Murray, S.M. Frailey and A.S Lawal, "New Approach to CO2 Flood: Soak Alternating Gas", SPE 70023 presented at the SPE Permian Basin Oil and Gas Recovery Conference held in Midland, Texas, 15-16 May 2001.

52. M. Dong, S. Huang and K. Hutchence, "Methane Pressure-Cycling Process with Horizontal Wells for Thin Heavy-Oil Reservoirs", SPE 88500, April 2006 SPE Reservoir Evaluation and Engineering.

53. P. Luo, C.D. Yang and Y.G. Gu, "Enhanced Solvent Dissolution into In-Situ Upgraded Heavy Oil under Different Pressures", Science Direct, Fluid Phase Equilibria 252 (2007) 143-151. Available online at www.sciencedirect.com.

54. G.Q. Wu and A. Kantzas, "Experimental Study of Gas Solvent Flooding for Lloydminster Heavy Oil Reservoirs", paper 2008-135, proceeding at the Canadian International Petroleum Conference/ SPE Gas Technology Symposium 2008 Joint Conference, Calgary, Alberta, Canada, 17-19 June 2008.

55. H.W. Yarranton, A. Badamchi-Zadeh, M.A. Satyro and B.B. Maini, "Phase Behaviour and Physical Properties of Athabasca Bitumen, Propane and CO2", Paper 2008-120, The Petroleum Society's 59th Annual Technical Metting, Calgary, Alberta, Canada, 17-19 June 2008.

56. P. Luo and Y.G. Gu, "Characterization of a Heavy Oil–Propane System in the Presence or Absence of Asphaltene Precipitation", Contents lists available at ScienceDirect, Fluid Phase Equilibria 277 (2009) 1-8. Journal homepage: www.elsevier.com/locate/fluid.

57. F.I. Syed, A.H. Tunio and N. A. Ghirano, " Compositional Analysis and Screening for Enhanced Oil Recovery Processes in Different Reservoir and Operating Conditions", International Journal of Applied Science and Technology, Vol. 1, No. 4; July 2011.

58. S.X. Zheng, H.Zh. Li and D.Y. Yang, "Pressure Maintenance and Improving Oil Recovery with CO2 Injection in Heavy Oil Reservoirs", SPE 150169 presented at the SPE Heavy Oil Conference and Exhibition held in Kuwait City, Kuwait, 12-14 December 2011.

59. A. Emadi, M. Sohrabi, M. Jamiolahmady, S. Ireland and G. Robertson, "Reducing Heavy Oil Carbon Footprint and Enhancing Production through CO2 Injection", Chemical Engineering Research and Design 89 (2011) 1783-1793.

60. A. Firoozabadi, "Mechanisms of Solution Gas Drive in Heavy Oil Reservoirs", Journal of Canadian Petroleum Technology, Vol. 40, No.3, March, 2001, page 15-20.

61. A. Mai, J. Bryan, N.N. Goodarzi and A. Kantzas, "Insights into Non-thermal Recovery of Heavy Oil", Journal of Canadian Petroleum Technology, March 2009, Volume 48, No. 3.

62. A. Johnson, "What is The Maximum and Minimum Void Ratio of Ottawa Sand (Silica Sand)?" http://www.newton.dep.anl.gov/askasci/env99/env156.htm.